1971

Superconductivity of Pb-Bi alloys under high pressure

Robert Edwin Jones Jr.
Iowa State University

Superconductivity of Pb-Bi alloys under high pressure

by

Robert Edwin Jones, Jr.

A Dissertation Submitted to the
Graduate Faculty in Partial Fulfillment of
The Requirements for the Degree of
DOCTOR OF PHILOSOPHY

Major Subject: Physics (Solid State)

Approved:

Signature was redacted for privacy.

In Charge of Major Work

Signature was redacted for privacy.

For the Major Department

Signature was redacted for privacy.

For the Graduate College

Iowa State University
Ames, Iowa

1971

TABLE OF CONTENTS

CHAPTER I. INTRODUCTION

Gordon and Deaton (1) recently identified a double-hexagonal close-packed (dhcp) phase in the Pb-Bi alloy system at pressures above 16 kbar. They identified the structure using a high pressure x-ray technique and also measured the volume change and electrical resistivity as a function of pressure. The pure dhcp region was found to be quite narrow with a range from about 60 to 64 atomic percent Bi (hereafter atomic percent concentration will be indicated by %). The transformation into the high pressure phase is quite slow (approximately 2 hours at the critical pressure) but at room temperature was found to be reversible on complete relief of pressure. The high pressure phase initially had been discovered, but not identified, by the resistance and compression measurements of Bridgman (2) whose report of broad, irreversible transformations may have resulted from their inherent sluggishness.

The temperature-dependent phase diagram of the Pb-Bi system is well-known at atmospheric pressure (3) and is shown in Figure 1. There are three single phase regions: 1) α, the rhombohedral or Bi-rich phase in which less than 1 % Pb is soluble, 2) β, the hexagonal close-packed (hcp) or intermediate phase which contains from 24 to 34 % Bi at room temperature, and 3) γ, the face-centered cubic (fcc) or Pb-rich phase in which up to 20 % Bi is soluble. Concentrations intermediate between these regions are mixtures of the two neighboring phases. At low pressures the concentrations associated with the dhcp or δ phase are in the α-β mixed region and contain roughly half of each of the phases. The dhcp structure is a close-packed arrangement of hexagonal planes with ABACABAC stacking which

is intermediate between hcp (ABAB) and fcc (ABCABC) stacking and can be considered to contain half of each of these simpler structures. Gordon and Deaton have suggested that the high pressure dhcp phase possibly is formed by conversion of the α phase component into the Bi V phase which may be fcc (4).

Bridgman suggested that for pressures of 15 kbar or above all α-β mixtures at least partially convert into the δ phase with an α-δ mixed phase for concentrations of Bi above the pure δ region and a β-δ phase below. He also reported distinct, reversible transitions to the Bi II (25 kbar) and Bi I-II (27 kbar) structures in both the pure Bi phase and the α component of the presumed α-δ phase, but no such transitions were seen at lower Bi concentrations. In addition, he found a transformation of the γ phase to a high pressure phase with a critical pressure which increased rapidly with increasing Pb concentration. Pure Pb has a high pressure polymorph above 161 kbar (5) which is presumedly related to the high pressure γ phase transition and Klement (6) has suggested that this is an hcp phase related to the β phase of the Pb-Bi system. A pressure-dependent phase diagram (at room temperature) constructed from the reports discussed above is shown in Figure 2.

The Pb-Bi system at atmospheric pressure has been extensively studied for superconducting behavior and all alloys except those in the α phase are superconducting. These alloys, which generally exhibit type II behavior, have relatively high transition temperatures and unusually high critical fields for a non-transition element material. The present work investigates the dhcp phase for superconducting behavior and hopefully

extends our knowledge of this alloy system which, perhaps, has been studied more than any other composed entirely of non-transition metals. A second objective will be to measure the volume dependence of Pb-Bi superconducting properties since much is known about the effect of pressure on elemental superconductors but there exists a paucity of reported data on alloys. Perhaps the most intriguing aspect of this study arises from the high pressure phase having the relatively rare dhcp structure* which is one of two La phases at atmospheric pressure. Lanthanum has certain unusual superconducting properties (which will be discussed later in this chapter) and it would be interesting to compare these with the properties of another dhcp superconductor. Some of the theoretical and experimental considerations which are important for the pursual of these investigations are presented in the following sections of this chapter.

Superconductivity and Type II Behavior

At the present time, there is a wealth of knowledge about superconducting behavior and the overt experimental features are in good agreement with theoretical predictions. Superconductivity is associated with the obvious property of zero electrical resistance below some critical temperature, T_c, (11) but the behavior in a magnetic field is an even more fundamental aspect and the division of superconductors into two types is

---

*Elemental dhcp phases at atmospheric pressure are found only among the rare earths and only La is superconducting whereas the others are magnetic (7). The dhcp structure has been found in Ag alloys, Mg, and perhaps Cd at high pressures (8) and in Au-In (9) and Au-Ga (10) alloys at atmospheric pressure, but there have been no reported investigations for superconducting behavior.

based on the manner in which they tend to exclude an applied field. An additional classification of superconductors is based on more subtly different properties which are related to presumed differences in the mechanisms leading to superconducting behavior.

Figure 3 shows the magnetization curves which result (neglecting geometrical considerations) when an external field is applied to an ideal superconductor of each type. For type I at a given temperature, $M = -H/4\pi$ up to the critical field, H_c, then precipitously drops to zero with the concurrent return of electrical resistance. The difference between the Gibbs free energy of the superconducting state at $H = 0$ and that of the normal state at H_c is given by the area under the magnetization curve, $VH_c^2/8\pi$, plus a negligible magnetostriction term. For type II, the perfect diamagnetism ceases at the lower critical field, H_{c1}, but M does not become zero until a higher critical field, H_{c2}, is reached and zero electrical resistance persists up to H_{c2}. By analogy, a thermodynamic critical field can be defined by $VH_c^2/8\pi = -\int MdH$. An important experimental observation is that for a suitable sample either type of magnetization curve is reversible (12, 13, 14). Many superconductors are not reversible and the superconducting properties of the α-β phase of Pb-Bi are extremely irreversible (15). The critical fields are temperature-dependent and a "similarity principle" exists in that most superconductors deviate only slightly from $h(t) = 1 - t^2$ where $h = H_c/H_c(0)$ and $t = T/T_c$. The above discussion of magnetization properties does not hold near the surface where the external field dies out over a short distance characterized by the London skin depth, λ_L.

The discovery of the isotope effect, $T_c \propto 1/\sqrt{M}$, raised the possibility of lattice participation in the origin of superconductivity. Cooper (16) found that pairs of electrons with opposite momentum states near the Fermi surface could take advantage of an electron-phonon interaction with a resulting net attractive potential. The theory of Bardeen, Cooper, and Schrieffer (BCS) (17) shows that such an attractive interaction can lead to superconductivity by considering the effects of correlating many pairs at once over a spatial extent limited by a coherence distance, ξ. BCS predicts an energy gap, $2\Delta(0)$, in the density of states at the Fermi surface and relates this to T_c by

$$kT_c = \frac{2\Delta(0)}{3.52} .$$

The transition temperature also is related to the attractive interaction, J, the density of states in the normal state, N(0), and the Debye temperature, Θ_D, via

$$T_c = 0.85\Theta_D \exp(-1/N(0)J) . \qquad (1)$$

BCS and subsequent modifications of this microscopic quantum mechanical theory predict most of the salient features of type I behavior and there have been some extensions of BCS to type II superconductivity near T_c (18).

The absent or suppressed isotope effect in Ru (19) and other transition metals (20) was the first of several indications that the electron-phonon interaction may not provide an adequate explanation of superconductivity in all cases. Matthias (21) recently has described four different classes of superconductors: 1) the non-transition metals, 2) the transition metals, with partially filled d states, 3) the rare earths and actinides, with partially filled f states, and 4) materials with high Debye

temperatures, including borides and beryllium compounds. This classification is based on a modified periodic chart with Lu replacing La which is added to the beginning of the rare earth series (22, 23). Differences among the superconducting behaviors of the members of the first three groups under pressure tend to support this division and will be discussed in the next section. One of the first theoretical treatments of the transition metal superconductors (24) developed a two band model related to the s and d states, and extension of this work (25) considered coupling between the bands and particularly related this to the behavior of La with presumed s and f states. Kuper, Jensen and Hamilton (23, 26) proposed a slightly different model for La and U which considered a narrow f band lying just above the Fermi surface and predicted a suppressed isotope effect and certain other properties in disagreement with BCS. However, Garland (27, 20) suggested modifications of BCS which could explain the observed behavior of transition metal superconductors, and Johnson and Finnemore (28) measured the specific heat of dhcp and fcc La with results in apparent agreement with BCS. The mechanisms for superconductivity in the second and third classes remain unsettled questions, and Fröhlich (29) recently proposed a collective electronic mode or acoustic plasmon model which Rothwarf (30) successfully has applied to a number of superconducting and normal state phenomena.

The present understanding of type II superconductivity is based on the solution by Abrikosov (31) and Gor'kov (32, 33) of the Ginzburg and Landau (34) theory and these works collectively are often called the GLAG theory. Ginzburg and Landau, who formulated the problem of superconductivity in

terms of surface energies and an order parameter $\psi(r)$, were able to reduce the problem to a dependency on a parameter κ for temperatures near T_c. For $\kappa > 1/\sqrt{2}$ a surface energy instability developed in the solution resulting in a mixed state or type II superconductivity and conversely if $\kappa < 1/\sqrt{2}$ the superconductivity is type I. Abrikosov solved the type II problem and found

$$H_{c2} = \sqrt{2}\kappa H_c \tag{2}$$

and also that near H_{c2} the slope of the magnetization curve was related to κ by

$$\frac{dM}{dH} = \left[(1.18)(4\pi)(2\kappa^2 - 1) \right]^{-1} . \tag{3}$$

He also was able to show that

$$H_{c1} = \frac{1}{\sqrt{2}\kappa} (\ln\kappa + 0.08) H_c$$

for the case where $\kappa \gg 1$.

Gor'kov extended the solution to all temperatures, but it was necessary to introduce a new parameter, ℓ, the electronic mean free path, and he found

$$H_{c2} = \kappa(1.77 - 0.43t^2 + 0.07t^4) H_c$$

for ℓ infinitely long. He also expressed κ as a sum of two components, $\kappa = \kappa_o + \kappa_e$, each of which involves physically measurable parameters with

$$\kappa_o = 0.96\lambda_L(0)/\xi = 0.53\lambda_L(0) \frac{kT_c}{\hbar v_F}$$

and

$$\kappa_e = 7.53 \times 10^3 \rho_n \gamma^{\frac{1}{2}}$$

where v_F = Fermi velocity, ρ_n = normal state resistivity, and γ = electronic specific heat. It unfortunately would be extremely difficult to determine all these parameters for a sample in a high pressure apparatus.

Maki (35) has taken Equations 2 and 3 above and redefined κ to be a variable in each case so that the equations will hold at all temperatures. Hence, κ_1 is defined by

$$H_{c2} = \sqrt{2}\kappa_1 H_c$$

and κ_2 by

$$\left.\frac{dM}{dH}\right|_{H_{c2}} = \left[(1.18)(4\pi)(2\kappa_2^2 - 1) \right]^{-1} .$$

He obtains numerical evaluations of these parameters as a function of temperature in the "dirty" limit where $\ell \ll \xi$. Maki (36) also shows that at T = 0,

$$H_{c1} = \frac{\ln \kappa_3(0)}{\sqrt{2}\kappa_3(0)} H_c$$

where $\kappa_3(0) = 1.53\kappa$. He then lets κ_3 become a temperature-dependent variable so $\kappa_3(t)$ replaces $\kappa_3(0)$ and he again presents a solution in the dirty limit.

Caroli, Cyrot, and de Gennes (37) have recalculated κ_2 in the dirty limit and found that κ_2 is very nearly equal to κ_1 at all temperatures. Some of the various numerical results for these temperature-dependent parameters are shown graphically in Figure 4.

It should be mentioned that Abrikosov (31) and Goodman (38) established a criterion for determining the type of superconducting behavior from the coherence distance and the London penetration depth. If $\xi/\lambda_L > 1$ the material is type II and if less than 1 the material is type I.

Saint James and de Gennes (39) predicted the possibility of superconductivity existing in a thin surface sheath for fields up to 1.695 H_{c2}. Both the existence of this effect and the approximate value of the coefficient experimentally were verified (40). It subsequently was found, how-

ever, that the ratio H_{c3}/H_{c2} was somewhat greater than 1.7 for most temperatures, but that it rapidly dropped toward unity as T approached T_c (41).

The above paragraphs were not intended to be a complete review of type II superconductivity since the purpose rather was to establish the concepts, definitions, and results necessary to discuss the present work. Additional information about superconductivity can be found in the books by Shoenberg (42), Schrieffer (43), de Gennes (44), and also in the two volumes edited by Parks (45).

The first superconducting Pb-Bi alloy was reported by de Haas, van Aubel, and Voogd (46) who found the eutectic (~ 56 % Bi) to be superconducting at 4.2 K but did not investigate the transition temperature, T_c. They also reported that the transition temperatures of Tl, Sn, and Au could be increased by the addition of Bi (46, 47) which is not superconducting in the pure state at atmospheric pressure. This work prompted McLennan, Allen, and Wilhelm to undertake further studies of Bi alloys (48) the results of which are summarized in Table I.

Table I. Superconducting transition temperatures of some Bi alloys

Alloy	T_c
$Pb_{0.42}Bi_{0.58}$	8.8 K
Rose's Metal, Bi_2SnPb	8.5
Newton's Metal, $Bi_{0.50}Sn_{0.19}Pb_{0.31}$	8.5
Wood's Metal, $Bi_{0.50}Sn_{0.12\frac{1}{2}}Cd_{0.12\frac{1}{2}}Pb_{0.25}$	8.2
Bi_5Tl_3	6.4

The tendency for increased T_c upon alloying with Bi is demonstrated again, but the T_c of 8.8 K for Pb-Bi was of particular interest since it was the highest transition temperature known at that time. Meissner and Westerhoff (49) investigated Pb-Bi alloys as a function of concentration and found that T_c increases above $T_c(Pb)$ = 7.2 K as the Bi concentration increases until T_c = 8.8 K at about 35 to 40 % Bi. The transition temperature then remains fairly constant with increasing Bi concentration until superconductivity disappears with the onset of the α phase. More recent reports (50, 51) also show this same general behavior but indicate a lower T_c for the 40 % Bi alloy (8.67 K) and a slight decrease in T_c with further increase in Bi concentration. Metallurgical problems which affect the transition temperature will be discussed later.

The superconducting behavior of Pb-Bi alloys has been studied extensively by a group of workers at the University of Cambridge (15, 52, 53, 54) (hereafter called CEDW). CEDW studied the magnetization curves of various alloys at 4.2 K and found H_{c2} increased with increasing Bi concentration up to the limit of the β phase, then H_{c2} remained constant at 18.7 kG for higher concentrations as shown in Figure 5. CEDW also report H_c, H_{c1}, and the temperature-dependent $\varkappa$ parameters as a function of concentration up to 40 % Bi and that the superconducting properties of an α-β mixture depend only on the superconducting properties of the β phase. Reversibility of the magnetization curve is quite adversely affected by the presence of the α phase which provides pinning sites. The limit of Bi in the β phase is 33.4 % at room temperature and Bi rapidly precipitates out of the β phase at higher concentrations unless the alloy is quenched directly in liquid nitrogen after annealing. Hence, an α-β sample left

for a few hours at room temperature will have a superconducting β phase matrix which contains approximately 35 % Bi (rather than about 41 %) and has a correspondingly lower H_{c2} and T_c. A second but slower aging effect afflicting α-β alloys is the growth of the Bi or α phase precipitate size, which is a change in microstructure, not the composition. The effect of the α precipitate size on the magnetization curves and flux pinning has also been investigated by CEDW. Other workers have reported two gaps for α-β alloys (55, 56, 50) and Adler and Ng suggest that this is the result of a proximity effect rather than a second gap due to the α phase as assumed in the other two reports. Other investigations on the superconducting behavior of Pb-Bi alloys have been reported, but the above discussion includes the results most relevant to the present work.

Superconductivity under High Pressures

The effects of pressure on superconducting behavior have been widely studied during the past several years as various high pressure, low temperature techniques have been developed. The most obvious type of study is to investigate the properties of a superconductor as a function of pressure or volume change and the most commonly observed parameters are the transition temperature and critical fields. Other properties such as specific heat or thermal expansions are technically difficult to measure at high pressures due to the required massive structures surrounding the sample. A second type of investigation involves a search for high pressure polymorphic phases of known atmospheric pressure superconductors. These high pressure phases generally have been found to be superconducting but with properties which sometimes are quite different from those of the usual

phase. The creation of high pressure superconducting modifications of materials which ordinarily are non-superconductors constitutes a third class of investigation which is closely related to the second. At the present time, approximately one-third of the known elemental superconductors exist only in some high pressure phase.

As was previously mentioned, the behavior of superconductors under pressure can be classified to a great extent by their position on the periodic chart. The non-transition elemental superconductors include the good metals at the right of the periodic chart (beginning with column IIB) and all have a negative dT_c/dP of moderate absolute value ($\sim$ 2-4 x 10^{-2} K/kbar), except for Tl for which T_c increases with pressure up to a maximum at about 2 kbar but at somewhat higher pressures behaves as other members of this group. Jennings and Swenson (57) first noted that T_c of Sn varied linearly with the volume, not the pressure, and this type of analysis has been extended successfully by Smith and Chu (58) to other non-transition metals. Eight additional elements in this class become superconductors only upon transformation at high pressure from semiconducting or semimetallic phases to metallic phases which are superconducting at low temperatures. The pressure effect, dT_c/dP, is relatively small and negative for two of these high pressure polymorphs (Si and Bi III) and the detailed properties of a few others are unstudied. There have been only limited studies under pressure on alloys and compounds composed entirely of non-transition metals and the reported pressure effects are both positive and negative but tend to be of the order of magnitude characteristic of the class. Fischer and Olsen (59) have measured the Ginzburg-Landau κ as a function of pressure for an In- 14 % Tl alloy with κ = 0.82 and found

$d\alpha/dP = - 0.46 \times 10^{-2}$ kbar^{-1}.

The second class of superconductors (transition metals) tend to have pressure effects which are an order of magnitude smaller than those of the non-transition metals and which may be either positive or negative. This class is affected by a marked dependence of dT_c/dP upon sample condition (impurities, strains, annealing), and this has resulted in several discrepancies among the earlier reported data. There has been a fairly successful attempt (60, 61) to relate the sign and relative magnitude of the pressure effect to the empirical relationship of T_c to valence number (62) by considering pressure as an effective increase in the valence number. This behavior and the other observed characteristics generally hold for alloys between transition metals.

The few superconductors found at the beginning of the rare earth and actinide series often are considered together with the transition metals but their unusual behaviors under pressure tend to justify a separate classification. Metallurgical problems in La have hampered efforts to completely resolve the pressure dependency of the dhcp and fcc phases below 23 kbar (63, 64, 65) but above this pressure only the fcc phase is stable. Regardless of phase, the pressure effect in La is positive and unusually large ($\sim 14 \times 10^{-2}$ K/kbar) and T_c increases to 12 K at the highest reported pressure (140 kbar). Alpha-uranium was thought to be superconducting at atmospheric pressure but recent investigations attribute this to internal strains. Gardner and Smith (66) report that dT_c/dP is exceptionally large ($\sim 60 \times 10^{-2}$ K/kbar) at low pressures with T_c rapidly rising from 0 to about 2 K then going through a broad maximum before finally decreasing as pressure is increased. Th has a less exciting

pressure dependence and its behavior is similar to those of the non-transition metals. A high pressure Ce polymorph produced above 50 kbars (67) loses its magnetism and becomes superconducting. Various fundamentally different models (68, 69, 67) have been proposed to explain the behavior of La and related superconductors under pressure. Any appropriate model of these elements as a group will have to consider the newly discovered superconducting high pressure polymorphs of Ba (70), Y, and Cs (71) and it likely will be desirable to return La to its original position in the periodic chart. It is interesting to note that monovalent Cs should not be superconducting according to certain empirical rules of Matthias (62) and that Y and Ba have transition temperatures which increase rapidly with increasing pressure.

There has been considerable theoretical interest in superconductivity under pressure, not only in an attempt to better understand the observed results but also to predict whether pressure can destroy superconductivity within a given crystal phase. The earliest theoretical efforts applied thermodynamic arguments to the previously mentioned difference between the Gibbs free energies of the normal and superconducting states. It can be shown that the change in the critical field under pressure is related to the volume change at the phase boundary by

$$\frac{dH_c}{dP} = \frac{4\pi}{H_c} \frac{V_n - V_s}{V_s} \quad . \tag{4}$$

In addition, the pressure effect is related to the volume thermal expansion, $\alpha = V^{-1} (\partial V/\partial T)_{P,H}$, the bulk modulus, $B_k = - V(\partial P/\partial V)_{T,H}$, and the specific heat, C, via

$$\frac{dT_c}{dP} = \frac{B_{kn} - B_{ks}}{B_k^2(\alpha_n - \alpha_s)} = VT_c \frac{\alpha_n - \alpha_s}{C_n - C_s} \quad . \qquad (5)$$

It is sometimes possible to obtain sufficiently accurate experimental values of the parameters on the right side of Equation 4 but usually not for those of Equation 5.

Many of the more recent theories are based on BCS and often involve consideration of the pressure dependence of the various terms in Equation 1. The logarithmic volume derivative of this equation can be written as

$$\frac{\partial \ln T_c}{\partial \ln V} - \frac{\partial \ln \Theta_D}{\partial \ln V} = \ln \frac{0.85\Theta_D}{T_c} \frac{\partial \ln N(0)J}{\partial \ln V} \quad , \qquad (6)$$

where $-\partial \ln \Theta_D / \partial \ln V$ is the Grüneisen parameter, γ_G, which can be determined experimentally from the Grüneisen relation $\alpha = \gamma_G C_V / B_k V$. The pressure dependence of J is quite difficult to predict, but it is possible to relate the pressure dependence of N(0) to experimental observables although these have been determined only for P = 0. Rohrer (72) noted that at low pressures several non-transition metals had values of $\partial \ln N(0)J / \partial \ln V$ between 2 and 3. Olsen *et al.* (73) considered this term to be a constant, φ, for all pressures and used this assumption to integrate Equation 6 with the result $\ln(T_c/\Theta_D) \propto V^{-\varphi}$ so that T_c approaches zero asymptotically. Brandt and Ginzburg (74, 75) suggested a pressure-dependent transition temperature related to a critical pressure, P_c, by

$$T_c(P) = 0.85\Theta_D \exp - \frac{A}{P_c - P}$$

where A is a constant, and they predicted critical pressures for some non-transition metals. Critical pressures which are higher than these have been predicted by Seiden (76) who has investigated $T_c(V)$ in terms of a

strong coupled superconductor (77). All of these theories predict T_c to be linear with V at low pressures in agreement with experimental observations for non-transition metals. Indeed, Smith and Chu have extrapolated this linear behavior to predict critical pressures which are smaller than any of those mentioned above, but such a behavior would require the superconducting interaction potential to drop preciptiously to zero at the critical volume. The experimental results presently do not extend to great enough pressures to select definitively which, if any, of the existing models is valid.

Additional information about experimental results can be found in the review articles by Swenson (78) and Brandt and Ginzburg (60, 79) and in the literature cited by these authors. These reviews also discuss some of the theoretical aspects of superconductivity under pressure as well as details of the apparatus and techniques. There remain several types of unusual superconducting systems which virtually are unstudied under pressure at the present time. Layered, quasi-two-dimensional superconductors form such a group and we report investigations of the effect of pressure on NbS_2 in Appendix A.

CHAPTER II. EXPERIMENTAL DETAILS

The purpose of this research was to investigate the superconducting properties of certain Pb-Bi alloys as a function of pressure. In particular it was desired to measure the critical field curves of the high and low pressure phases of alloys near the $Pb_{0.4}$-$Bi_{0.6}$ concentration. This objective required the use of high pressure-low temperature apparatus with associated techniques to accurately determine the temperature, pressure, and superconducting transitions. Strong, homogeneous magnetic fields also were needed and all of the various experimental aspects had to be compatible. The equipment and techniques used to meet these requirements are described in the following sections of this chapter.

High Pressure Apparatus

High pressures at low temperatures were obtained using a modification of the clamp technique originally developed by Chester and Jones (80). Two different types of piston and cylinder pressure cells were employed in the present investigations. The piston-cylinder devices were chosen over Bridgman anvils which are also in common use in low temperature work. While the latter are capable of higher pressures they do not come nearly as close to achieving hydrostatic conditions. Piston-cylinder devices can be designed so as to be compatible with a.c. susceptibility measurements of the superconducting transitions. This technique has the distinct advantage that no electrical leads into the high pressure sample chamber are required.

Pressure cells

The initial pressure cells were constructed entirely of heat treated beryllium-copper alloy (Berylco 25) and consisted of a thick-walled

cylinder with a movable piston in each end of the bore. The external end of each piston had a large head for mechanical support and better alignment. A Teflon disk placed at each inner piston face provided a seal between the piston and the cylinder bore. Beryllium-copper was chosen for these pressure cells because it has a high tensile strength but does not become brittle at low temperatures. Also, it is non-magnetic which is necessary for the use of the a.c. susceptibility measurements. It can be readily machined in the half-hard form then heat treated at 600° F (316° C) for 2 hours to obtain maximum tensile strength.

It is possible to predict the maximum internal pressure which can be supported by these devices, since at its limit, a thick-walled cylinder with supported ends will fail due to some combination of the tangential and radial strains in the wall.* The pressure at which failure occurs is a function of the material's mechanical properties and K, the ratio of outer to inner radii. Due to the physical limitation imposed by the clamp, all cylinders had an outside diameter of 0.60 inches hence K became dependent on the bore size. Pistons will fail above tne compressive strength of the material (13.8 kbar for Berylco 25), and for these cells it was not difficult to use a K sufficiently large so that the pistons would fail before the cylinder. Pressures slightly above the compressive strength were achieved with the additional pressure supported by the deformed shape of the pistons, and several sets of pistons were destroyed by use above the compressive strength but no cylinders ever failed.

---

*There are several models for determining the combined effects of tangential and radial strains. The experimental behaviors of various materials are approximated by different models (81, 82).

In order to achieve higher pressures, it became necessary to use a stronger piston material, but most of the likely candidates exhibited some disadvantage such as magnetic behavior, brittleness, or difficult fabrication. Finally, a cemented tungsten carbide (WC) with a compressive strength of 40 kbar was chosen, and rods of this material were cut to the proper lengths with a diamond wheel. While the ferromagnetic cobalt binder in these small pistons resulted in a large field-dependent contribution to the a.c. susceptibility, we found it could be subtracted satisfactorily from the superconducting transition contribution.

At the same time that the WC pistons were adopted, a new pressure cell was developed. This cell, shown in Figure 6, has a prestressed double wall cylinder to sustain higher internal pressures. It also is designed to allow the use of small, cylindrical pistons and still provide adequate alignment. Brass disks are situated at the piston ends to act as protective cushions, and brass extrusion rings sit on the disks at the inner piston faces. These rings are used in conjunction with Teflon disks to seal the sample chamber. All parts of this pressure cell are made from beryllium-copper except for those specifically mentioned above. Only the upper piston is movable and this is driven by a larger diameter plunger which fits snugly in the bore of the outer wall. This bore is straight between points A and B, but is tapered from point B to point C ($\sim 1^\circ$ included angle) to facilitate assembly of the cylinder during prestressing. The prestressing is accomplished by having the inner wall at a much lower temperature than the outer, then quickly pressing the two together. Further details about the prestressing as well as the strengths of double and single wall cylinders appear in Appendix B.

Pressure transmitting media

Two different pressure transmitting media were used in these experiments in order to obtain nearly hydrostatic application of pressure. In the first technique the sample and a superconducting manometer (described below) were surrounded by powdered Teflon, and no special sealing methods were used other than those previously mentioned. In the second technique, the sample and manometer were placed in a Teflon capsule and the remaining volume was filled with a 1:1 mixture of isoamyl alcohol and pentane. The self-sealing capsule which is used in conjunction with the usual high pressure seals is shown as a Teflon capsule body and lid together with the two Teflon disks at the right of the pressure cell in Figure 6.

Clamp and clamp technique

The clamp along with associated parts for pressurization is shown in Figure 7 with a single-walled pressure cell employing a powdered Teflon medium contained within the clamp. The holes in the bottom of the clamp provide mounting locations for two resistance thermometers but in this experiment only one, GR-65, was employed. The clamp body and lock nut were fabricated of beryllium-copper as was the thrust piston. The three-pin hex spanner was made from stainless steel and the pressure stand assembly was machined from a cold rolled steel rod.

The use of the clamp is fairly straightforward. The loaded pressure cell is placed inside the nylon sleeve and both are inserted into the clamp; the sleeve provides alignment while preventing the cylinder from expanding into the clamp wall under pressurized conditions. The lock nut then is screwed into place and the remaining parts of the apparatus are assembled. A hydraulic press applies force to the cell *via* the thrust

piston and the pressure is retained by torquing down the lock nut. The clamp, lock nut, and internal parts which collectively are called the "bomb" are attached to the cryostat by four machine screws through the upper shoulder of the clamp. This shoulder is cylindrical except for two opposing faces which are cut off so that the clamp mates with a slot in the pressure stand to prevent twisting of the clamp while the lock nut is being tightened. The narrowest cross-section of the shoulder is shown in Figure 7.

Superconducting manometers

Several superconductors with sensitive, well-known T_c vs P relations are commonly employed as manometers in cryogenic pressure experiments (83). The pressure is determined directly at low temperatures and hence, the method is particularly well-suited to the clamp technique since differential thermal contractions within the bomb change the applied pressure upon cooling.

The careful work of Jennings and Swenson (57) on Sn to 10 kbar has become the standard calibration for this most widely used manometer. Over this range the decrease in transition temperature is expressed by

$$\Delta T_c = -4.74 \times 10^{-2} P + 3.6 \times 10^{-4} P^2$$

where P is in kbar. This expression or other polynomial forms (58) cannot be extrapolated accurately beyond the range of their fit.

Smith and co-workers (83) have established manometer calibrations on a more fundamental basis. It had been noted that for many non-transition elements the decrease in T_c is proportional to the volume change (57, 58). They assume this to be true for all pressures so the "superconducting Grüneisen parameter"

$$\gamma_s = \frac{\partial \ln T_c}{\partial \ln V}$$

is a constant which can be evaluated from the low pressure data. The volume dependence was assumed to follow the Birch relation (84)

$$P = (3B_k/2)(Z^7 - Z^5)\left[1 - (3 - 3B_k'/4)(Z^2 - 1)\right]$$

where B_k is the isothermal bulk modulus, B_k' is its pressure derivative at zero pressure, and Z is related to the volume change as

$$Z = \left[\frac{V(0)}{V(P)}\right]^{\frac{1}{3}} .$$

They discuss the consistency of the low temperature values of the appropriate experimental parameters for Sn, Pb and Zn. Their values of B_k = 575 kbar, B_k' = 5.86, and γ_s = 7.21 for tin were used along with the experimentally determined T_c = 3.721 K to provide a pressure calibration for the present experiment. A computer program was used to provide a T_c vs P table with millidegree increments.

One experimental problem arose from the use of a Sn manometer. The 99.9999 % pure tin rods which were obtained from United Mineral and Chemical Corporation had such a small normal state resistance at cryogenic temperatures that bulk pieces cut from these rods exhibited a strong skin effect which was dependent on temperature and magnetic field. This resulted in a large temperature- and field-dependent background for the a.c. mutual inductance readings. An example of this effect is shown in Figure 8. The problem was finally overcome by extruding the Sn into a wire which both reduced the cross-section and increased the strain.

Cryostat

Temperatures in the 1 to 20 K region were obtained using a cryostat with a He^4 refrigerator and an electric control heater. In use the cryostat was suspended in a glass dewar filled with liquid helium which in turn was surrounded by an outer glass dewar filled with liquid nitrogen. The helium bath usually was vented into a recovery system; however, this exhaust could be closed and the pressure controlled by a manostat and vacuum system.

The lower section of the cryostat (shown in Figure 9) is connected to the vacuum systems at room temperature by stainless steel pumping lines. The diameter of these lines increases part way up the cryostat and again as the lines emerge from the dewar top. Isolation of the pot and experimental section is achieved by evacuating the vacuum jacket via the smaller line. By providing an overpressure of helium in the larger or pot pumping line, liquid condenses and runs down into the pot. The temperature of the pot then can be regulated between 1 and 4.2 K by controlling the pressure in this line. A small orifice (0.040 in. diameter) at the pot entrance prevents excessive film flow of superfluid helium II.

A stainless steel tube extends from the bottom of the pot to support a copper heater block around which a 1000 Ω bifilamentary electric heater of # 44 Manganin wire is wound. The Speer carbon resistor control thermometer is mounted in this block using Apiezon N-grease. The bomb is bolted to this block with thermal contact assured by a thin layer of N-grease at the interface. GR-65 and the search secondary coil are detachable from the bomb and thermal contact again is provided by N-grease. The electric leads which enter the vacuum jacket are first thermally anchored to the pot and

then to the heater block. The leads to GR-65 and the search secondary continue on from here.

A thin copper strip provides a limited amount of thermal contact between the brass pot and the heater block. The thermal conductivity of this strip is chosen to be large enough to provide adequate cooling yet small enough so that the bomb can be heated to several degrees above the pot temperature.

The vacuum can is soldered to the can top by Wood's metal and this seal can be broken to effect repairs. A detachable tail section to allow easy access to the bomb is provided by an indium vacuum seal consisting of an indium ring placed between stainless steel male and female flanges which are held together with stainless steel bolts. (All other parts of the vacuum can are of brass.) The search primary coil, the reference primary and secondary coils, and the 20 kG superconducting solenoid are mounted on the tail. All of the electrical leads to these components pass through the miniature Winchester electrical connector which readily disconnects to allow removal of the can.

The Westinghouse superconducting solenoid was equipped with a persistent mode switch and was rated for 20 kG at 16.4 amps with a 1 % uniformity over a 1 in. diameter x 2 in. long cylinder about the center. A Lambda regulated power supply with remote programed voltage and current controls energized the solenoid and the current was determined by potentiometric measurement of the voltage across a standard shunt in series with the solenoid. An opposing brace of avalanche diodes (GE semiconductor rectifier 1N1186) were connected in parallel across the current terminals to protect the solenoid from high voltages. These high voltages could result from

too rapid current changes or from accidental "quenching".

Mutual Inductance Bridge

Superconducting transitions can be detected using an a.c. mutual inductance bridge technique. The operational principle of this technique is to use the sample as a core in a set of transformer coils so that the mutual inductance between the primary and secondary coils is dependent on the properties of the sample. A low frequency current is driven through the primary coil and some voltage of undetermined amplitude and phase appears across the secondary coil. A null condition can be obtained in the secondary circuit of the bridge by the proper combination of measured inductive and resistive reference voltages in series with the secondary coil. The reference voltages necessary for null vary as the sample undergoes a transition from the superconducting to the normal state with associated changes in electromagnetic properties.

A schematic diagram of the modified Hartshorn bridge used in this experiment is shown in Figure 10. This bridge employes a 33.1 Hz oscillator with a quartz crystal frequency control to drive the primary circuit (including the search primary coil) via a Gertsch isolation transformer ST248B. The search primary is a set of Helmholtz coils with 630 turns of copper wire in each coil. A Helmholtz coil configuration was chosen because it is physically more compact than a solenoid with comparable homogeneity over the sample region. The search secondary has a 1700 turn central portion with 875 turn astatic coils at each end while the inductive reference voltage is provided by a replica set of coils with a dummy sample of Pb at their center. Placing the reference coils in the

helium bath provided a much more noise-free and stable reference than would have been possible at room temperature. The output of the reference secondary feeds into the secondary or null circuit of the bridge via a Gertsch Ratio Transformer 1011 which is an accurately calibrated voltage divider. The resistive reference voltage is supplied to a resistor in the secondary circuit by connecting it in parallel with a resistor in the primary circuit but with attenuation of voltage by a calibrated resistor in one of the voltage leads. Null conditions in the secondary are detected by a dual-phase lock-in detector with a Geoformer input. The detector is adjusted so that one channel is in-phase with the resistive reference and the other with the inductive reference.

The oscillator generates a sinusodial voltage of the form $V_o \sin \omega t$ where $\omega = 2\pi(33.1)$ sec^{-1}. The amplitude, V_o, is controlled by a variable resistor whose dial reads directly in volts provided that the load impedance is sufficiently high. During actual operating conditions the current through the primary circuit of the bridge was measured to be 3.4 ma per volt of output. The field produced at the center of the Helmholtz coils was calculated to be 258.3 G per ampere so that when driven by this circuit an oscillating field $h = h_o \sin \omega t$ is generated with amplitude $h_o = 0.9V_o$ G/ volt. This oscillating field was parallel with the axis of the superconducting solenoid.

Thermometry

Temperatures were measured using a Honeywell type II germanium resistance thermometer, GR-65. This thermometer previously had been calibrated against constant-volume gas thermometry at 121 points in the range 4.2 to

20 K (85). It also had been calibrated against the He^4 vapor pressure at 140 points between 1.1 and 4.2 K (86). The polynomial,

$$\ln T = \sum_{n=0}^{7} A(n) \left[\ln \frac{R}{R0}\right]^n ,$$

was fit to the resistance vs temperature data in three overlapping temperature ranges between 1 and 20 K. Rather arbitrarily, R0 was set equal to the largest resistance in each fit range. The coefficients, their range of validity, and the measuring currents are listed in Appendix C.

A standard four-lead potentiometric technique was used to measure the resistance of GR-65. The potentiometric circuit employed a Leeds and Northrup K-3 Potentiometer with battery substitute, a Keithly 155 Null Detector, an Eppley Standard Cell (No. 802720), and a General Radio 1 kΩ standard resistor. The measuring current was supplied by a series battery of 10 "D-size" mercury cells connected in series with variable resistors, the standard resistor and the thermometer. The auxiliary emf of the K-3 was used in setting the measuring current.

Once the experimental section obtained a desired temperature, it was maintained there using a Speer carbon ($\frac{1}{2}$ W, nominal 470 Ω, grade 1002) resistance thermometer in a control circuit (Figure 11). A three-lead d.c. Wheatstone bridge compared the carbon thermometer resistance with a variable decade resistance; the bridge off-balance voltage was amplified by a Leeds and Northrup Microvolt Indicating Amplifier and could be displayed on the internal meter or on a strip-chart recorder. Two functions were performed by an interface circuit. 1) The 10 mv full-scale output of the amplifier was reduced to 2 mv full-scale by use of a voltage divider. 2) The inherent zero-left of the recorder was converted to a zero-center by supply-

ing a constant 1 mv off-set voltage. Two 45 volt batteries in series provided current to the control heater via a system of variable resistors arranged so that a certain current was continuously supplied and an additional amount could be supplied on demand via a switch mechanically linked to the zero-center of the recorder. The continuous and incremental currents could be adjusted either individually or jointly and judicious setting of these currents allowed the temperature to be controlled with Speer resistance fluctuations of less than 0.1 Ω, the minimum increment of the decade resistor.

As is common with carbon thermometers the R vs T curve may shift slightly upon cycling between room and cryogenic temperatures. For a given calibration, the resistance of Speer carbon thermometers as a function of temperature can be expressed reasonably well by the two parameter relationship (87)

$$\left[\frac{\log R}{T}\right]^{\frac{1}{2}} = C \log R + D \, .$$

The deviation from this expression for one particular calibration is shown in Figure 12. A more accurate description can be made by fitting the parameters in several temperature ranges. Typically we found values of C = 2.8 and D = -7.7 which are in agreement with other reports for nominal 470 Ω, $\frac{1}{2}$ W Speer resistors (87, 88).

Magnetoresistance effects in the germanium and Speer carbon resistance thermometers have been a major experimental problem, and these can result in thermometry errors greater than 0.1 K under conditions commonly obtained in the present work. Due to the spatial limitations of the cryostat it was impossible to extend the thermometers outside the solenoid field.

A preliminary set of magnetoresistance effect measurements to 19.4 kG

were made at 4.2 K by filling the vacuum jacket with liquid helium to obtain isothermal conditions. The deviation of the apparent temperature from 4.2 K was of the same order of magnitude, but of opposite sign, for the germanium and carbon resistors.*

Fortunately GR-65 had been calibrated by D. L. Johnson at eight fields between 0 and 17.07 kG for each of eleven temperatures in the range 1.221 to 7.223 K (95). In his experiment, as well as in the present one, the applied field was perpendicular to the axis of the thermometer. The magnetoresistance effect at a given temperature is defined as $\Delta R/R(0)$ where $\Delta R \equiv R(H,T) - R(0,T)$ and $R(0) \equiv R(0,T)$. At the warmer temperatures $\Delta R/R(0)$ displayed the expected parabolic behavior with field (96, 97). However, as the temperature was decreased below about 3 K there was an increasing tendency for the magnetoresistance effect to rise more rapidly than H^2. In the present studies we extended the analysis of these data and found that the temperature dependence could be expressed analytically by

---

*Speer and Allen-Bradley are the two brands of carbon resistors commonly used as low temperature thermometers but the Speer resistors are in more general use in this laboratory. Although there has been extensive disagreement among the measured magnetoresistance effects in Allen-Bradley resistors, the reported absolute value of the apparent temperature discrepancy (89, 90, 91, 92) is one or two orders of magnitude smaller than that which we observed. Previous evidence for the larger discrepancy of the Speer thermometers had been given by Black, Roach, and Wheatley (93) and Jon Carlson (94) at lower temperatures where the observed magnetoresistance effect was decreasing rapidly with increasing temperature. Extrapolation of their results to 4.2 K would have suggested a smaller magnetoresistance effect than we observed. The percentage change in resistance with field in either brand is similar in absolute magnitude but the greater sensitivity of the Allen-Bradley thermometers results in a smaller apparent temperature discrepancy. In retrospect it appears the use of an Allen-Bradley thermometer would have been more satisfactory in the present experiment.

$$\frac{\Delta R}{R(0)} = \left[2.50 + \frac{7.96}{T^2}\right] \times 10^{-4} \; H^2 \quad ,$$

where H is in kG. This expression is also in quite good agreement with our preliminary data at 4.2 K. The empirical formula and the Johnson data at 12.2 kG are shown in Figure 13. Data at 7.3 and 17.1 kG also are plotted in the form of error bars to indicate the magnitude of non-parabolic behavior. This empirical expression was employed to extend the range of the calibration to 8.80 K and 19.5 kG.

This knowledge about GR-65 allowed us to obtain a desired temperature in the presence of a known magnetic field and then to measure the resistance of the carbon thermometer. In the region where the Johnson data existed, these rather than the empirical expression were used. The carbon thermometer was calibrated from 3.35 to 8.80 K in fields up to 19.5 kG. The magnetoresistance effect was found to be expressed best by

$$\frac{\Delta R}{R(0)} = - (8.45 - 0.38 \; T) \times 10^{-4} \; K(H) \; H \quad ,$$

where $K(H)$ is a slowly varying function of H and is nearly unity between 10 and 20 kG. $K(H)$ is shown graphically in Figure 14 with the 6.25 K data superimposed. Some data and the empirical fit of the temperature-dependent magnetoresistance effect are shown in Figure 15. In both Figures 14 and 15 the error bars are indicative of the minimum Wheatstone bridge sensitivity. The physical explanation of the field dependence is not understood. Our results are similar to the recent work of Saito et al. to 75 kG (88) who found an initial negative magnetoresistance and a high field positive effect with a minimum between 10 and 30 kG.

Samples

Lead-bismuth ingots were alloyed from 99.9999 % pure Pb and 99.999+ % pure Bi. The Pb was obtained from Cominco American Incorporated while the Bi orginially was received from Oak Ridge National Laboratory but within Ames Laboratory had been analyzed by Spectographic Group (98) and had been re-cast by Harvey Jensen of this Laboratory. Small chunks of the constituent metals were cut, cleaned according to ASARCO recommendations,* and then weighed. The desired ratio of these metals was melted in a pyrex crucible under vacuum. To minimize Bi precipitation, the melt was quenched by rapidly cooling the crucible in air.

The first ingot, REJ-I, was cast in a 3/8 in. diameter pyrex tube. A central section of this ingot was re-cast under vacuum in a special pyrex crucible having a thin-walled lower section of 0.1 in. bore. This lower section with the thin ingot, REJ-Ia, was cut off and the glass eaten away with HF. Eventually this ingot was cut into several samples which were numbered sequentially from the top after the uppermost slag portion was discarded.

The second ingot, REJ-II, was cast in a single step in a $\frac{1}{2}$ in. diameter tube, but a stainless steel paddle was used to insure mixing. Several samples were cut from the central portion of this ingot using a jewelers saw, and final shaping was done with a sharp blade.

All samples used in this experiment were of right cylindrical shape.

---

*ASARCO, American Smelting and Refining Company, handling recommendations: Clean Bi surface in dilute C. P. hydrochloric acid. Clean Pb surface with 1:3 solution of 30 % hydrogen peroxide plus C. P. grade acetic acid. After etching either surface, rinse with distilled or deionized water several times. Then dry in air or on ashless filter paper.

The diameters were about 0.1 in. and the length of each was 1 to $1\frac{1}{2}$ times the diameter. The surface of each sample was etched using a 1:1 bath of HCl and H_2O.* When inserted into the pressure cell, the sample axis was oriented parallel with the bomb axis and hence with the applied magnetic field.

A portion of each sample-yielding ingot was chemically analyzed for Pb content by Analytical Chemistry Group I of this Laboratory (then under the direction of the late Dr. C. V. Banks). The balance of the composition was assumed to be Bi. These results as well as the proportions calculated from initial weights are given in Table II. The atomic percentages were calculated from the 1961 International Atomic Weights M_{Pb} = 207.19 and M_{Bi} = 208.98).

Table II. Composition of Pb-Bi alloys

Initial weights	REJ-I	REJ-II
Pb	37.2 %	37.7 %
Bi	62.8 %	62.3 %
Analytical analysis	**REJ-Ia(4)**	**REJ-II(3)**
Pb	42.5 %	37.8 %
Bi	57.5 %	62.2 %

Procedure

Due to the nature of the clamp technique, it was necessary to warm the cryostat to room temperature in order to change the pressure. The period

*WARNING: Bi and high concentration Bi alloys cannot be electropolished in a chilled perchloric acid and methanol solution. The bismuth reacts rapidly and the results can be dangerous.

between cooling down to cryogenic temperature and warming up to room temperature is defined as a run. Hence, we generally had a different pressure associated with each run. The cryostat has been described previously and its operation employed standard techniques which will not be discussed further. However, there are several salient features about the data taking methods and these will be pointed out below.

With rare exceptions for special investigations, all of the data for this experiment were taken under equilibrium conditions. The temperature was controlled using the manostat and the Speer carbon control heater system; the superconducting solenoid was always in the persistent mode. After each change in temperature or magnetic field a few minutes wait was allowed to insure thermal equilibrium. Then the mutual inductance bridge was balanced and the values of the Gertsch Ratio Transformer (Gertsch) and the variable resistor setting (℟) were recorded. The current through the solenoid had been measured just prior to switching into the persistent mode. The resistance of the Speer carbon was noted and the temperature determined from the resistance of GR-65 (at least in zero field). This set of data was collectively called a data point and these data points were assigned consecutive numbers (KPT).

The experimental procedure involved obtaining a set of data points (called a sweep) which established a path through the critical field curves on an H vs T diagram. For each sweep the voltage amplitude of the oscillator was noted. Changes in the mutual inductance of the sample are related to the critical fields and the details will be discussed in the following chapter. All investigations were carried out on virgin samples (i.e. the sample had been cooled through T_c in zero field) and once a field had

been applied, H and T were controlled so as to be essentially monotonically non-decreasing.

The first action in each run was to determine the pressure from the zero field Sn transition. The He^4 pot was pumped to some temperature below T_c of Sn and held at that temperature with the manostat, while the control heater system was used to warm the experimental section through the transition in a series of small steps with a data point recorded for each. After the Sn transition had been determined, the point-by-point temperature sweep was continued upward to find the zero field Pb-Bi transition. The zero field sweeps completed the run unless the critical fields were to be measured.

It was important to measure the Sn transition before using the superconducting solenoid for two reasons. 1) The solenoid is not entirely reversible on return to zero current and can trap a field in its bore of the order of 10 G. This problem does not occur while the solenoid is still unused for that run. 2) The magnetic properties of the ferromagnetic Co binder in the WC pistons (if used) are extremely irreversible. This difficulty is overcome by degaussing the pistons at the end of each run during which the solenoid is used in preparation for later zero field studies. When saturated, these pistons apply a non-homogeneous field on the Sn manometer and result in a depressed, smeared-out Sn transition. Experimentally, the difference between the half height of such a transition and that of the degaussed case indicated that the average field applied to the manometer was roughly 30 or 40 G. These two effects could result in a pressure determination error of several kbar. However, these extraneous fields are insignificant in comparison with the measured critical field curves of the

Pb-Bi alloys.

Two techniques were used to observe the critical fields. 1) A sweep of the magnetic field at "constant" temperature. Actually, the Speer carbon resistance was held constant so the temperature decreased slightly with increasing field. 2) A sweep of the temperature at constant field.

Field sweeps always began at H = 0 so the temperature could be determined from GR-65 and the Speer calibrated against it. This initial temperature was called T* and deviations from T* were determined from the magnetoresistance of the Speer. Usually these data points in a field were incomplete in that the resistance of GR-65 was not measured. The field sweeps had the disadvantage that the mutual inductance of the bomb and cryostat was a function of field, so, it was necessary to make a background sweep at a temperature above T_c for each run. Also there is the problem that the seasoning sweep during which the pistons are saturated does not have the same background as subsequent sweeps.

Temperature sweeps at constant field appeared to have little or no background. However, in order to determine the temperature from the Speer it was necessary to calibrate the Speer at zero field during that run. For several temperature sweeps the resistance of GR-65 also was measured. In a few cases the lock-in detector output was fed to a dual-pen recorder and the temperature swept at a known rate (recorded on another strip-chart recorder). These non-equilibrium studies were used only for investigating the effect of varying h_o, the measuring field amplitude.

The pistons were degaussed by applying the solenoid field in alternating directions and decreasing the magnitude of the field with each change

of direction. Degaussing began at about 2.2 kG* and the magnitude was decreased each step by 60 G. This continued until the minimum output current of the solenoid power supply was reached (H ~ 30 G). Then the reversing switch was thrown back and forth with shorter and shorter times in each position. These times (10 sec. to less than 1 sec.) are of the same order or less than the characteristic energization time of the solenoid at minimal current.

---

*The saturation magnetization of Co is 1446 G at 0 K and its Curie temperature at 1400 K is the highest known.

CHAPTER III. RESULTS

The previously reported superconducting properties at zero pressure of Pb-Bi alloys with Pb concentrations of about 40 % have been discussed in the first chapter. In the present experiment, we re-examined the superconducting behavior of this low pressure or α-β phase and in addition measured the pressure dependence of these properties. We find the high pressure dhcp phase to be superconducting with properties which are not drastically different from those of the α-β phase. We report in this chapter the observed critical field curves of both phases including effects of pressure and discuss the various corrections and the analysis of the data.

Observed Transitions and Interpretation

The transitions from the superconducting state to the normal state are observed with a low frequency ac mutual inductance technique as was discussed previously. This widely employed technique measures the complex ac susceptibility, $\chi = \chi' - i\chi''$, as a function of temperature and the applied magnetic field, $H + h_o \sin\omega t$. The resulting measurements of χ are fairly unambiguous for the determination of T_c or for the investigation of the critical field of most type I superconductors. The ac susceptibility usually exhibits a more complicated behavior for type II materials or type I superconductors with $H_{c3} > H_c$, and the nature of this behavior often has not been completely understood. This lack of understanding has been promoted by the confusing differences between the observed ac susceptibilities associated with the transitions of various samples. Rollins and Silcox

(99) and van der Klein et al. (100) have reported both theoretical and experimental research on ac susceptibility measurements and quite recently Clem (101) has investigated the theoretical aspects of this problem. It now is possible to sketch some of the general features of χ as a function of H, h_o, ω, and sample properties, although all of the details may not be completely established.

Magnetic fields do not penetrate into the bulk of a superconductor in the Meissner state which results in the ac susceptibility having the values $\chi' = -1/4\pi$ and $\chi'' = 0$. The complex ac susceptibility is usually very small in the normal state, but this is not true if there are large resistive losses or if the skin effect resulting from a very small normal state resistivity screens much of the sample. As H is increased from zero at a given temperature, the Meissner state values of χ' and χ'' may be maintained to above H_{c1} or even H_{c2} if the interior of the sample is screened from the oscillating field in this dynamic situation by surface currents or flux pinning. It is important to notice that the ac susceptibility is related to the oscillating field, $h_o \sin\omega t$, which may be excluded from the bulk of the sample even though the static field, H, penetrates the sample creating a mixed state. If the Meissner state values persist above H_{c2}, the absolute value of χ' begins to decrease and χ'' commences to increase simultaneously at some higher value of H where the oscillating field begins to penetrate the bulk of the sample. As H is increased further, $4\pi\chi''$ reaches a maximum of approximately $1/\pi$ when $-4\pi\chi' = \frac{1}{2}$, and then both terms decrease to the normal state values at H_{c3}. The χ'' vs H curve is symmetrical about $H(\chi_{max}'')$, and this field

decreases rapidly with increasing h_o but is only slightly dependent on ω. If h_o is increased sufficiently (or if sample conditions warrant), then χ' and χ'' depart from the Meissner state values below H_{c2} and the shapes of the $\chi'(H)$ and $\chi''(H)$ curves become more complicated, but from experimental reports an inflection point or a spike is expected at H_{c2}. The ac susceptibility may deviate from the Meissner value as low as H_{c1} if h_o is sufficiently large for that particular sample, and this behavior may be manifested as either a spike or an inflection point in the $\chi'(H)$ and $\chi''(H)$ curves. There are no reasons to expect a fundamentally different behavior of χ if the sample is taken from the superconducting to the normal state by increasing the temperature at a fixed field.

Details of observed χ transitions

In the present experiment there is always a large background contribution to the observed ac susceptibility measurements due to the susceptibility of the bomb and cryostat and possibly to the search secondary not being truly astatic. The observed values of χ' and χ'' are taken to be the change in the measured susceptibility from this background. The mutual inductance bridge is not calibrated in the sense that the absolute values of χ' and χ'' can not be measured, but it is possible to determine the relative magnitudes of the two terms by direct comparison of the associated voltages. The Gertsch Ratio Transformer setting (G) is directly proportional to the real component (χ') of the total ac susceptibility under null conditions. The dial reading of the 111,100 Ω variable resistor (called 100 kΩ in Figure 10) is $\mathfrak{R}$ = (111,100 Ω - actual resistance) and $\mathfrak{R}$ has the same sense as the imaginary component (χ'') but

is not actually proportional to it. It can be shown that if the amplitude of the voltage across the resistive network in the primary circuit is held constant then the total imaginary ac susceptibility is proportional to

$$\frac{R_L R_H}{111{,}100 + R_L - \mathcal{R}}$$

where R_H is the resistance in the primary circuit which is connected in parallel with the resistance R_L in the secondary circuit. It is seen from this relation that χ'' is nearly proportional to the change in $\mathcal{R}$ if $\Delta\mathcal{R}/(111{,}100 - \mathcal{R})$ is small, which is generally the case.

The transition temperature, T_c, of the Pb-Bi alloys is defined at the half height of χ' which is measured during a temperature sweep in zero field with $h_o = 0.9$ G. Typical $X'(T)$ and $\chi''(T)$ curves are shown in Figure 16.* The beginning and ending temperatures of the transition are called T_L and T_H respectively if we can neglect the rounding of the $\chi'(T)$ transition curve, and in this case, the transition temperature also is determined by $T_c = (T_L + T_H)/2$.

It can be seen from Figure 16 that X'' in the normal state does not return to the Meissner state value and the effect of a peak nearly is suppressed. A relatively higher peak generally is observed for transitions in a magnetic field and the source of this discrepancy is not understood but perhaps arises from the peak being quite narrow in zero field. Never-

---

*In Figure 16, as elsewhere, we follow the convention of displaying $-\chi'$ rather than χ' without explicit mention of the minus sign since arbitrary units are used.

theless, the difference between the χ'' values in the Meissner and normal states eventually led to an investigation of various phase angles associated with the mutual inductance bridge. A dual-trace oscilloscope was used to compare the phase angles of voltages across certain components and these traces were photographically recorded. Careful analysis of these photographs confirmed suspicions that the phase angle of the reference secondary voltage (and hence the inductive reference voltage, V_G) is not orthogonal to the resistive reference voltage with the angle of error, Θ, being about 16.6°. However, the voltage across the search secondary is with 1° of being orthogonal to the resistive reference voltage. The cause of this phase angle problem probably is related to eddy current losses in the numerous metal parts of the cryostat.

An analysis of the phase angles and measurements involved shows that no serious errors are incurred in the results, and no attempts were made to correct the reference coils since the phase measurements were made after much of the data had been taken. The dual-phase lock-in detector is phased to the inductive and resistive references so it obviously shows no disagreement with the non-Cartesian, but unique, coordinate system established by the non-orthogonal references. Figure 17 shows a phase diagram with V_G and V_R which are associated with χ' and χ'' respectively. The actual ac susceptibility is $\bar{\chi} = \bar{\chi}' - i\bar{\chi}''$ so that a change in $\bar{\chi}''$ results only in a change in χ'', but a change in $\bar{\chi}'$ results in changes in both χ' and χ''. The relation between the real and observed ac susceptibilities is given by the equations

$$\bar{\chi}' = \chi' \cos\Theta$$

and $$\bar{\chi}'' = \chi'' - \chi' \sin\Theta \quad .$$

Figure 18 illustrates the resulting effects where the true shape of the $\bar{\chi}''$ transition is preserved but the observed shape of the $\bar{\chi}''$ transition is altered. It should be noted that $\bar{\chi}'(T) = \frac{1}{2}$ when $\bar{\chi}''(T)$ is a maximum and that $\bar{\chi}''_{max}/\Delta\bar{\chi}' = -1/2.5$ in comparison with the value of $-1/\pi$ predicted by various theories. The normal state value of $\bar{\chi}''$ which still is above the Meissner state value presumedly results from large normal state resistive losses and the $\bar{\chi}''$ curve is similar to that reported for a Pb- 6 % Tl alloy (102).

Critical field measurements

The observed critical field, H_{cr}, is defined as the field at which χ'' becomes a maximum and unless otherwise stated a measuring field with amplitude h_o = 0.9 G is used. In this experiment, H_{cr} is between H_{c2} and H_{c3} and is related to the properties of the superconducting sheath, but the exact location of H_{cr} is dependent on h_o. Due to broad χ transitions at high fields and to a field-dependent background susceptibility, measurement of H_{cr} proves to be more feasible than determining the associated H_{c3} from the end point of the χ transition. No advantage would be gained by correcting the phase angle error of the χ'' curve since this error results in H_{cr} being closer to H_{c3}. No significant differences are found between H_{cr} determined by a field sweep and that determined by a temperature sweep. Both methods were employed in the present research, and both have certain experimental advantages, but the biggest advantage probably lies with the temperature sweep which avoids the field-dependent background problem. The transition temperature associated with H_{cr} for

the sweep of Figure 18 is taken as that corresponding to the maximum in the χ'' curve.

The background susceptibility, χ_{BG}, is measured by a field sweep at a temperature above T_c, and it generally is necessary to repeat these measurements for each run in which field sweep measurements of H_{cr} are employed. A computer program approximates the $\chi'_{BG}(H)$ and $\chi''_{BG}(H)$ curves by straight line interpolations between adjacent points, and then, for each data point of a field sweep below T_c, the χ_{BG} value at that field is subtracted from the observed susceptibility, χ_{unc}. Figure 19 shows χ'_{unc}, χ'_{BG}, and also the resulting corrected χ'_c, while Figure 20 shows χ''_{unc}, χ''_{BG}, and χ''_c as well as the point which determines H_{cr}. This large background arises primarily from two sources: 1) the ferromagnetic Co binder in the WC pistons and 2) presumed lead particles in a brass part of the vacuum jacket which cause the anomaly near 500 G. This anomaly appears at a field of about 650 G if the helium bath is cooled to 3.0 K, and both of these points roughly lie on the critical field curve of Pb.

Magnetoresistance thermometry corrections

The above determination of the observed critical field curves is not complete since the resistance thermometry must be corrected for magnetoresistance effects as discussed in Chapter II. There is no need to correct the temperature of each data point since we are only interested in the temperatures associated with H_{cr}.

The resistance of either thermometer in a field is called R*, and

the temperature that this resistance would represent in zero field is labeled T*. The actual temperature, T, is associated with a resistance R(0). The magnetoresistance effect can be written as

$$R(0) = \frac{R^*}{1 - HK(H)(8.45 - 0.38T) \times 10^{-4}}$$

for the Speer carbon thermometer. This equation can be solved for R(0) by making the approximation that T is equal to T* on the right hand side of the equation. This approximation can introduce an error of the order of 0.1 Ω for critical field points obtained in this experiment. For a temperature sweep, T* is not known and has to be calculated from R* and a two parameter fit to zero field thermometry data, but in any case such a thermometry fit is necessary to determine T from R(0).

The magnetoresistance effect of GR-65 can be written as

$$R(0) = \frac{R^*}{1 + H^2(2.50 + 7.96/T^2) \times 10^{-4}} \quad ,$$

and we can solve this equation by letting T become T* on the right hand side which essentially provides the first iterated solution. The error introduced by this approximation is kept to less than 1 mK by taking the second iteration of the above equation at high fields and low temperatures.

Measuring field dependence

The h_o dependence of the ac susceptibility was studied extensively by making temperature sweeps with various values of h_o. The dhcp phase was more carefully studied but the results of the brief investigations of the α-β phase of the same sample are quite similar. Curves fitted to the ac susceptibility data at various measuring fields with H = 200 G are shown in Figure 21 as a function of T* determined from GR-65. The results

of similar studies at 10.00 and 19.60 kG are shown in Figures 22 and 23, respectively, where it is seen that the h_o dependence becomes greater with increasing H. Slight irregularities in the susceptibility curves for $h_o < 0.9$ G should not be taken too seriously, particularly at high fields, since the sensitivity of the bridge is linear in h_o and the uncertainty becomes fairly large on the scale of the graphs. The $H_{cr}(h_o,T)$ data obtained from the above and other susceptibility measurements are listed in Appendix D and the effects of the h_o dependence on a critical field curve of the dhcp phase are shown in Figure 24. At any given H, the change in the temperature associated with $H_{cr}(h_o)$ is not linear in h_o, and a sensitive measure of the h_o dependence is made by plotting $T(h_o)$ - T(0.9 G) at various values of H_{cr} as in Figure 25.

The end point of the χ''(0.9 G) transition is defined experimentally as H_{c3}*. The values of H_{c3}* are difficult to measure accurately, especially at the higher fields, but the resulting data are listed in Appendix D. The H_{c3}*(T) data for fields from 5 to 10 kG indicate that the H_{c3} critical field curve is 11 to 13 % above the measured H_{cr}(0.9 G) curve. The H_{c3}*(T) data at lower fields indicate a greater deviation near T_c, and the high field data, which may be highly inaccurate, indicate up to 17-18 % deviation at low temperatures. It is believed that the limit of $H_{cr}(h_o)$ as h_o approaches zero is H_{c3}, but the non-linear h_o dependence of H_{cr} fails to suggest this limit.

One result of the above investigations is the evidence found in some susceptibility curves for the location of H_{c2}. Evidence of H_{c2} appears in both $\chi'(T)$ and $\chi''(T)$ curves for h_o = 7.2 G as shown in Figure 26. A

secondary peak is observed in the χ'' curves at 1.20 and 2.00 kG, but as H increases this peak progressively becomes more masked by the tail of the H_{cr} peak. The H_{c2} peak is difficult to observe near T_c, presumedly, because it falls within the H_{cr} peak. The H_{c2} peak is too broad to be useful in determining the H_{c2} curve, but its existence verifies that H_{cr} lies between H_{c2} and H_{c3}.

Sn Manometer and Transition Widths

The use and calibration of a Sn manometer already have been discussed as have the details of detecting the superconducting transition in zero field as the temperature is increased. A typical $\chi'(T)$ curve for a Sn manometer is shown in the Insert of Figure 27 where T_L and T_H are defined as previously with the transition temperature determined by $T_c = (T_L + T_H)/2$ and the transition width defined as $T_H - T_L$. The various transition widths observed in this experiment and the experiment reported in Appendix A are shown in Figure 27 as a function of the pressure at 4.2 K. Jennings and Swenson (57), who used solid hydrogen pressure transmitting media, report a minimum transition width of 0.02 K for polycrystalline Sn and any additional width is assumed to be a manifestation of a pressure gradient across the manometer. This nominal minimum transition width and the widths associated with a 0.5 kbar pressure gradient across the sample also are indicated in Figure 27. It is clear that there are no large deviations from hydrostatic conditions except for the one very broad transition which is associated with Run 17 where the pistons were seriously distorted.

Metallurgical Aspects

The metallurgical properties of Pb-Bi alloys are of interest in the present work since the superconducting behavior is dependent on these properties. The sluggishness of the transformation from α-β to dhcp at 16 kbar, together with the known high mobility of the atoms in the α-β phase at room temperature (54), suggests that the transformation involves rearrangement of the atoms over long distances on an atomic scale. We assumed that the transformation results in a more homogeneous arrangement of the atoms in the dhcp phase since it involves only a single crystal structure while the low pressure phase is comprised of regions of two different structures. A series of micrographs of Pb-Bi alloys with different histories were made by H. H. Baker of this Laboratory in order to test the above hypothesis and to further investigate the known aging effects.

Figure 28 is a 500x micrograph of a polished surface of REJ-1a(1) which has been in the α-β phase continuously for one year since alloying. The light areas are identified as the α or Bi-rich phase and the dark areas as the β phase in agreement with CEDW (53). A similar micrograph of REJ-1a(3) which had been pressurized to over 75 % of the critical pressure indicates no significant differences between these two α-β microstructures. Figure 29 is a micrograph of REJ-1a(2) made 2 days after the pressure had been relieved which allowed the sample to revert from the dhcp to the α-β phase. The sample presumedly is in the α-β phase but the microstructure is quite fine which supports the hypothesis that the arrangement of Pb and Bi atoms is much more nearly homogeneous in the dhcp phase. Micro-

graphs of this same sample at later dates are shown in Figures 30 and 31 which illustrate the growth of the α phase regions with time. It appears that the sample eventually will regain its initial "fishbone" structure. It should be mentioned that these investigations study only the slower of the two aging processes where there are no changes in the compositions of either phase.

Experimentally Observed Superconducting Behavior

A primary result of this work is that high pressure dhcp phase Pb-Bi is superconducting, with T_c approximately 8.0 K near the critical pressure. This transition temperature is not greatly lower than that of the α-β phase which is near 8.5 K at atmospheric pressure. Appendix D reports the transition temperatures measured at a number of different pressures for several Pb-Bi specimens of both phases. The considerable scatter in the $T_c(P)$ data is attributed to aging effects. Estimates of the time, t, at room temperature since the previous run or since alloying* also are listed in Appendix D, but most of the times which are listed as 1 day are actually 12 hours or shorter. Two pairs of consecutive runs (14-15 and 40-41) are of particular interest to the study of aging effects, since the clamp was unchanged between the runs of each pair. The transition temperature of an α-β specimen at about 1.7 kbar increased by 20 mK after 5 days at room temperature, and later, T_c of this sample in the

---

*It must be remembered that t as determined from date of alloying may not represent the aging of that sample since the metallurgical changes during quenching are neglected.

dhcp phase at about 18 kbar increased by 68 mK after 20 days at 300 K. The change in T_c of the α-β phase as a function of t can be associated with the recrystalization of the microstructure. This effect in the dhcp phase is more difficult to understand but may be related to completion of the sluggish phase transformation or to relief of internal strains by annealing.

These difficulties are minimized by considering only the $T_c(P)$ data for which t is 1 day or less. We are interested in the pressure effect, dT_c/dP, only within a single phase and it seems wise to consider data for α-β specimens which previously have not been in the high pressure phase. The $T_c(P)$ data which satisify these conditions are shown in Figure 32 where both phases exhibit a linear depression of T_c with increasing pressure. The pressure effect of the α-β phase is given by

$$\frac{dT_c}{dP} = - (1.23 \pm 0.01) \times 10^{-2} \text{ K/kbar},$$

and that of the dhcp phase by

$$\frac{dT_c}{dP} = - (1.35 \pm 0.05) \times 10^{-2} \text{ K/kbar}$$

where the limits indicated result only from consideration of scatter in the $T_c(P)$ data. Uncertainties in the determination of T_c and P increase these limits, but the largest and least determined errors quite possibly are introduced by the aging effects. It seems reasonable to state identical pressure effects for the two phases as

$$\frac{dT_c}{dP} = - (1.3 \pm 0.15) \times 10^{-2} \text{ K/kbar}$$

where it is assumed the calibration of the Sn manometer is correct.

Critical field curves (to 20 kG) of the α-β phase of REJ-1a(3) from Run 15 (P = 1.75 kbar) and Run 16 (P = 9.00 kbar) are shown in Figure 33 where it appears that these curves nearly follow a similarity principle. In contrast with these curves, Figure 34 shows a higher critical field curve for an α-β sample which has just reverted from the dhcp phase and a lower curve for an as-cast portion of the same ingot (REJ-11) at similar pressures (2.19 and 3.68 kbar, respectively). Aging apparently is the primary factor determining $(dH_c/dT)_{T_c}$ in the α-β phase, and this prevents us from successfully investigating the pressure dependence of the critical field curve. The $H_{cr}(T)$ data for these and all other runs are listed in Appendix D.

The critical field curve of the dhcp phase proves to be amenable to studies of its pressure dependence and Figures 35 and 36 show the critical field data obtained for two different samples from the REJ-1a ingot. Curves are fitted to the data of each run except those of Run 43 which lie too close to the curve for Run 38. These $H_{cr}(T)$ curves have a slight positive curvature near T_c, and this is carefully studied in Run 43. (A similar but less pronounced effect is seen in the α-β curves.) The h_o dependence or other systematic errors may account for this behavior, but it is likely that $H_{c3}(T)$ has a positive curvature near T_c as has been reported for Nb (103). The maximum absolute value of the slope occurs in a linear region of these curves from about 2 or 3 kG to 10 or 12 kG. This slope decreases linearly with increasing pressure as shown in Figure 37. The point shown for Run 41 is indirectly calculated on the basis of the similarity of this $H_{cr}(T)$ curve to that of Run 40. All other data points

for REJ-1a, regardless of history, are in good agreement with the fitted line for which the pressure dependence is given by

$$\frac{d}{dP}\left[-\frac{dH_{cr}}{dT}\right] = -0.10 \text{ kG/kbar - K} .$$

Samples from the second ingot, REJ-11, also were studied as a function of pressure, but these samples did not readily transform from the α-β to the dhcp phase nor back to the low pressure phase. This unwillingness to transform from one phase to another is illustrated by the series of zero field $\chi'(T)$ curves shown in Figure 38 and by the associated critical field curves shown in Figure 39. The pressure in Run 30 is 12.68 kbar which would have transformed a REJ-1a sample into the dhcp phase, but here the χ' transition appears to be that of a well-aged α-β specimen with a small secondary transition near 8.0 K. The associated critical field curve exhibits an initial slope not unlike that of an α-β sample, but the magnitude of the slope increases with increasing H until at high fields the curve appears to be that of a dhcp sample. We interpret these data to mean the sample is composed of regions of both high and low pressure phases. The manifestation of two transition temperatures indicates that the size of the regions must be larger than the coherence distance. The next run which is at a pressure of 14.00 kbar has a broad zero field $\chi'(T)$ transition from 7.9 to 8.4 K but with some evidence of two transitions. The critical field curve still has a positive curvature near T_c and a high field dhcp-like behavior. The zero field transition indicates the characteristic size of the microstructure regions is of the same order of magnitude as the coherence distance. The sample finally is transformed into the dhcp phase in the next run at 17.22 kbar. The pressure is only

partially relieved in Run 33 (P = 7.40 kbar), and both low and high pressure phases are evident. The pressure finally is relieved from the sample, and then Run 34 made at P = 2.19 kbar which shows only the behavior of an α-β specimen.

The above series of investigations employed isoamyl alcohol and pentane in a Teflon capsule as pressure transmitting media. All of our previous studies of Pb-Bi alloys under pressure had used powdered Teflon media. Runs 35 and 36 were made on REJ-II(4) using powdered Teflon media to investigate the possibility that this presumedly less nearly hydrostatic medium promoted the phase transformation, but the results basically are the same as those of Runs 30-34. The nature of this unwillingness to transform is not known.

This concludes the experimental findings of the present work in which we find dhcp Pb-Bi to be superconducting with T_c near 8.0 K. The pressure dependence of certain superconducting properties for both the dhcp and α-β phases were successfully measured, but metallurgical problems thwarted other of these investigations.

CHAPTER IV. DISCUSSION

The various experimentally observed superconducting properties of Pb-Bi alloys under pressure have been described in the previous chapter. In the present chapter, we discuss the critical field curves and associated superconducting parameters as well as their pressure dependence. The various results are compared with the theoretical and experimental results reported by other workers.

The depression of the transition temperature with pressure for these Pb-Bi alloys is given approximately by $dT_c/dP = -1.3 \times 10^{-2}$ K/kbar which is a factor of three smaller than the pressure effect reported for Pb, $dT_c/dP = -4.5 \times 10^{-2}$ K/kbar (60). The pressure effect in Pb-Bi also is smaller than that of any elemental non-transition metal other than Tl and Bi III, but it is within the range of values reported for various non-transition metal alloys.

This depression of T_c also can be discussed in terms of the volume change since the relation between volume and pressure from 0 to 20 kbars is reported by Gordon and Deaton (1) for similar Pb-Bi alloys. Using their results, we find the volume dependence of T_c to be given by

$$V_o \frac{dT_c}{dV} = 3.2 \pm 0.4 \text{ K}$$

for either phase. They also report a 2.5 % reduction in the volume during the transformation from the α-β to the dhcp phase. This volume change alone would account for an 0.080 K decrease in T_c, but we observe a larger decrease of about 0.365 K associated with the phase transition. Therefore, the differences between the superconducting properties of the

two phases, while small, must result principally from other than a simple volume effect.

One of the most important measures of the pressure effect for comparison purposes is the logarithmic derivative of T_c with respect to volume. This derivative is calculated separately for each phase, but it is satisfactorily given for either phase by

$$\frac{d \ln T_c}{d \ln V} = 0.39 \pm 0.05 \quad .$$

This is a considerably smaller value than those reported for Pb and many of the other elemental non-transition metal superconductors. Following Smith and Chu (58), we plot $T_c(V)/T_c(V_o)$ against $-\Delta V/V_o$ for both these Pb-Bi phases and other superconductors in Figure 40.* It is interesting to note that if these results are extrapolated to higher pressures, then Pb-Bi is the only material for which T_c is not completely suppressed as the volume is reduced to zero. Hence, none of the reports discussed in the first chapter predict a critical pressure for Pb-Bi without an additional phase transition.

The α-β phase critical field curve data from Run 15 is compared to three different theoretical models in Figure 41, and a similar comparison is made for the dhcp data from Run 38 in Figure 42 where H_{cr} for either case is assumed to be proportional to H_{c2} at a given temperature. For comparison purposes, critical field curves often are expressed in a reduced form with $t = T/T_c$ and $h_{c2}(t) = H_{c2}/H_{c2}(0)$. We deviate somewhat

---

*The results for Th are from previous work of the author to 10 kbar.

from this practice and present the theoretical and experimental results in terms of a reduced temperature, t, and a reduced critical field curve, $h_{c2}^*(t)$, defined by normalizing the slope near T_c so that $dh_{c2}^*/dt = -2$. Critical field curves for the Gor'kov "clean limit" and the Maki "dirty limit" models discussed in the first chapter are constructed by multiplying the appropriate temperature-dependent Ginzburg-Landau parameter by a parabolic $H_c(t)$ curve and then normalizing the slope at T_c. The choice of a -2 slope for standardization is not entirely capricious since $\varkappa h_c(0) = 1$ for the Gor'kov model; however, $\varkappa h_c(0)$ lies about 4 % higher for the Maki model. A third shape for the critical field is predicted by the Abrikosov and Gor'kov pair breaking (AG) theory (104, 105) where H is the only pair breaking mechanism for the present case so the basic equation reduces to

$$\ln \frac{T}{T_c} = \psi\left[\frac{1}{2} + 0.14 \frac{T_c}{T} \frac{H_{c2}(T)}{H_{c2}(0)}\right] - \psi\left(\tfrac{1}{2}\right) = 0$$

where ψ is the digamma function. The transition temperature and the absolute maximum value of the slope of the H_{cr} curve are used to normalize the experimental data. The agreement of the experimental data with the theoretical curves is sensitive to small variations of dH_{cr}/dT, but the AG theory apparently provides the best description of the observed critical field curve of either phase.

Characteristic critical field parameters for the present experimental results include T_c, $H_{cr}(4.2\ K)$, and $(-dH_{cr}/dT)_{max}$. The slope and the 4.2 K values of the H_{c2} and H_{c3} curves are estimated from these results by assuming that H_{c3} is 15 % higher than H_{cr} and also that $H_{c3} = 1.7\ H_{c2}$. The zero temperature values of H_{c2} and H_{c3} are calculated from the

relation

$$H_{c2}(0) = \frac{T_c}{1.40} (-dH_{c2}/dT)_{T_c}$$

which is a result of AG theory. The results of these calculations for the data of Runs 15 and 38 are shown in Table III along with additional results obtained from the data of Run 34 for comparison purposes.

Table III. Characteristic critical field parameters

PARAMETER	Run 15 α-β 1.75 kbar	Run 34 α-β 2.19 kbar	Run 38 dhcp 14.57 kbar
Experimental Results:			
T_c	8.400 K	8.635 K	8.020 K
$(-dH_{cr}/dT)_{max}$	3.95 kG/K	4.28 kG/K	5.716 kG/K
$H_{cr}(4.2\ K)$	15.90 kG	17.80 kG	20.35 kG
Derived Results:			
$H_{c3}(4.2\ K)$	18.29 kG	20.47 kG	23.40 kG
$H_{c3}(0)$	27.28 kG	30.36 kG	37.66 kG
$H_{c2}(4.2\ K)$	10.76 kG	12.04 kG	13.77 kG
$H_{c2}(0)$	16.04 kG	17.86 kG	22.15 kG

The superconducting properties of an α-β alloy are determined by the β phase which has a limiting stable Bi concentration of 33.4 % at room temperature. We assume the β phase of our α-β samples is near this concentration, therefore, the present results for $H_{c2}(4.2\ K)$ can be compared with those of CEDW (54) who report $H_{c2}(4.2\ K) = 13.4$ kG for a β phase Pb- 33.4 % Bi alloy. The discrepancies between the values of $H_{c2}(4.2\ K)$ probably result from metallurgical problems and the difficulty of accu-

rately determining H_{c3} from H_{cr}.

There is no direct measure of either κ or H_c in the present experiment, but we approximate $H_c(4.2\ K)$ for the α-β phase by using the CEDW value of $H_c(4.2\ K) = 738$ G for their 33.4 % Bi alloy. This approximation and the present result for $H_{c2}(4.2\ K)$ are used with the Maki model to predict $\kappa = 9.54$ and $H_{c1}(4.2\ K) = 109$ G for the α-β specimen of Run 15. An accurate calculation of κ is not possible for the dhcp phase since there are no reported values of H_c. Estimates of $H_c(4.2\ K) = 840$ G, $H_c(0) = 1160$ G, and $\kappa = 10.8$ for the dhcp specimen of Run 38 are obtained from a presumed parabolic H_c curve, the hypothesis that $H_c(0)/T_c$ is the same for the α-β and dhcp phases, and the CEDW results of $H_c(4.22\ K) = 909$ G and $T_c = 8.4$ K for a β phase Pb-40 % Bi alloy. However, this hypothesis is known to be only a rough approximation for the Pb-Bi alloy system since the CEDW critical field data indicates that $H_c(0)/T_c$ varies by 30 % as the Bi concentration increases from 0 to 40 %.

The measured effects of pressure on the critical field curve of dhcp Pb-Bi can be expressed in terms of calculated parameters for comparison with results for other superconductors. The AG relationship between the zero field H_{c2} and the slope of the critical field curve is differentiated with respect to P to obtain the equation

$$\frac{dH_{c2}(0)}{dP} = \frac{T_c}{1.40} \frac{d}{dP}\left[-\frac{dH_{c2}}{dT}\right] + \frac{H_{c2}(0)}{T_c}\frac{dT_c}{dP}$$

which we evaluate for the specimen of Run 38. The pressure derivative of the slope of the H_{c2} curve is determined easily from the experimentally determined $\frac{d}{dP}(-dH_{cr}/dT) = -0.10$ kG/kbar-K, and the other terms on the

right hand side of the equation have been measured or calculated. The first term on the right hand side is an order of magnitude larger than the second but the sum gives the result

$$\frac{dH_{c2}(0)}{dP} = -0.42 \text{ kG/kbar} \quad .$$

Other studies report the effects of pressure on H_c or on κ for various superconductors but H_{c2} is dependent on both of these parameters and there is no basis for separating their pressure dependence. If we assume $\kappa_1(0)$ to be a constant, then the decrease of $H_{c2}(0)$ is due to the decrease in $H_c(0)$, and we obtain

$$\frac{dH_c(0)}{dP} = -0.022 \text{ kG/kbar}$$

which is considerably higher than the value of -0.0079 kG/kbar reported for Pb (60). However, if we assume $H_c(0)$ to be a constant, then the decrease of $H_{c2}(0)$ is related to the decrease in $\kappa_1(0)$, and we find $d\kappa/dP = -0.21$ kbar^{-1} or $(1/\kappa)d\kappa/dP = -0.020$ kbar^{-1} where $\kappa_1(0) = 1.2\kappa$ from the Maki model. These results indicate a significantly greater pressure effect on κ than the $d\kappa/dP = -0.0046$ kbar^{-1} or $(1/\kappa)d\kappa/dP = 0.0056$ kbar^{-1} reported by Fischer and Olsen (59) for an In- 14 % Tl alloy.

In conclusion, the high pressure dhcp phase of $Pb_{0.4}$-$Bi_{0.6}$ alloys has been found to be superconducting with a slightly smaller T_c and a somewhat steeper critical field curve than those associated with the low pressure α-β phase. The shapes of the critical field curves of both phases are in fairly good agreement with that predicted by AG theory. The depression of T_c with pressure is nearly the same for both phases, but the magnitude of this effect is smaller than usually reported for non-

transition elements and their alloys. An interesting result is that no critical pressure for destruction of superconductivity is predicted for either phase. The depression of H_{c2} with pressure for the dhcp phase is noticeably larger than would have been expected from the results of pressure work on other superconductors. The Pb-Bi alloys have exceptionally high Ginzburg-Landau parameters for a non-transition metal superconductor, and hence, it is not distressing to observe some differences between their behaviors and those of other members of the group. The slight differences between the superconducting properties of the α-β and dhcp phases tend to indicate that the unusual properties of La are not related principally to the dhcp structure.

FIGURES

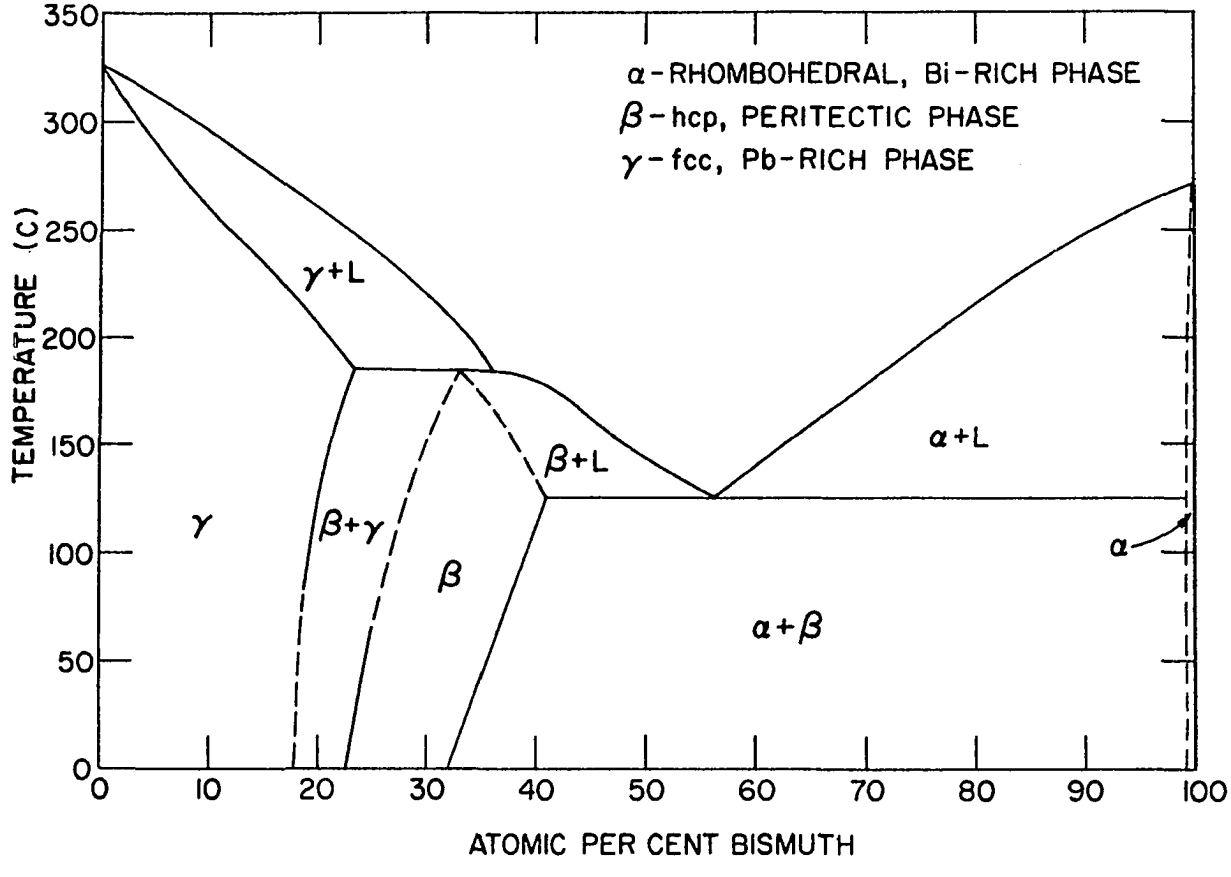

Figure 1. Phase diagram of Pb-Bi alloy system at atmospheric pressure

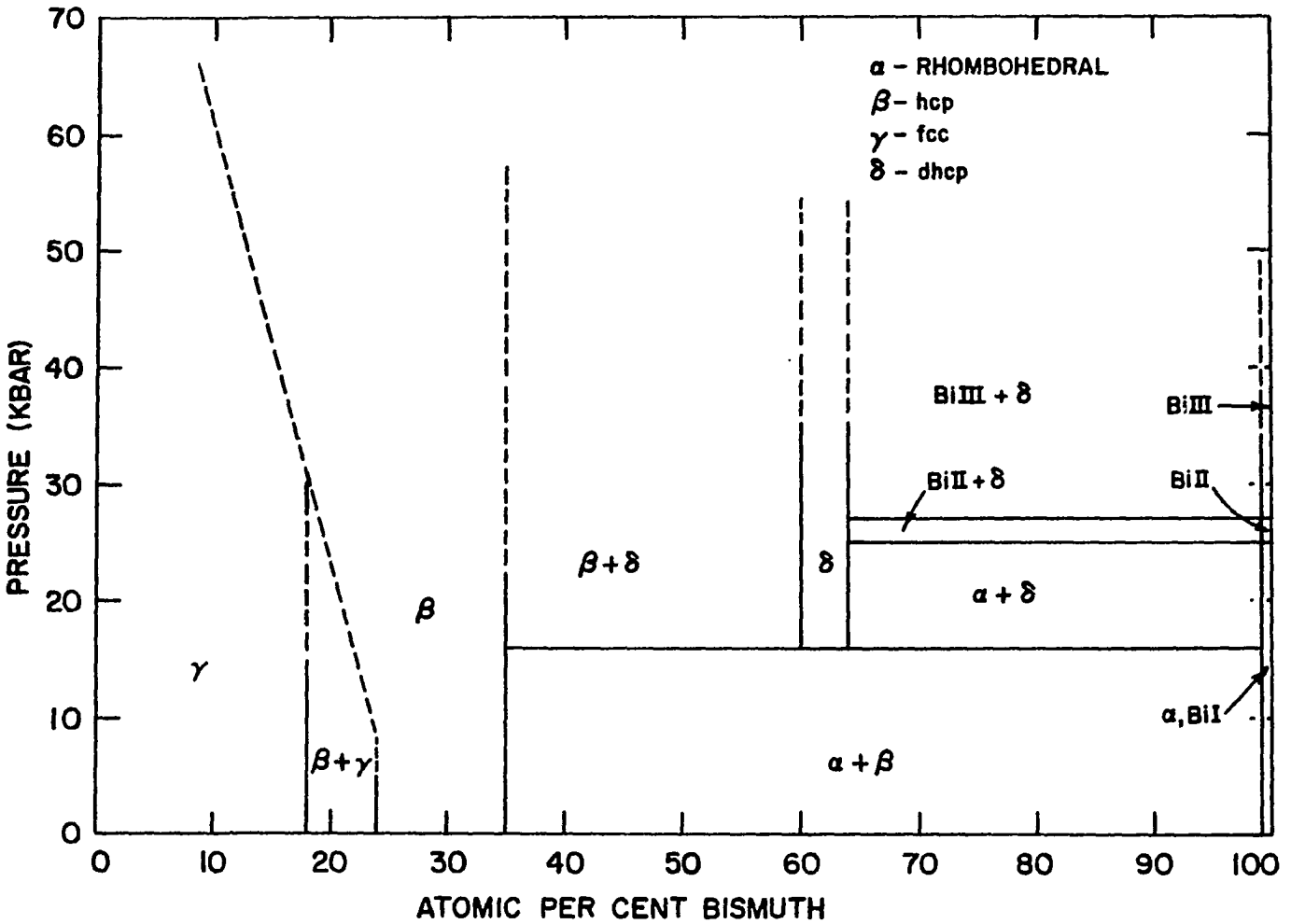

Figure 2. Pressure-dependent phase diagram of Pb-Bi alloy system at room temperature. Pressure calibration from reference (6)

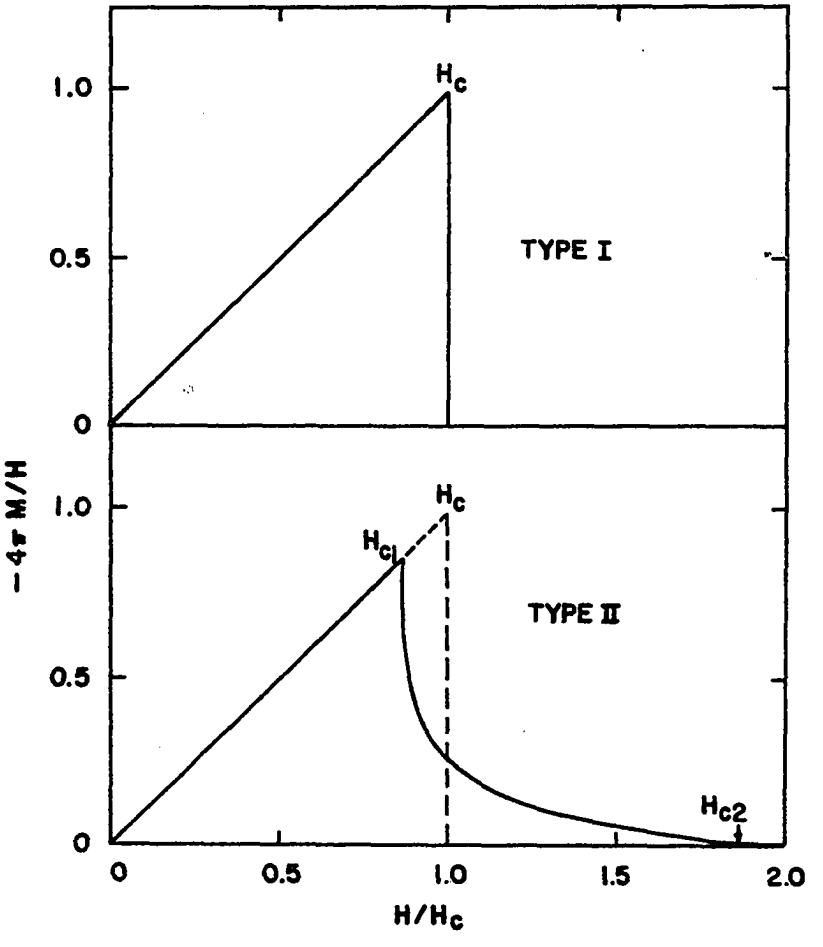

Figure 3. Magnetization curves for ideal type I and type II superconductors. The area under the type II magnetization curve (solid line) is equal to that of the triangle (dashed line) which defines the thermodynamic critical field, H_c

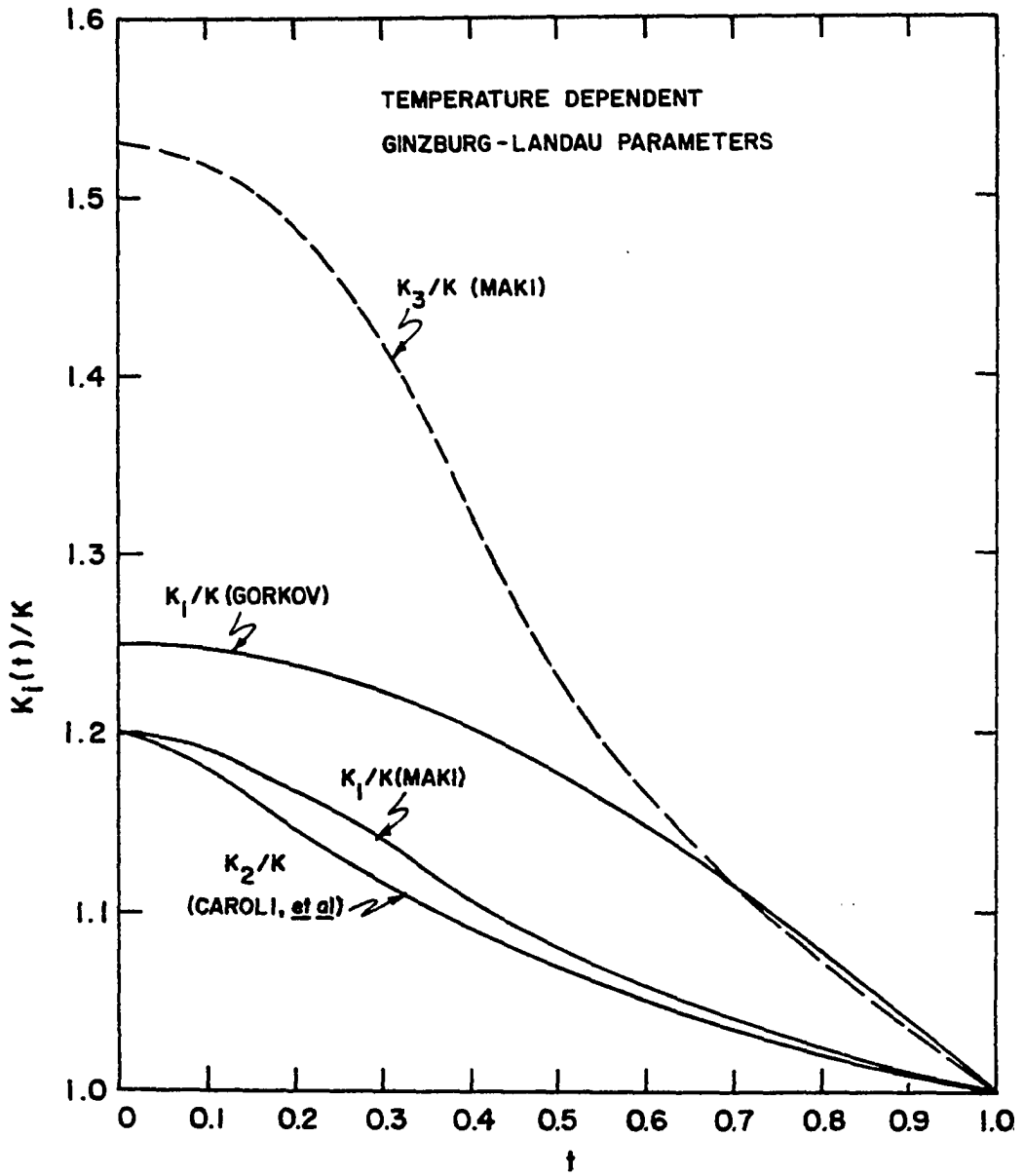

Figure 4. Temperature-dependent Ginzburg-Landau parameters

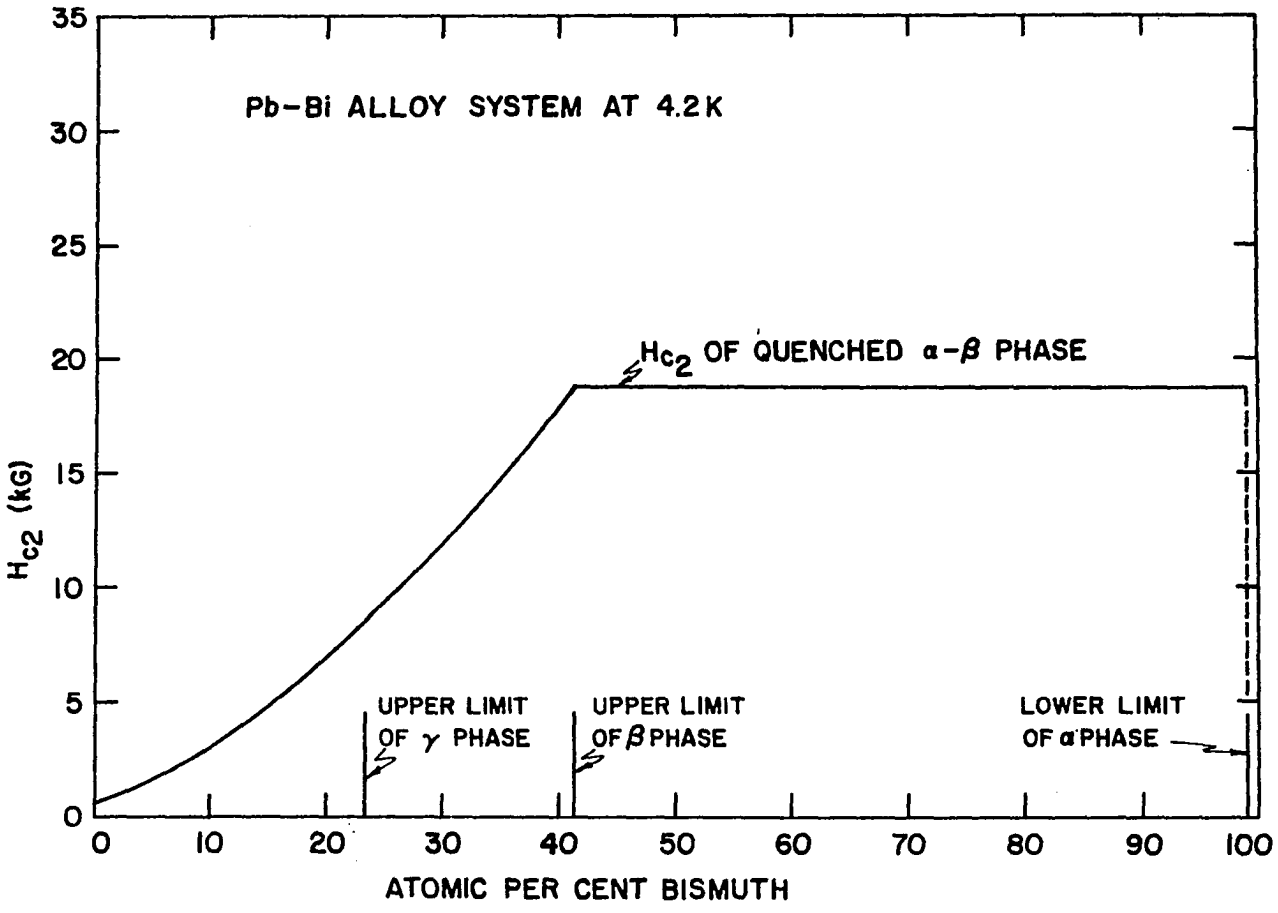

Figure 5. H_{c2} for the Pb-Bi alloy system at 4.2 K and atmospheric pressure

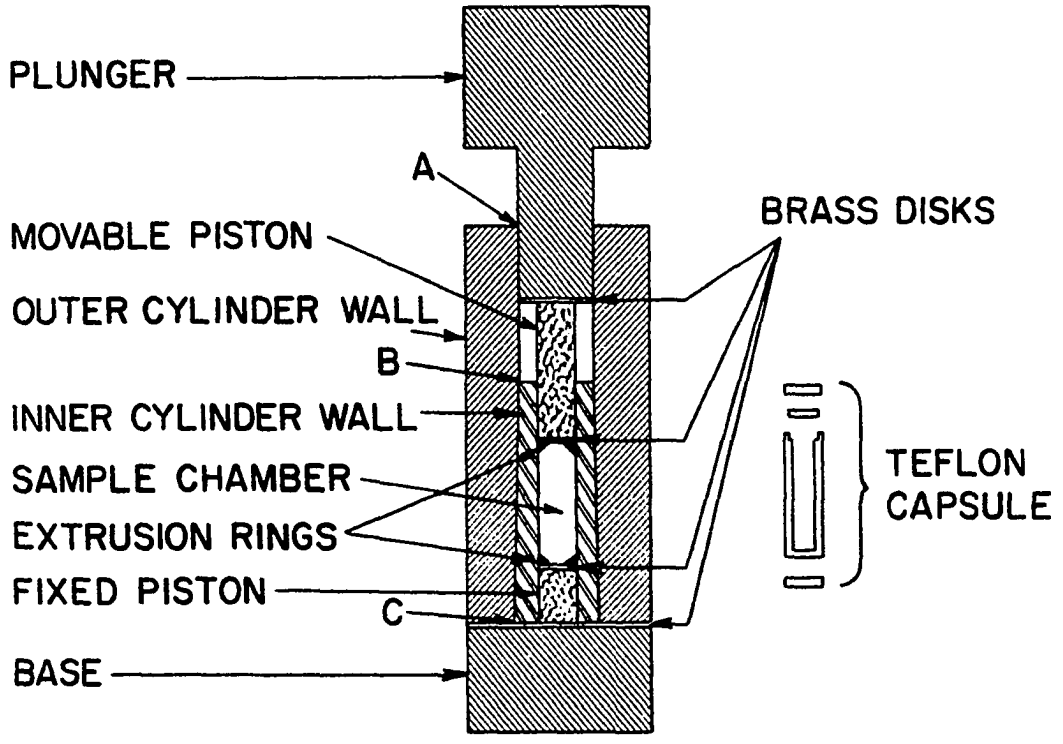

Figure 6. Double-walled high pressure cell with cemented WC pistons. Teflon capsule shown on right (scale drawing)

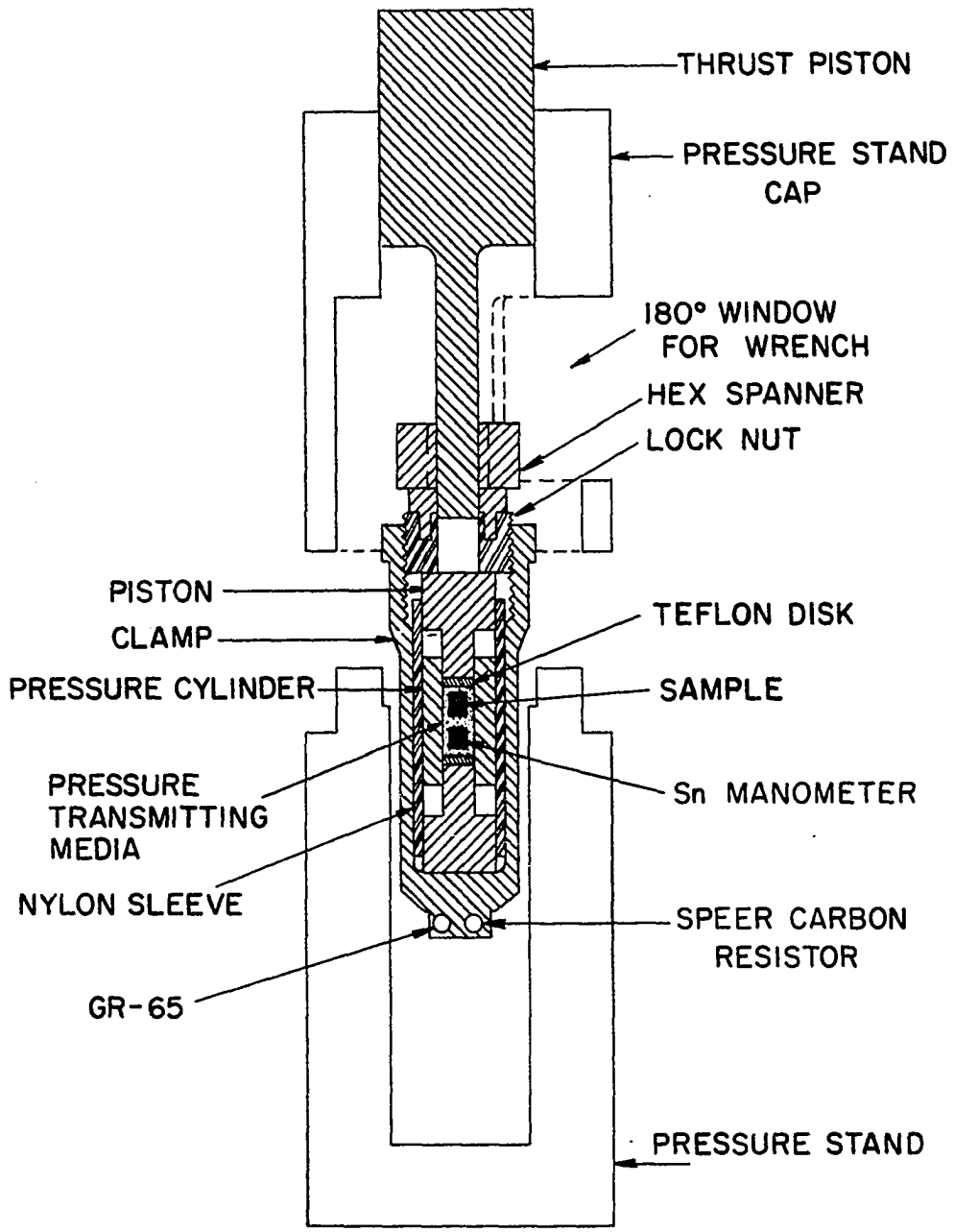

Figure 7. Clamp with associated pressurization apparatus. The clamp is loaded with a single-walled pressure cell (scale drawing)

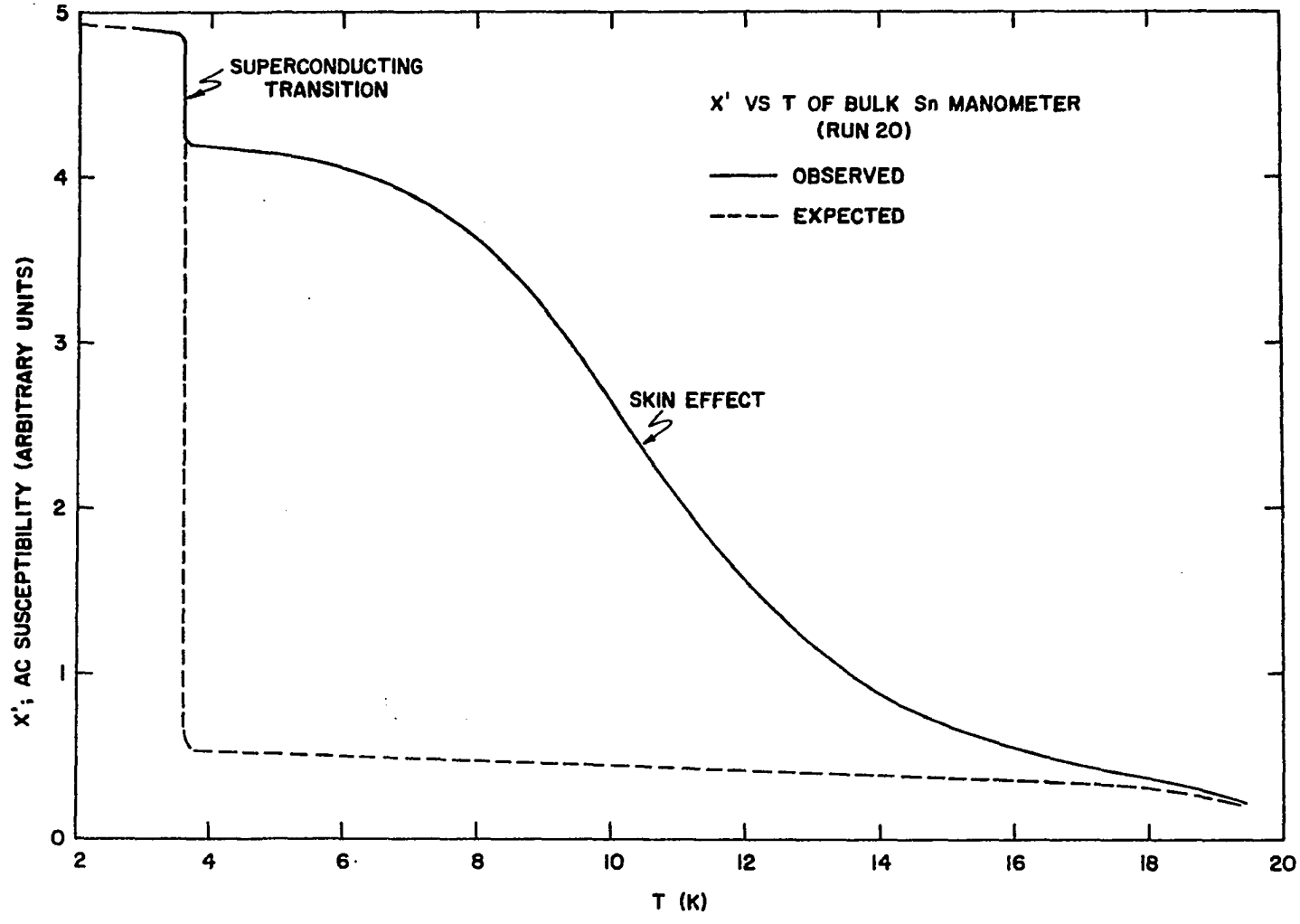

Figure 8. Anomalous transition due to skin effect in Sn. A small amount of temperature-dependent background is expected from the bomb

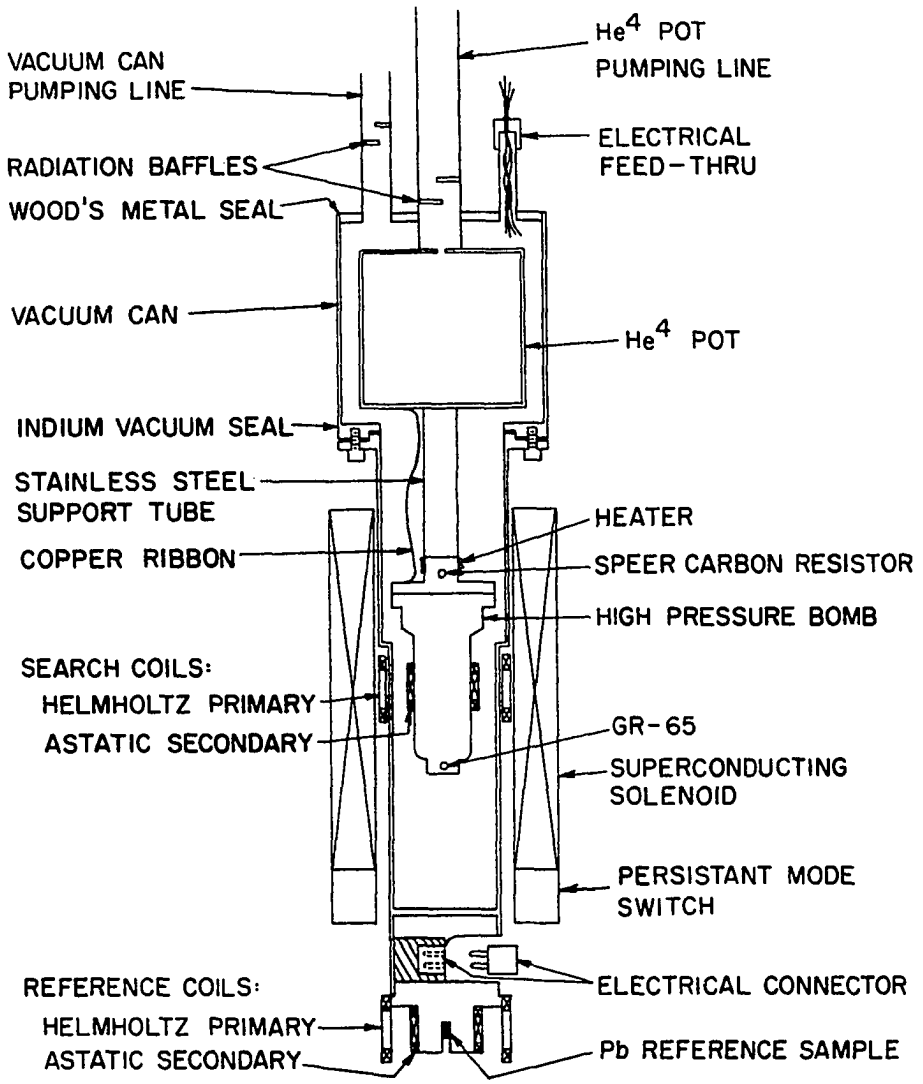

Figure 9. Lower section of He^4 cryostat (not to scale)

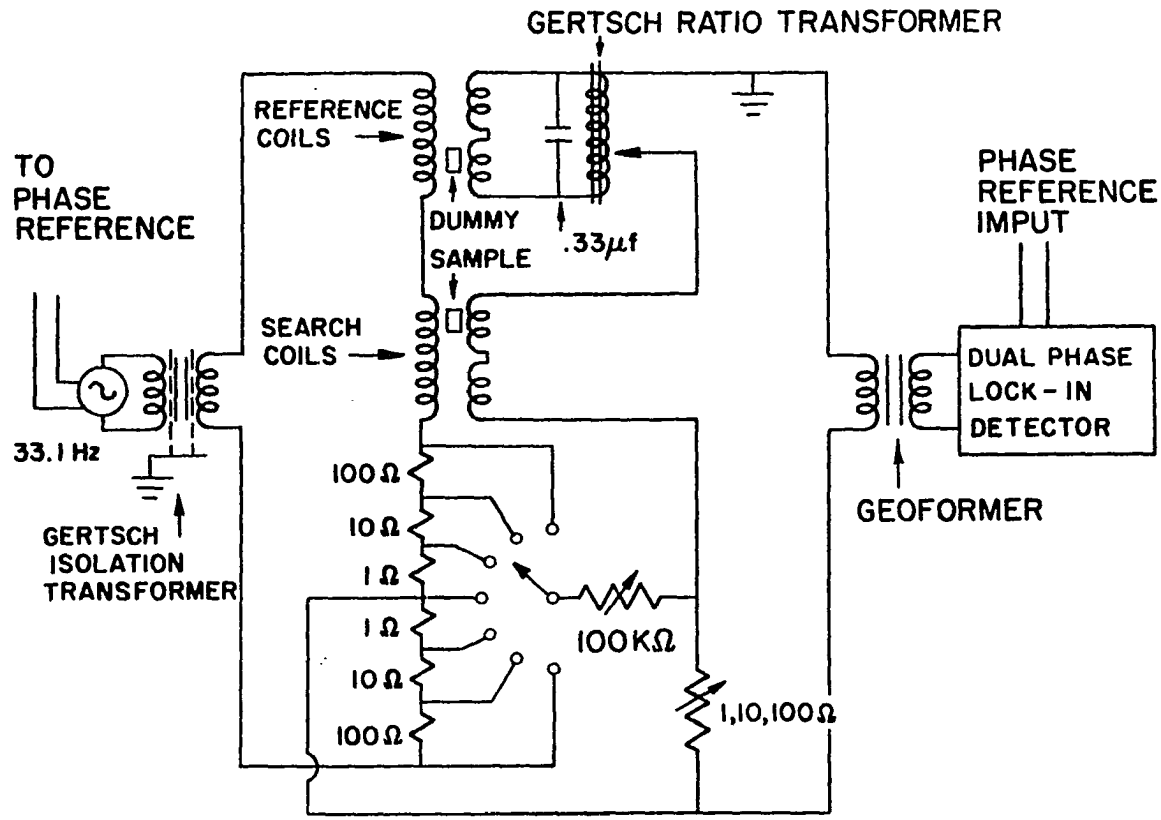

Figure 10. 33.1 Hz mutual inductance bridge

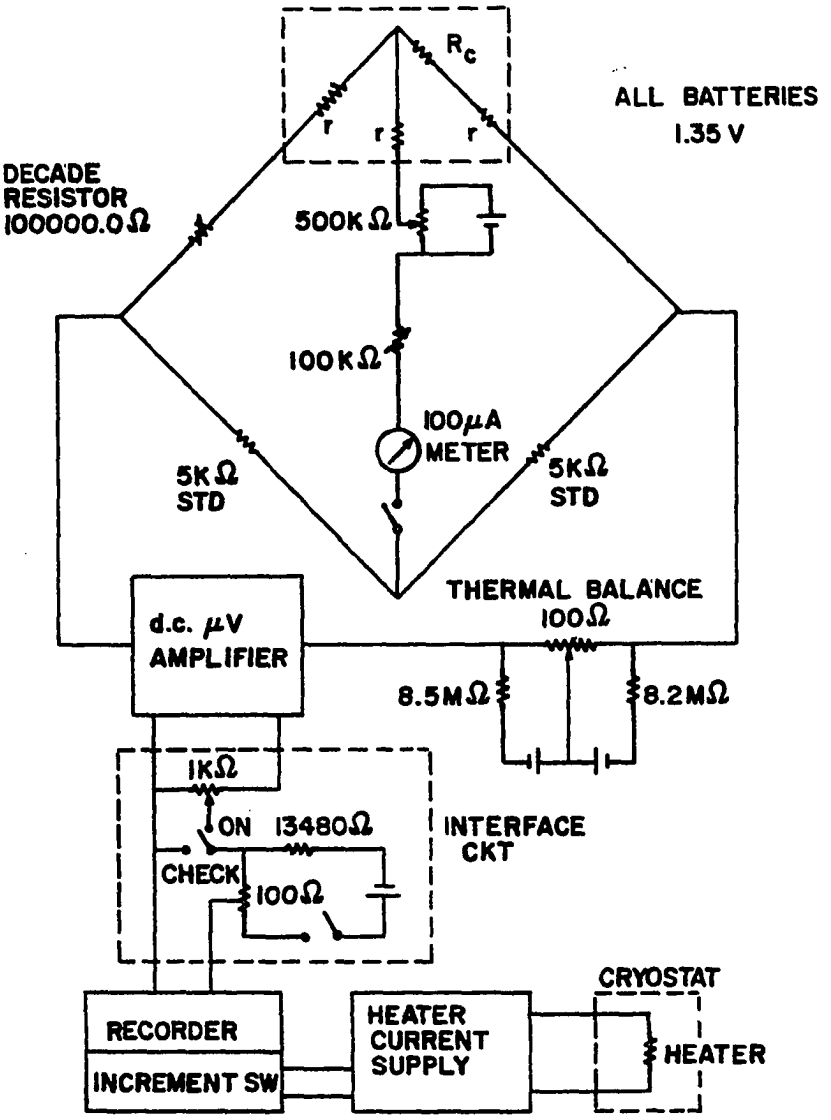

Figure 11. Wheatstone bridge and temperature control circuit

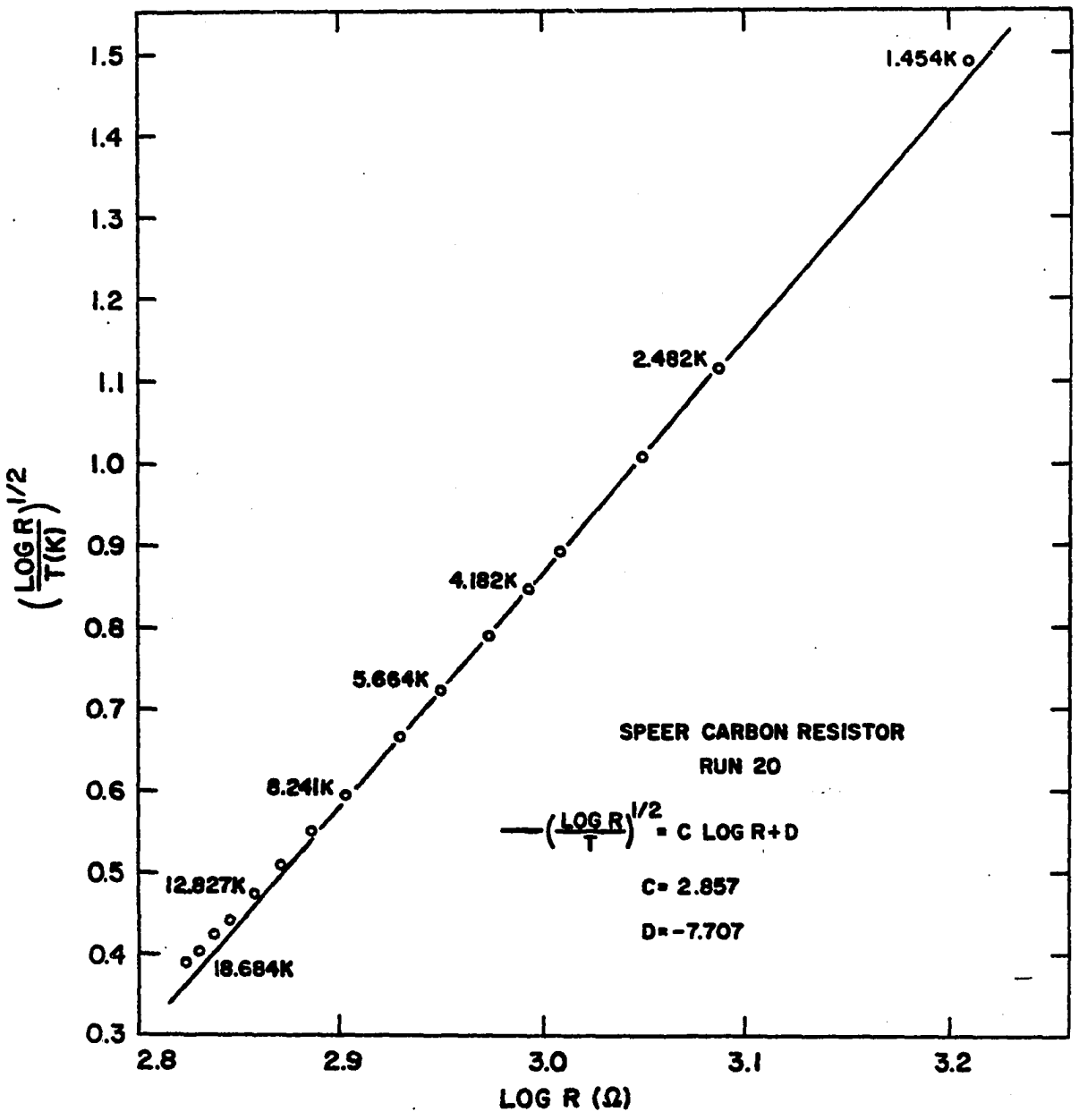

Figure 12. Temperature dependence of Speer carbon resistor

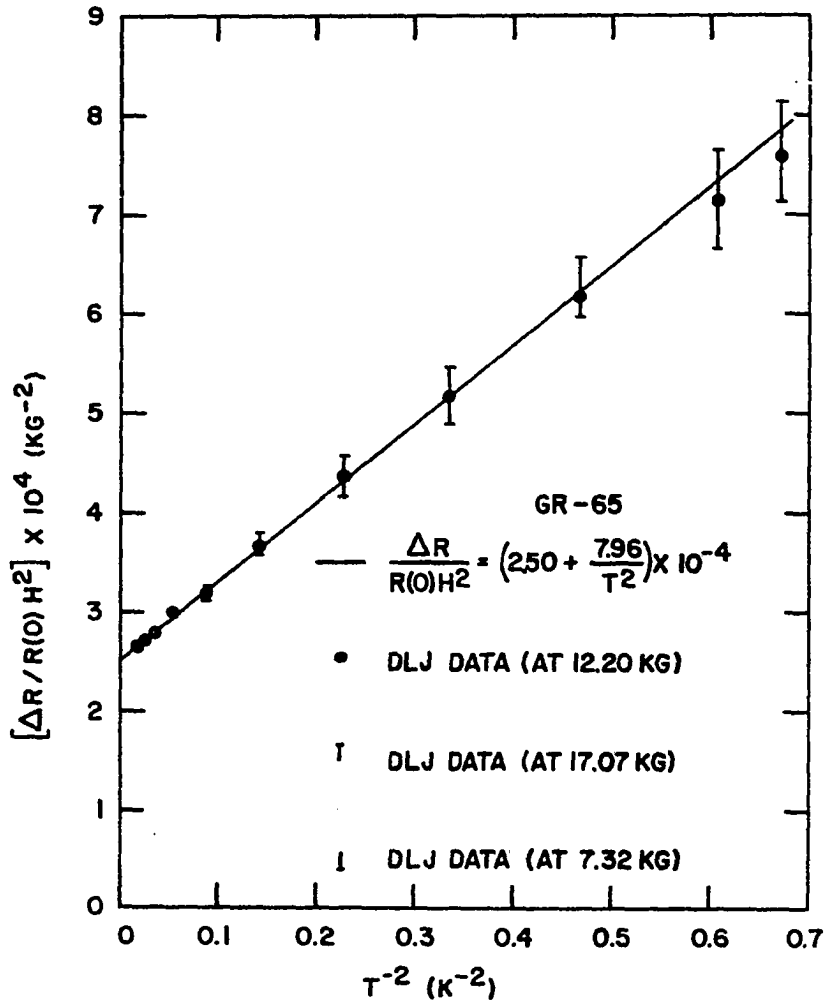

Figure 13. Temperature dependence of GR-65 magnetoresistance effect. The error bars are indicative of non-parabolic field dependence at low temperatures

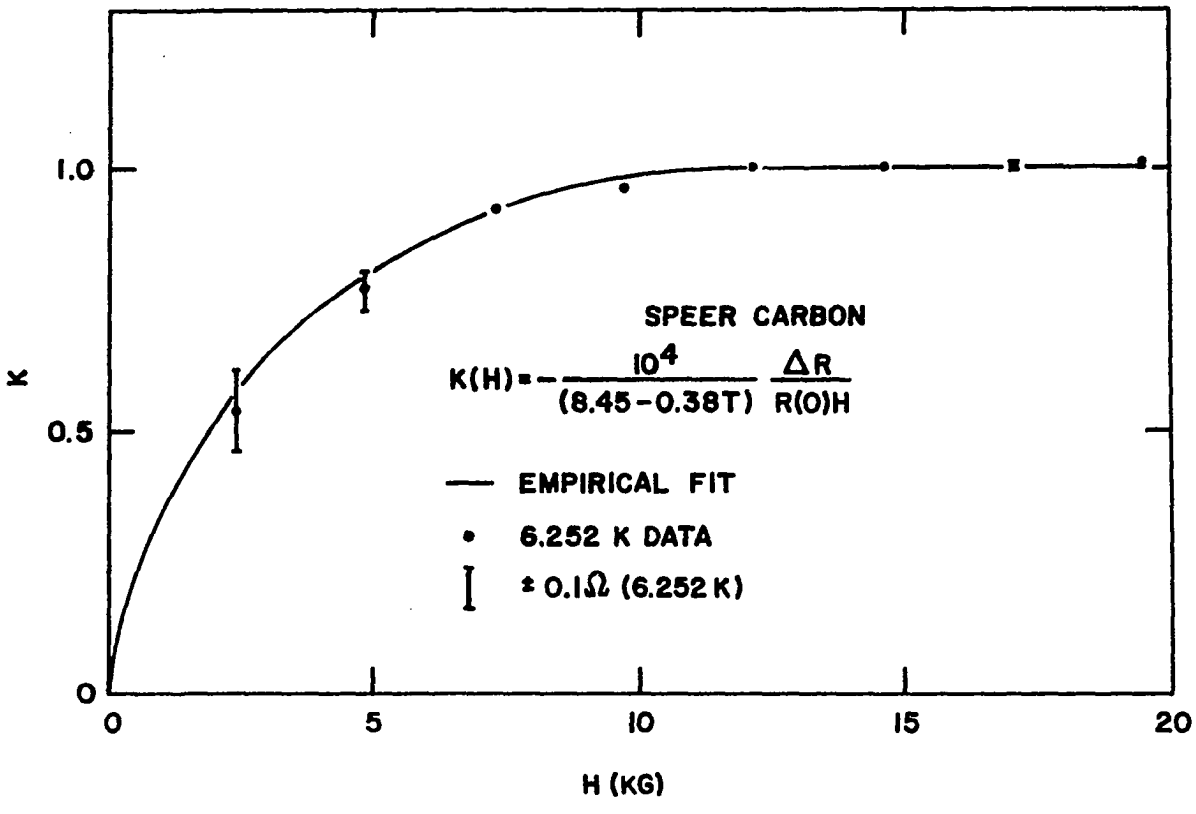

Figure 14. $\kappa(H)$, deviation from linear field dependence of Speer carbon magnetoresistance effect

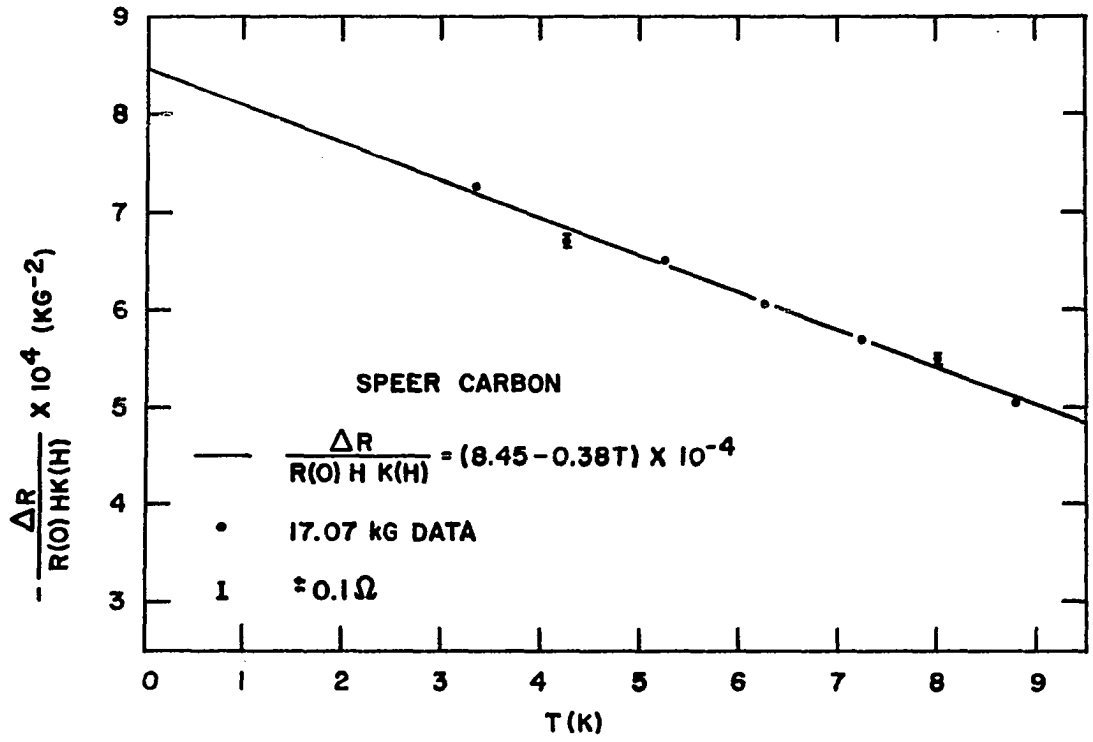

Figure 15. Temperature dependence of Speer carbon magnetoresistance effect

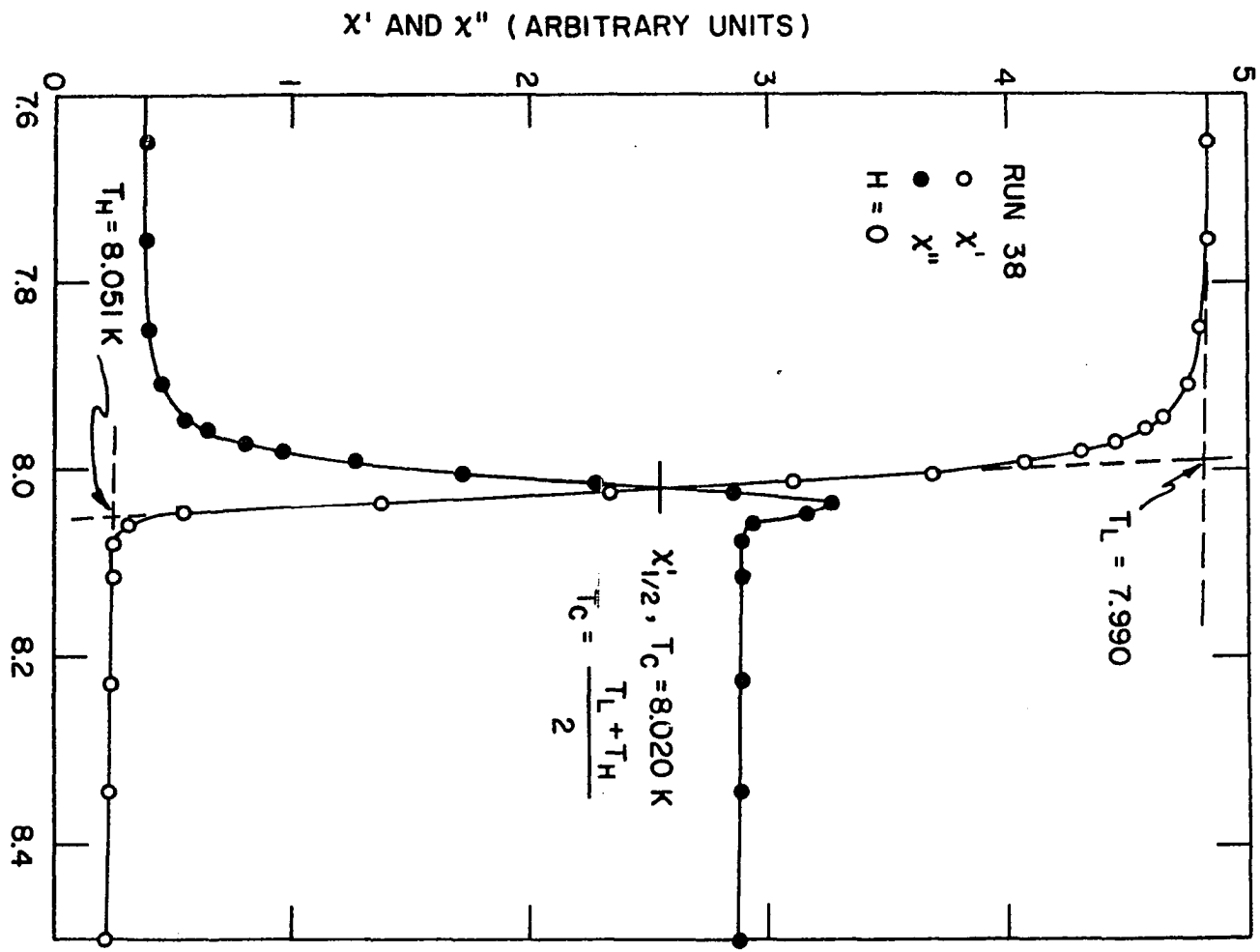

Figure 16. Zero field ac susceptibility transition with h_o = 0.9 G

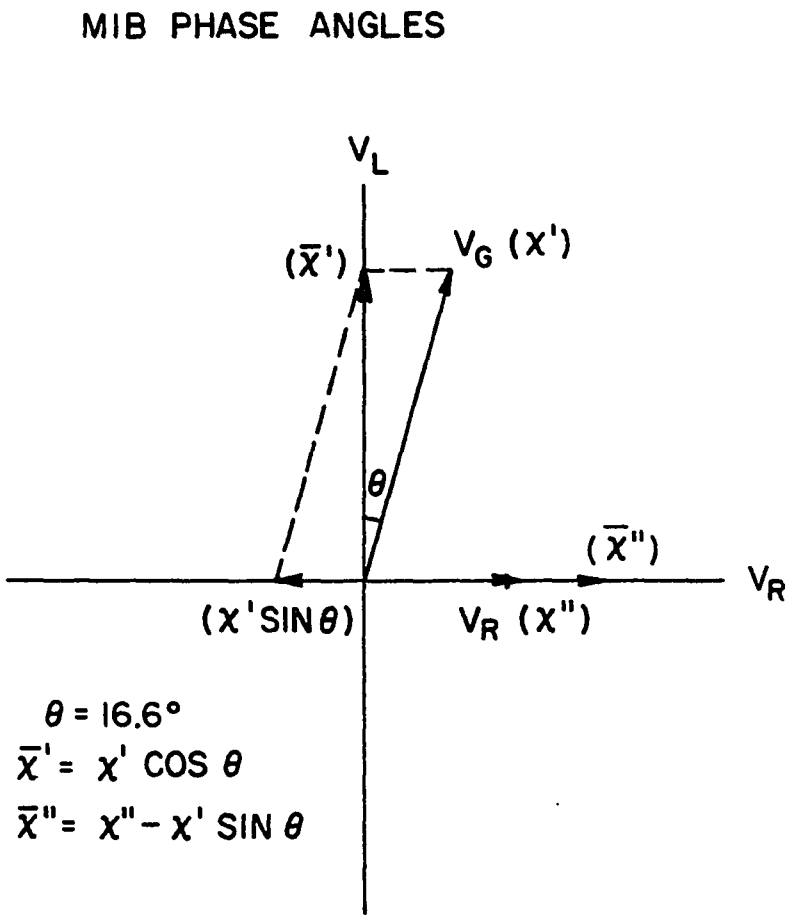

Figure 17. Voltage phase diagram of the mutual inductance bridge. Various ac susceptibility components, shown in parentheses, are proportional to the associated voltages

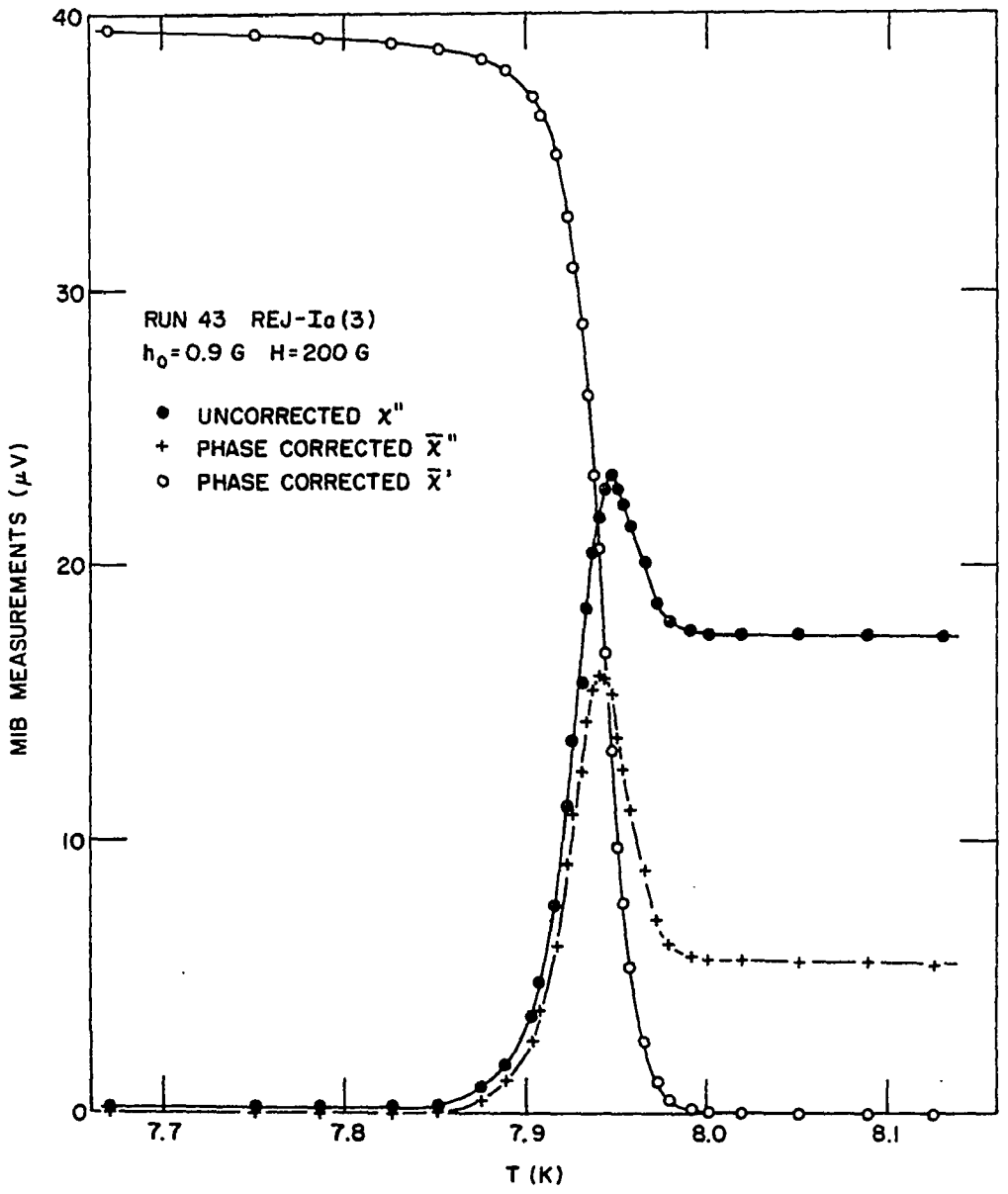

Figure 18. Effects of the mutual inductance bridge phase angle problem on ac susceptibility

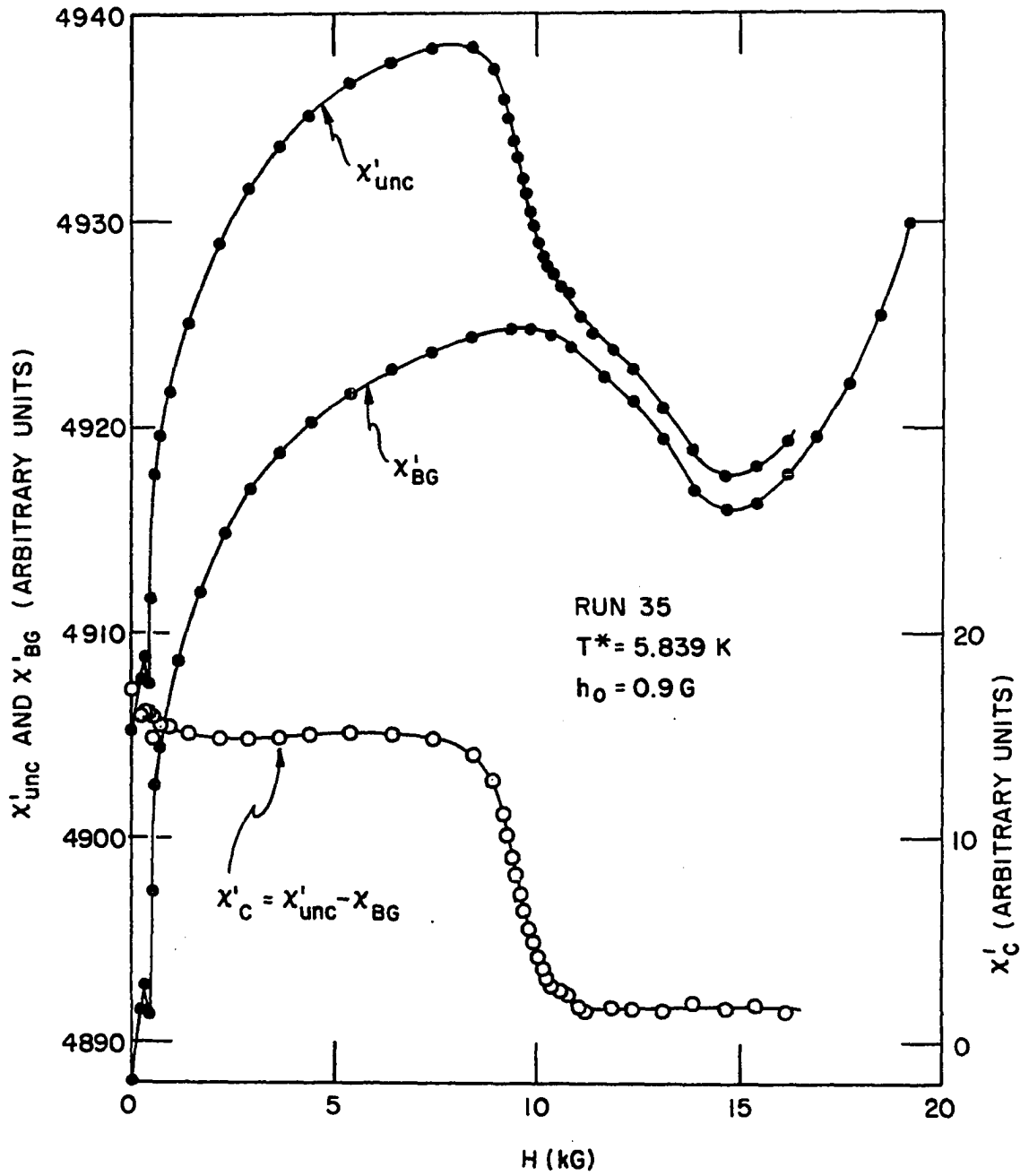

Figure 19. Subtraction of the background from the real part (χ') of the ac susceptibility transition associated with a field sweep. The numerical values are indicative of the actual relative magnitudes

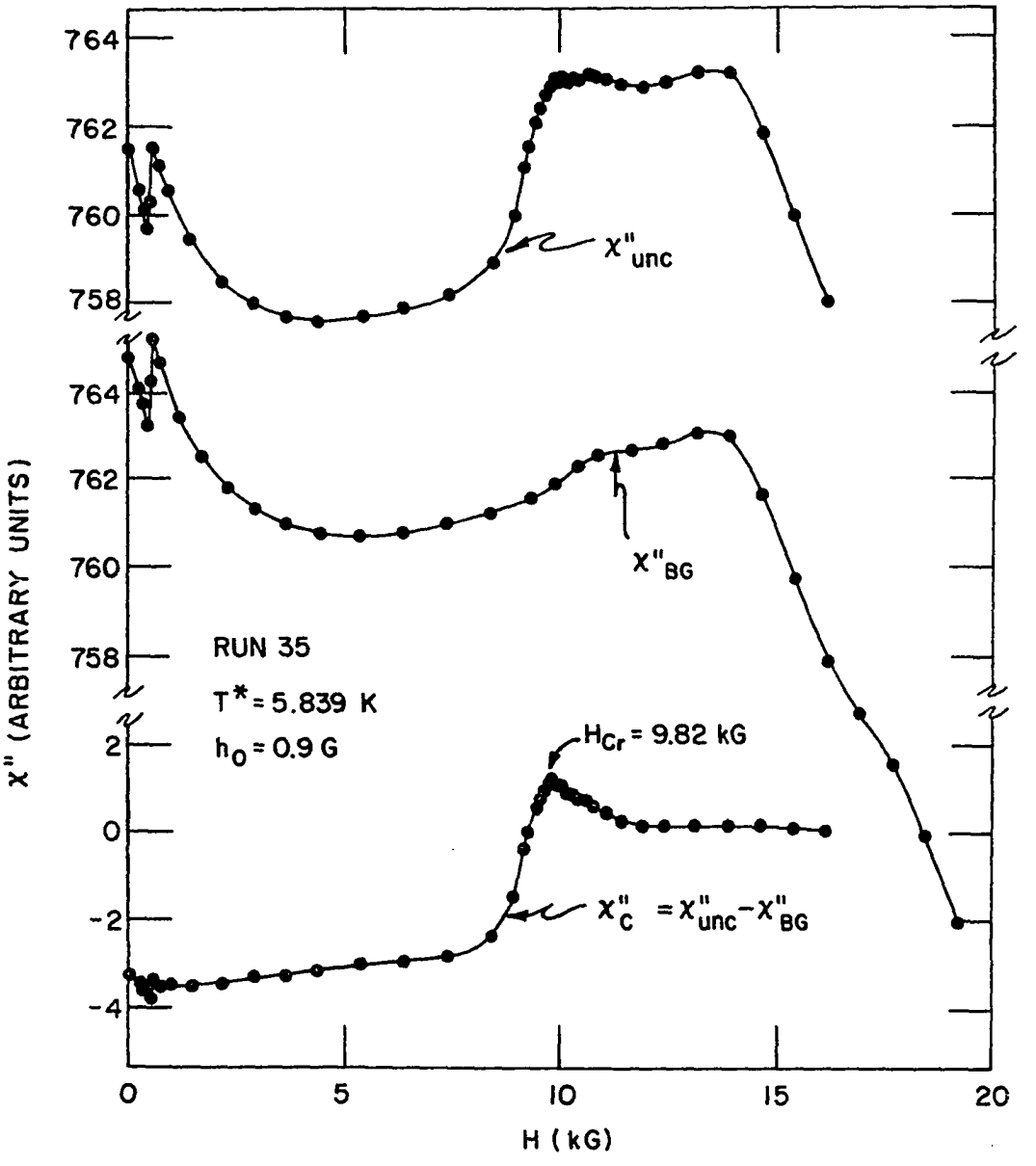

Figure 20. Subtraction of the background from the imaginary part (χ'') of the ac susceptibility transition associated with a field sweep. The numerical values are indicative of the actual relative magnitudes

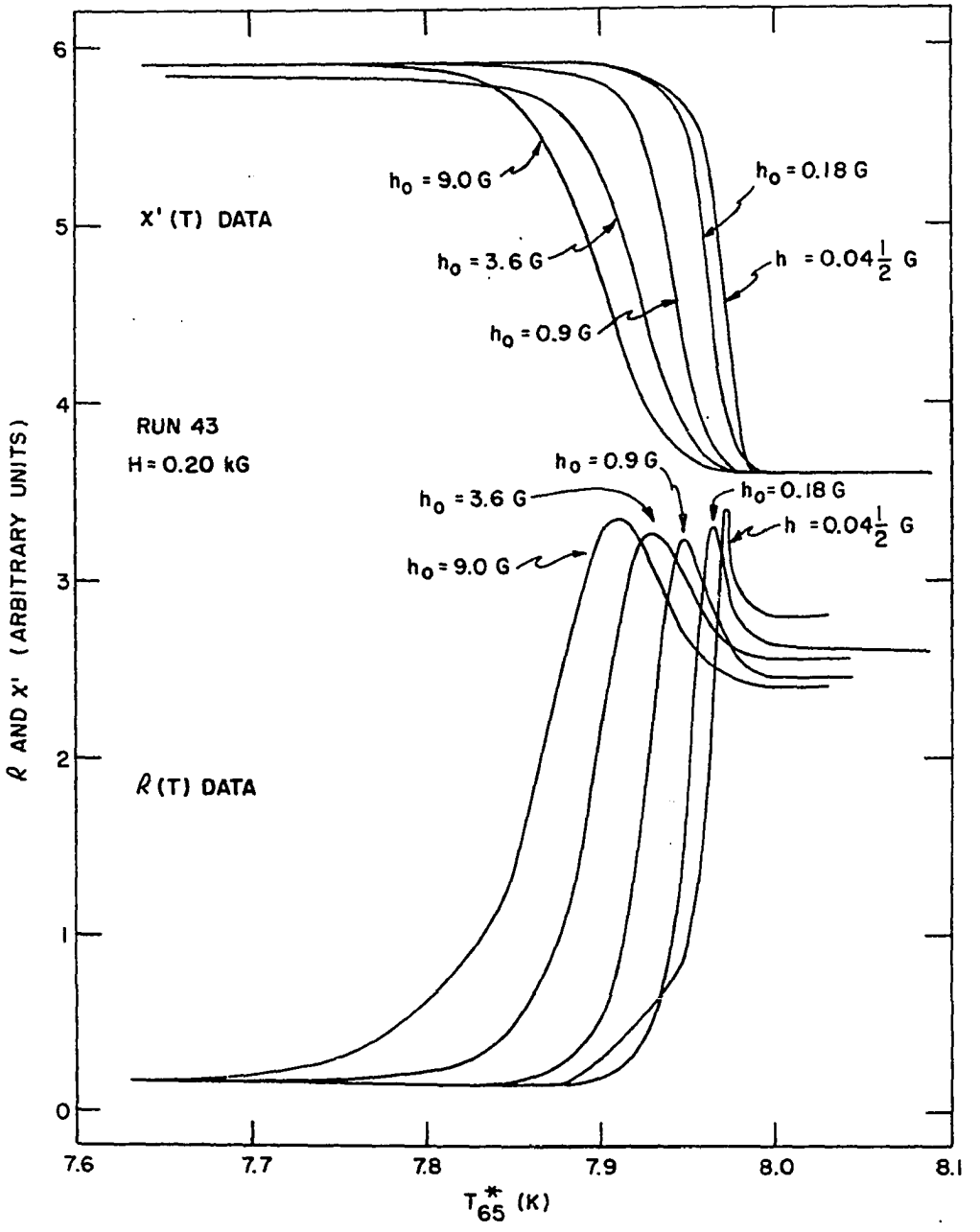

Figure 21. Measuring field dependence of the ac susceptibility transition for a temperature sweep at H = 0.20 kG

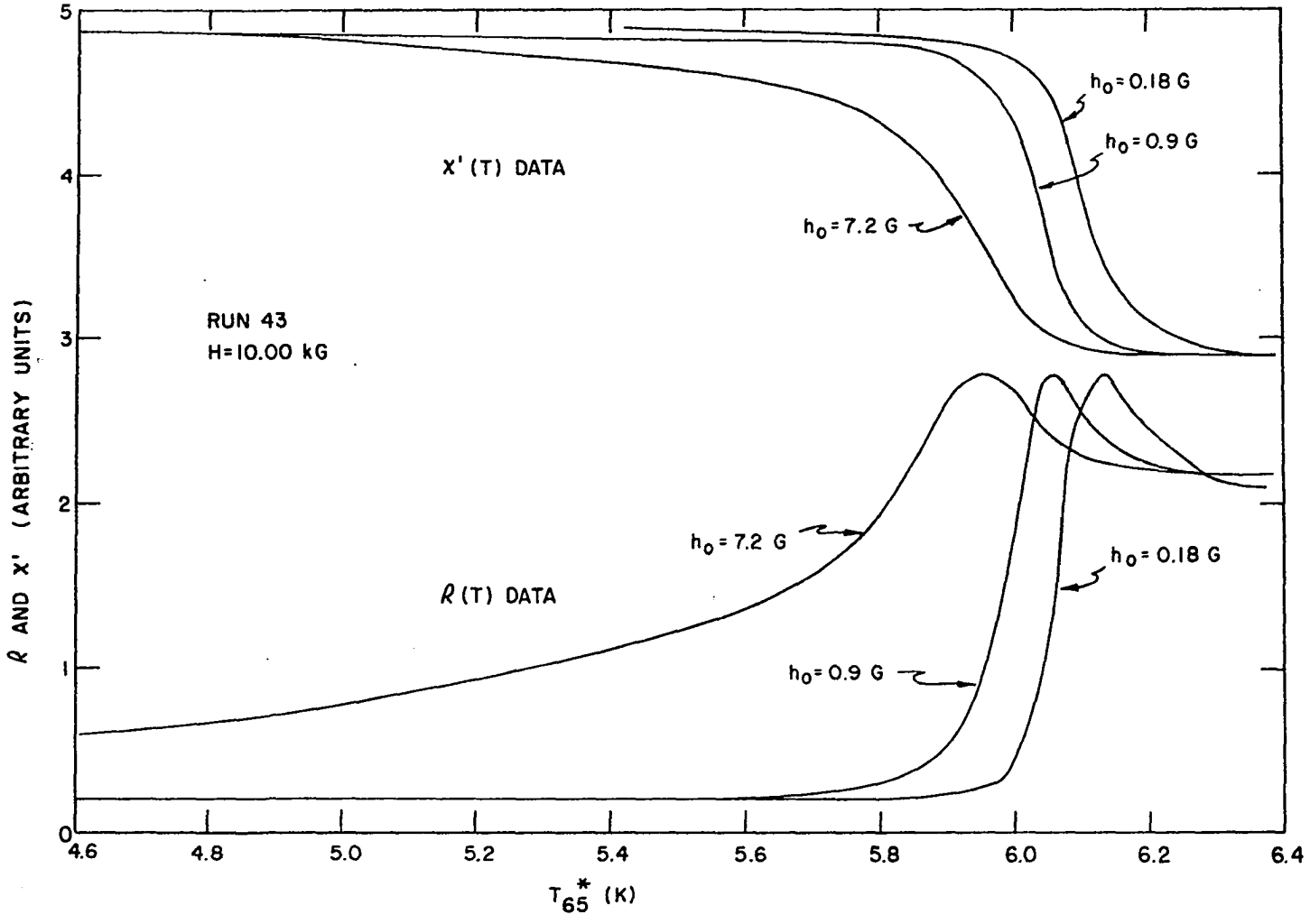

Figure 22. Measuring field dependence of the ac susceptibility transition for a temperature sweep at H = 10.00 kG

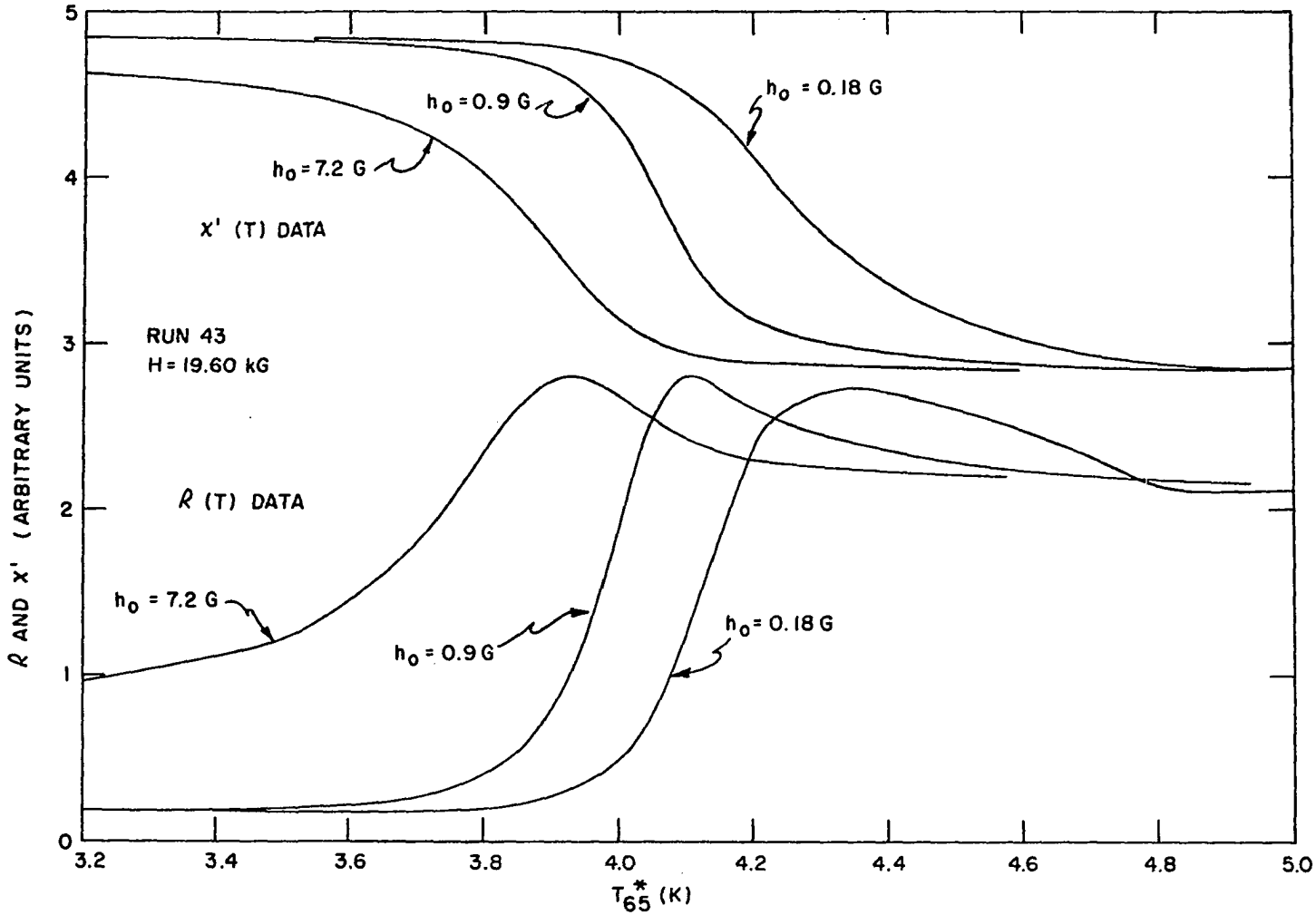

Figure 23. Measuring field dependence of the ac susceptibility transition for a temperature sweep at H = 19.60 kG

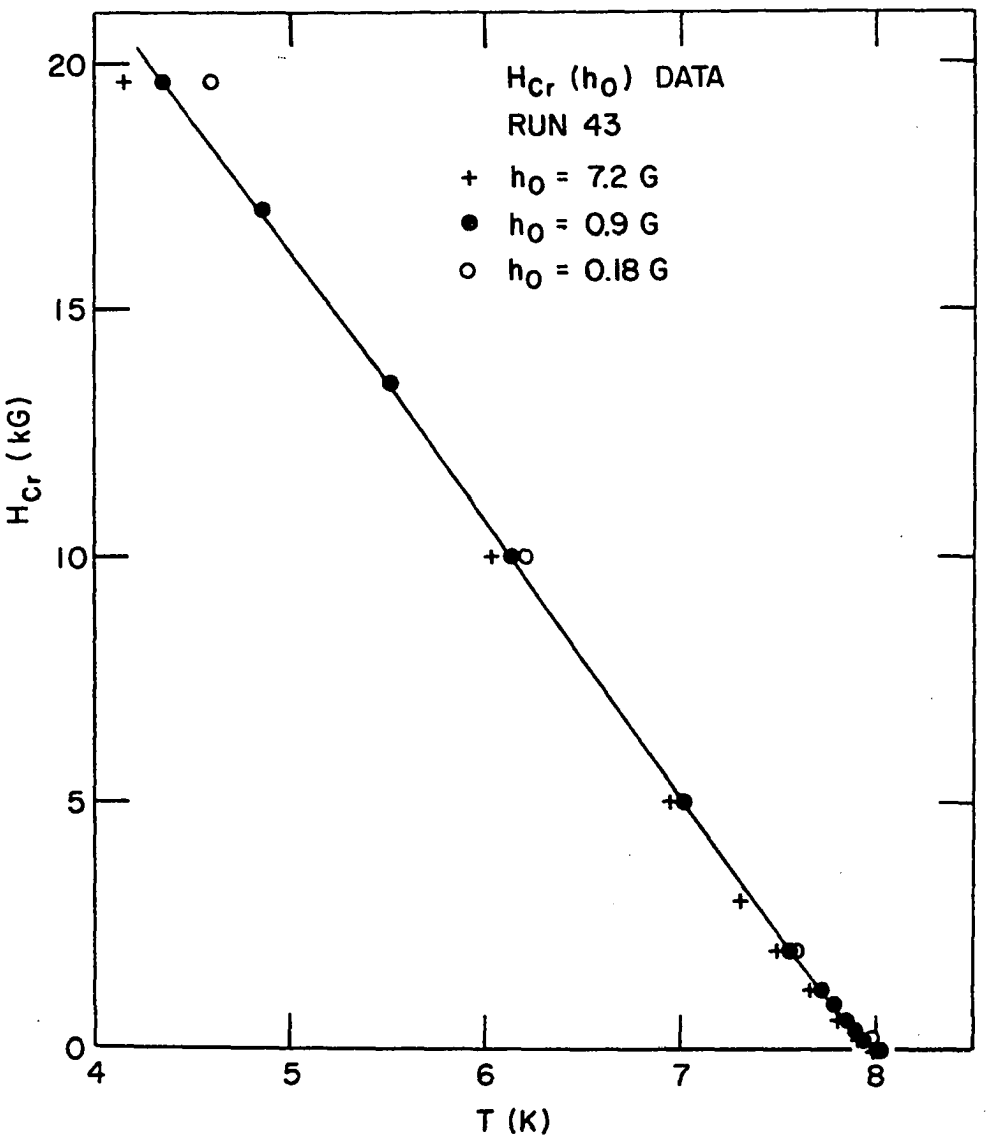

Figure 24. Effects of the h_o dependence of the observed critical field curve of a dhcp phase sample

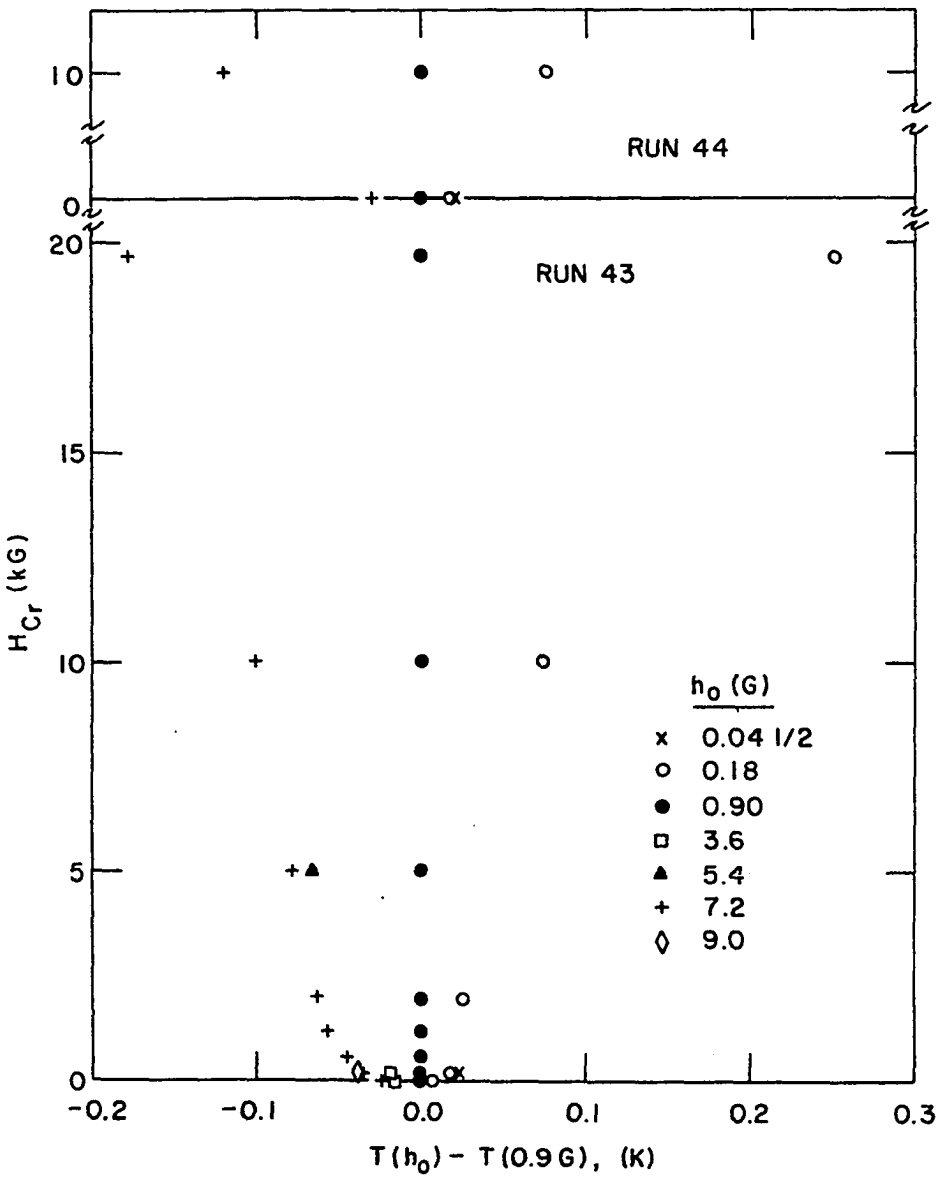

Figure 25. Differences in $T(H_{cr})$ as a function of h_o for temperature sweeps at a given H

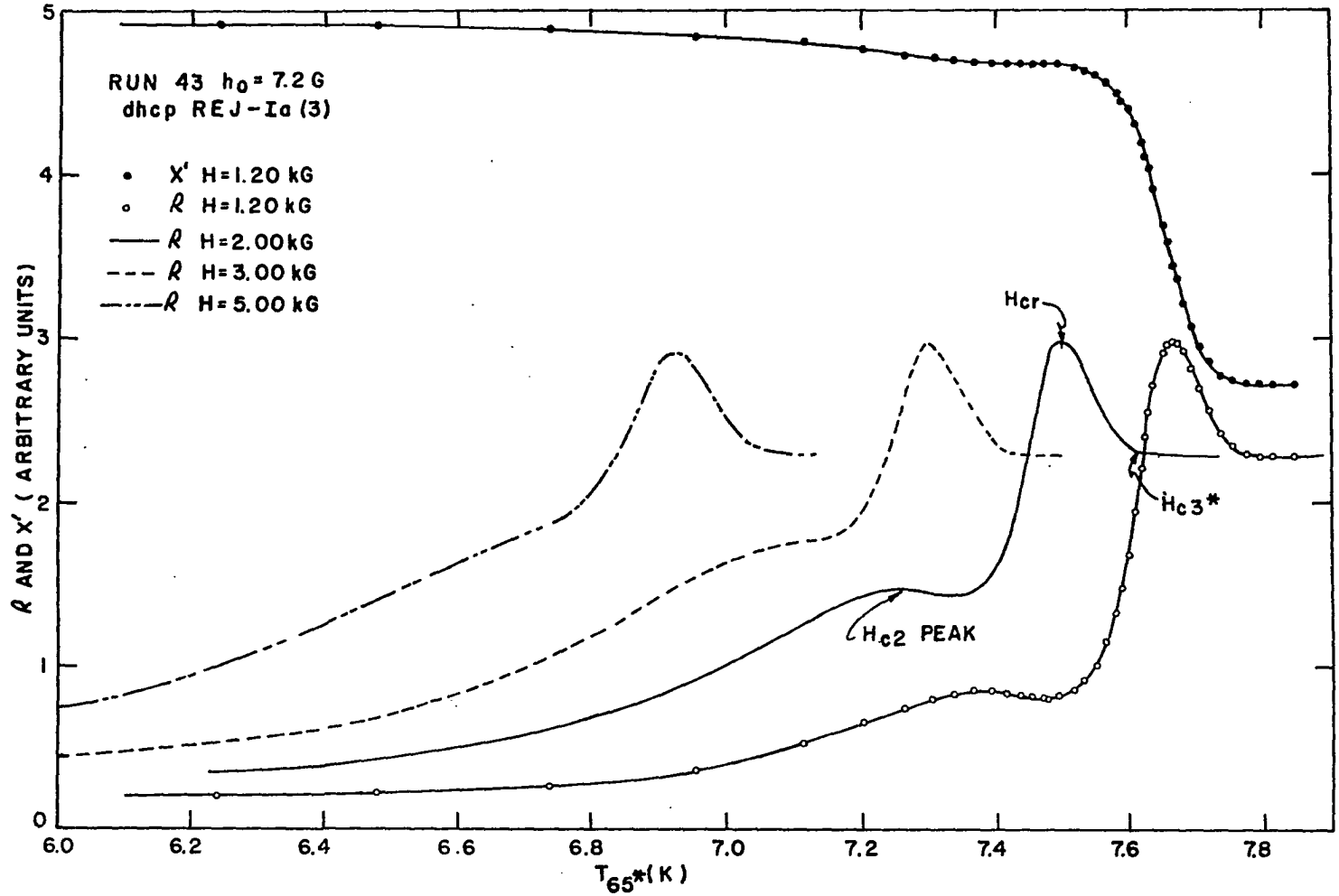

Figure 26. Evidence for the location of H_{c2}

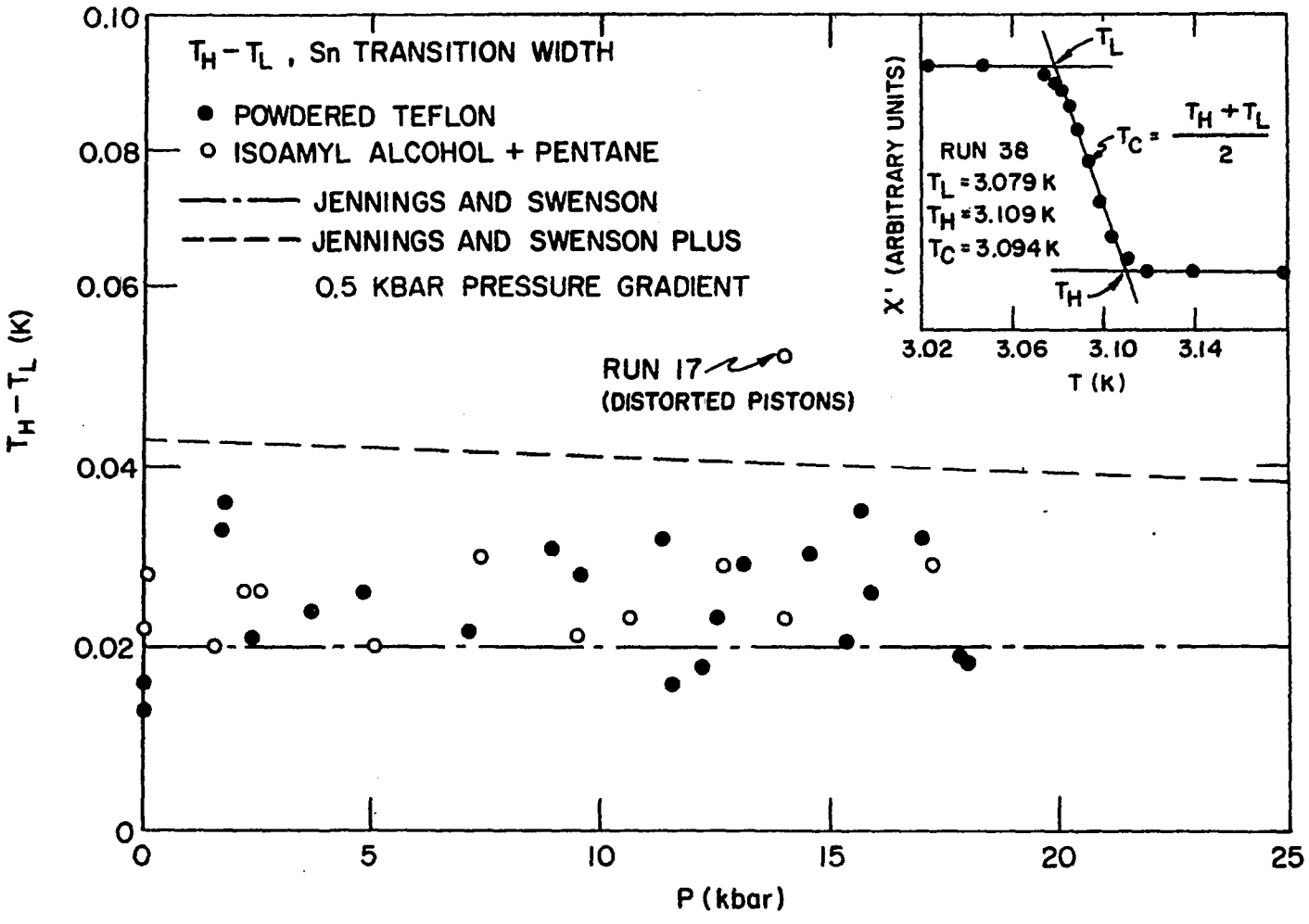

Figure 27. Widths of the zero field χ' transition of the Sn manometer. The insert shows a typical χ' transition of the Sn manometer

Figure 28. Micrograph of a well-aged α-β phase

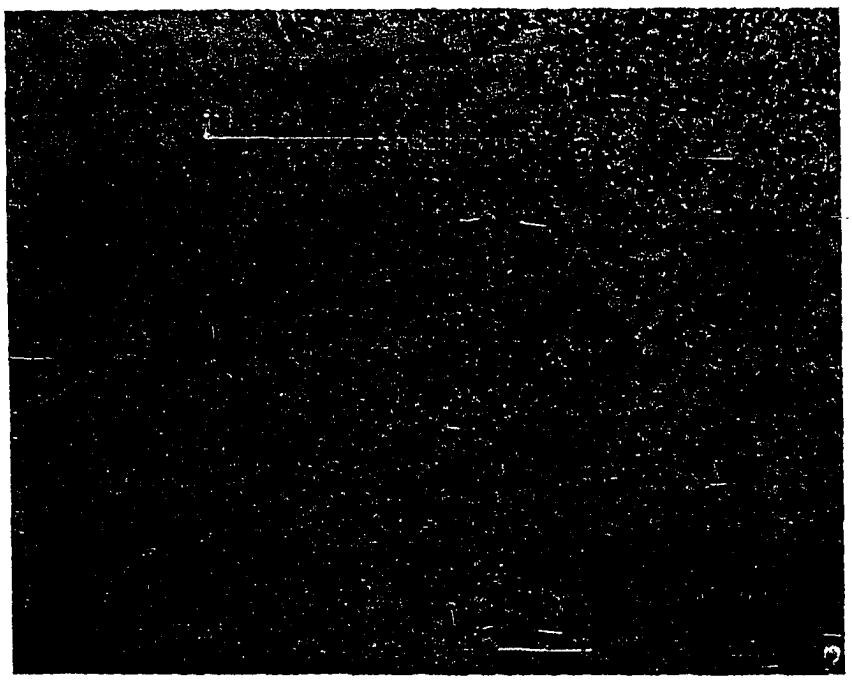

Figure 29. Micrograph of an α-β phase, t = 2 days

Figure 30. Micrograph of an α-β phase, t = 50 days

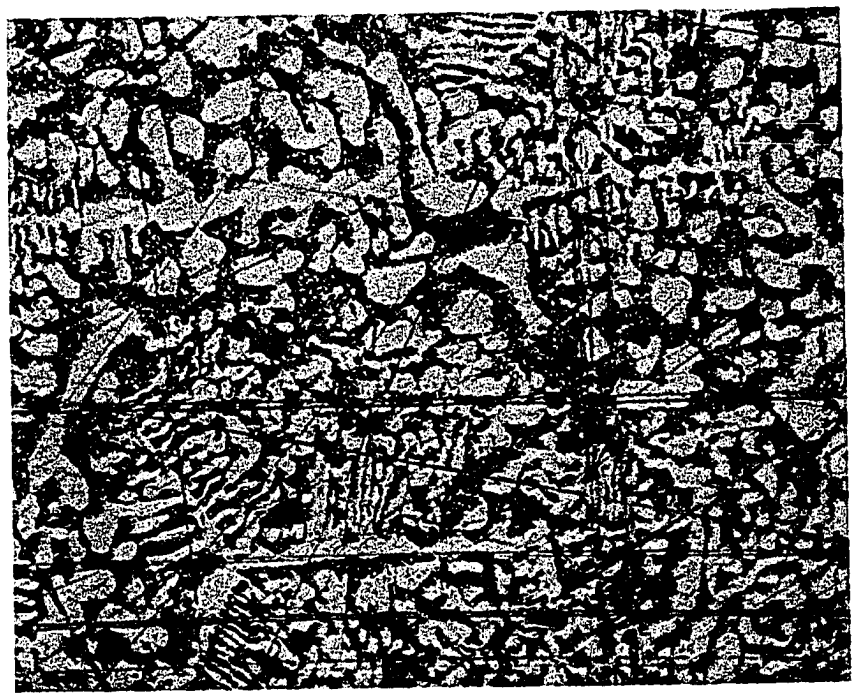

Figure 31. Micrograph of an α-β phase, t = 128 days

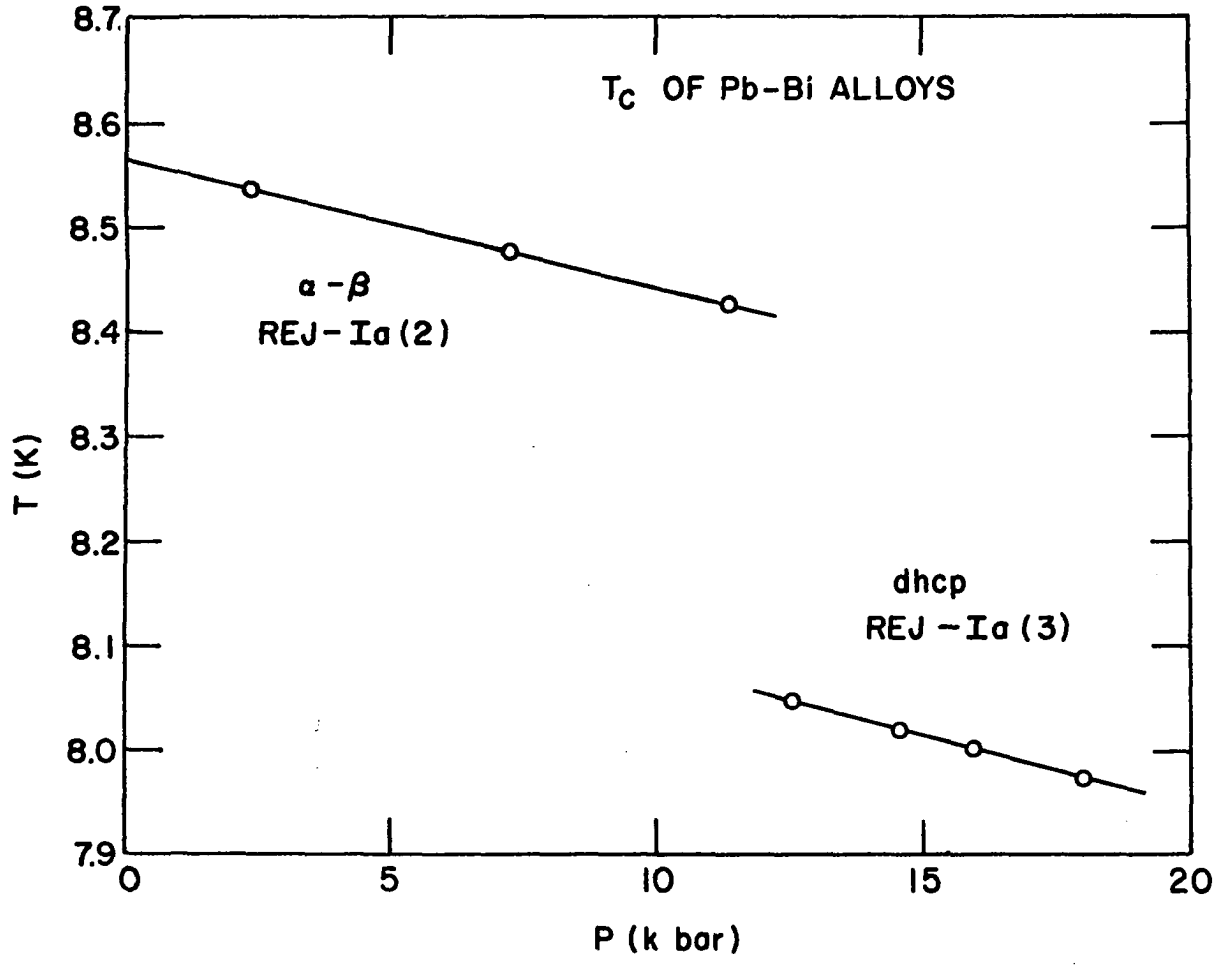

Figure 32. Pressure dependence of T_c

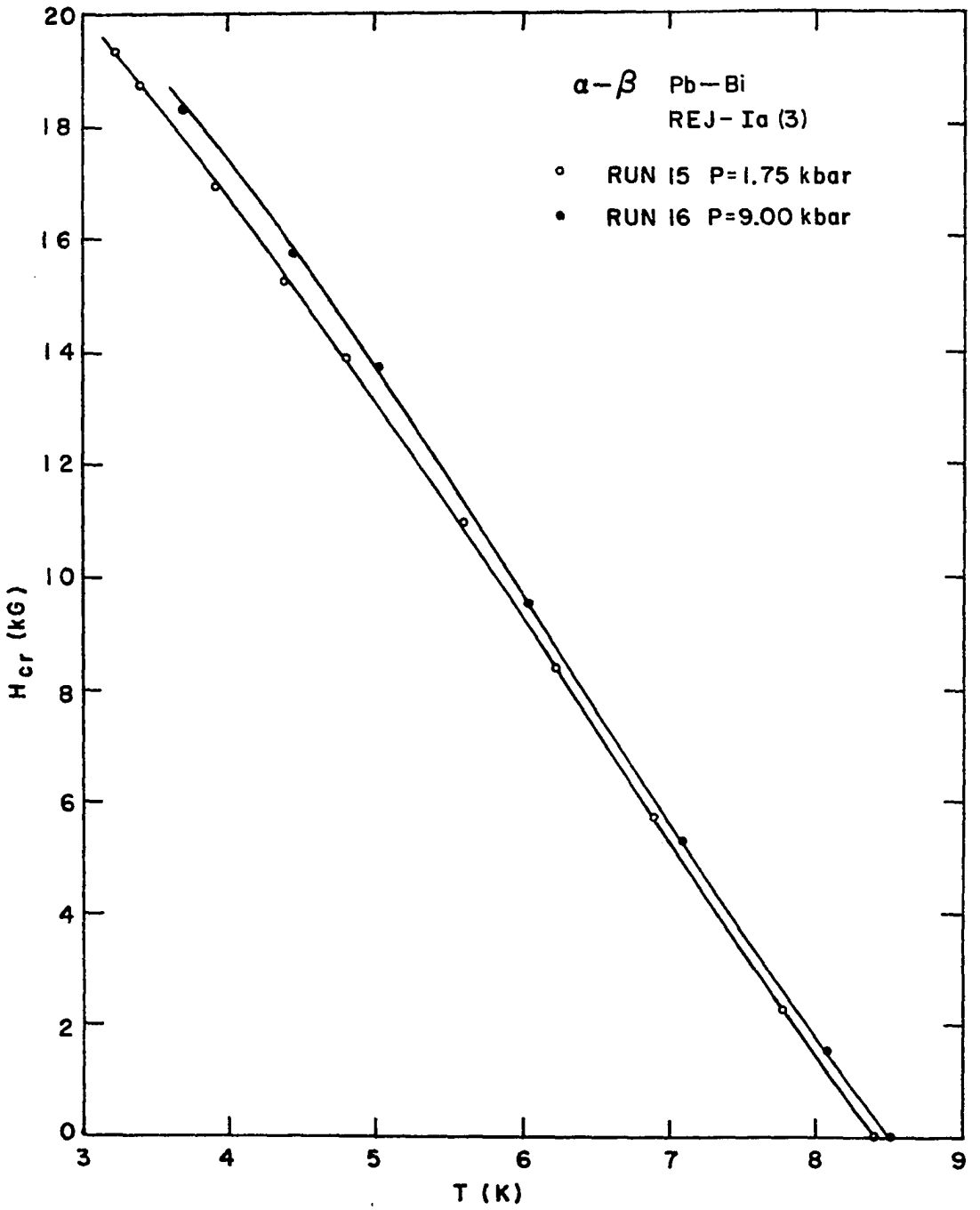

Figure 33. Observed critical field curves for the α-β phase of REJ-Ia(3)

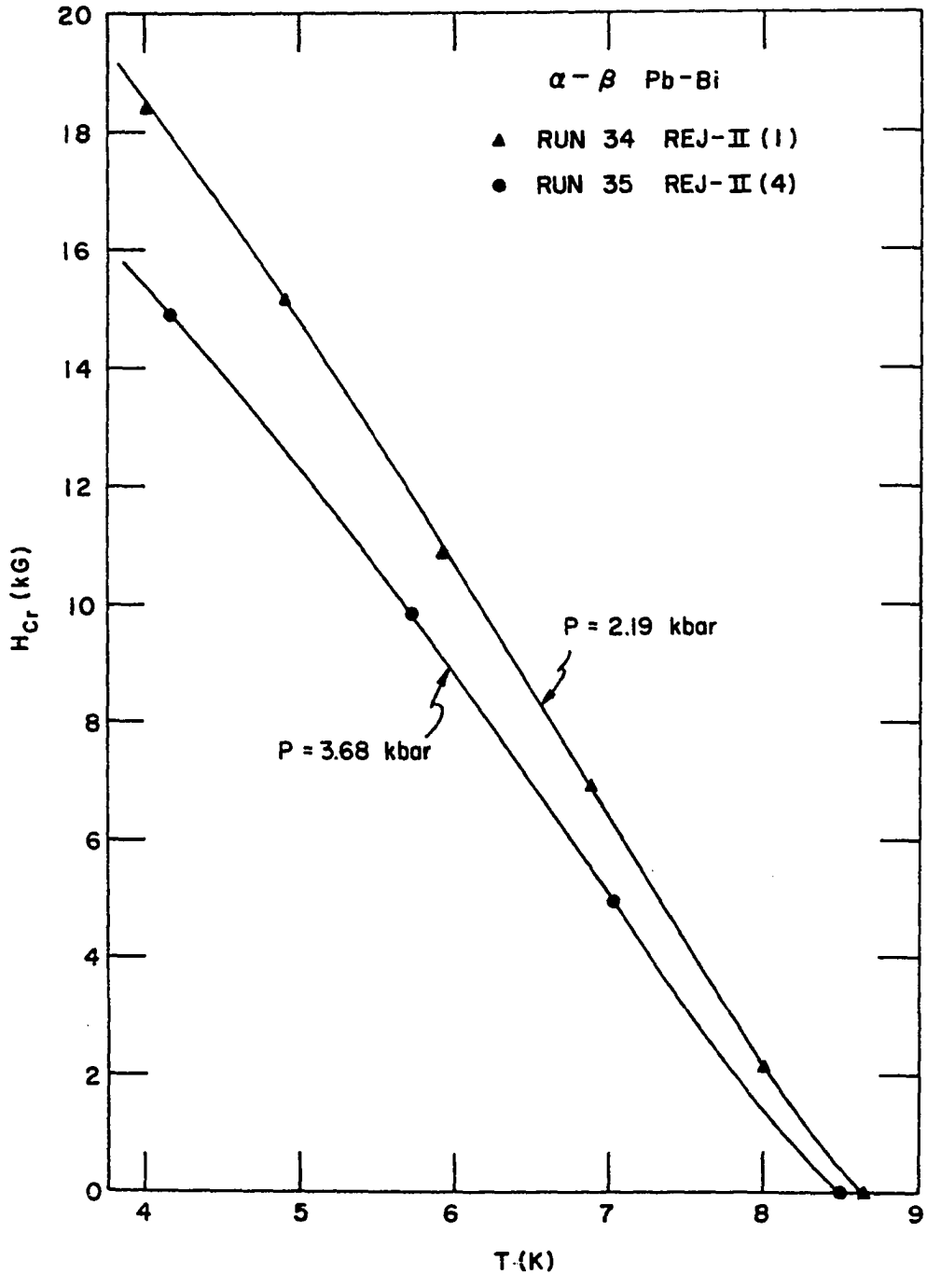

Figure 34. Observed critical field curves for the α-β phase of samples from REJ-II ingot

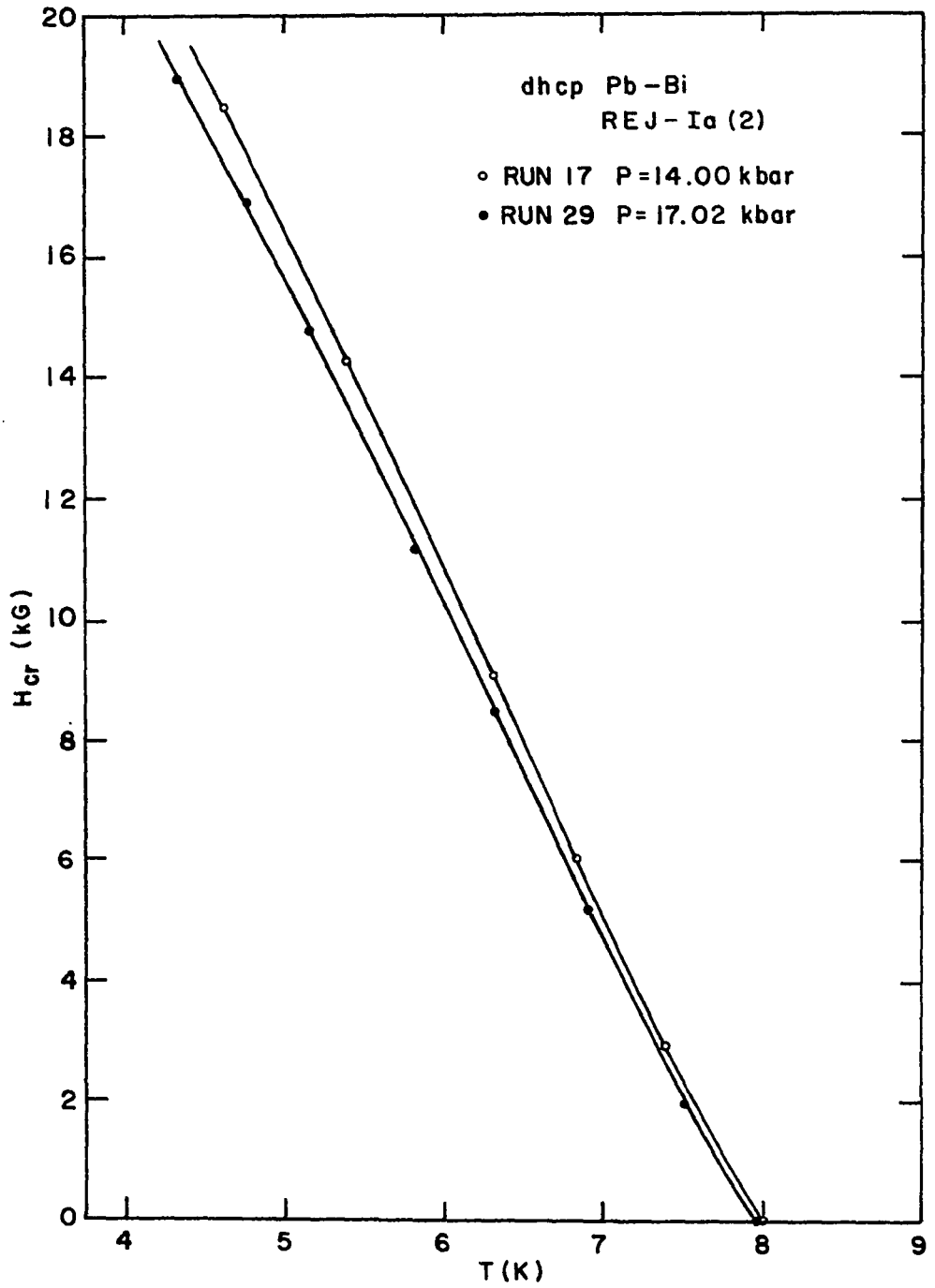

Figure 35. Observed critical field curves for the dhcp phase of REJ-1a(2)

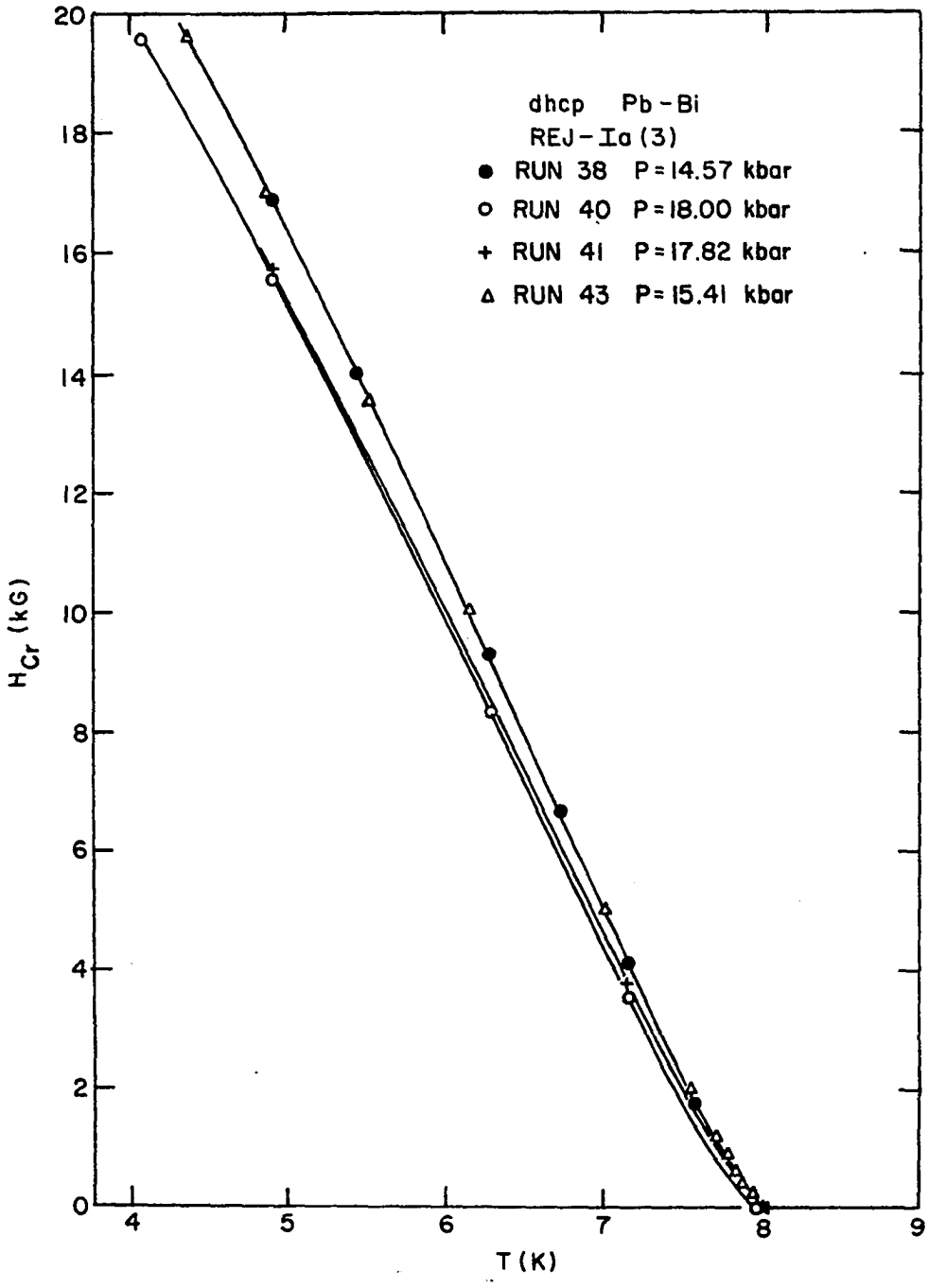

Figure 36. Observed critical field curves for the dhcp phase of REJ-Ia(3)

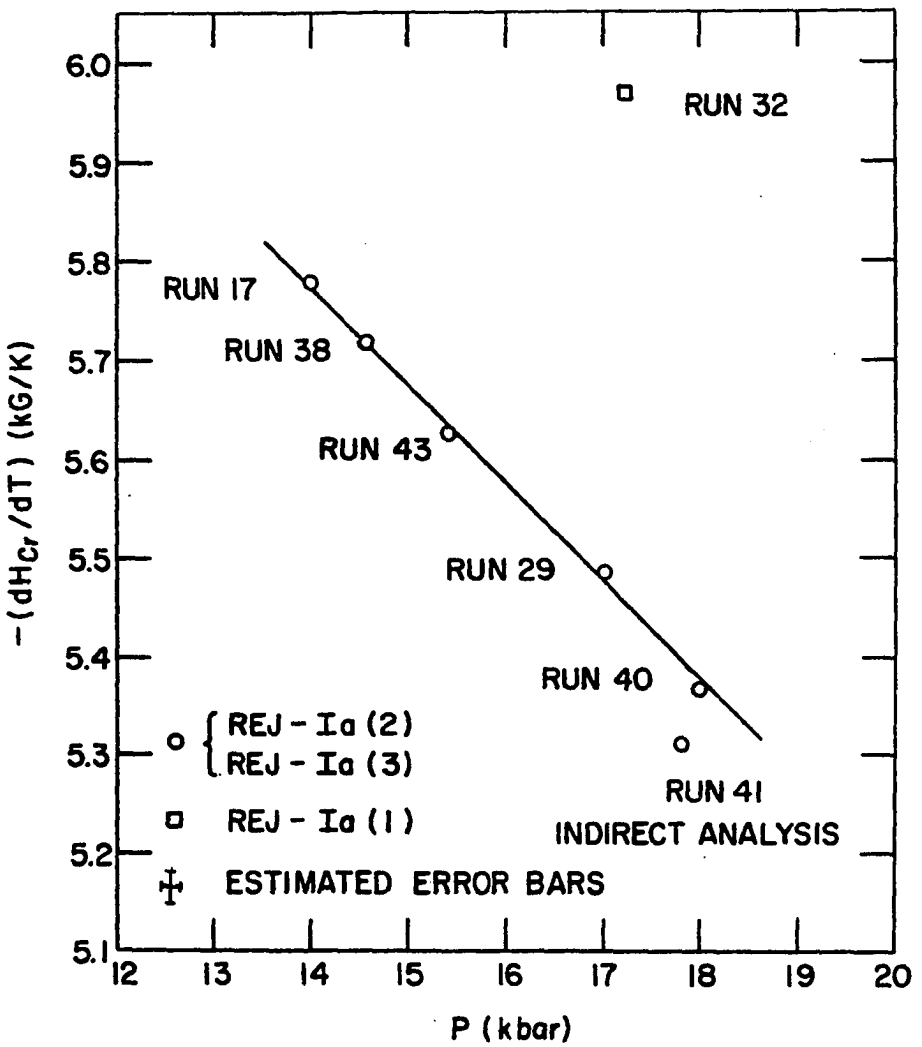

Figure 37. Pressure dependence of the maximum absolute value of the slope of the observed critical field curve

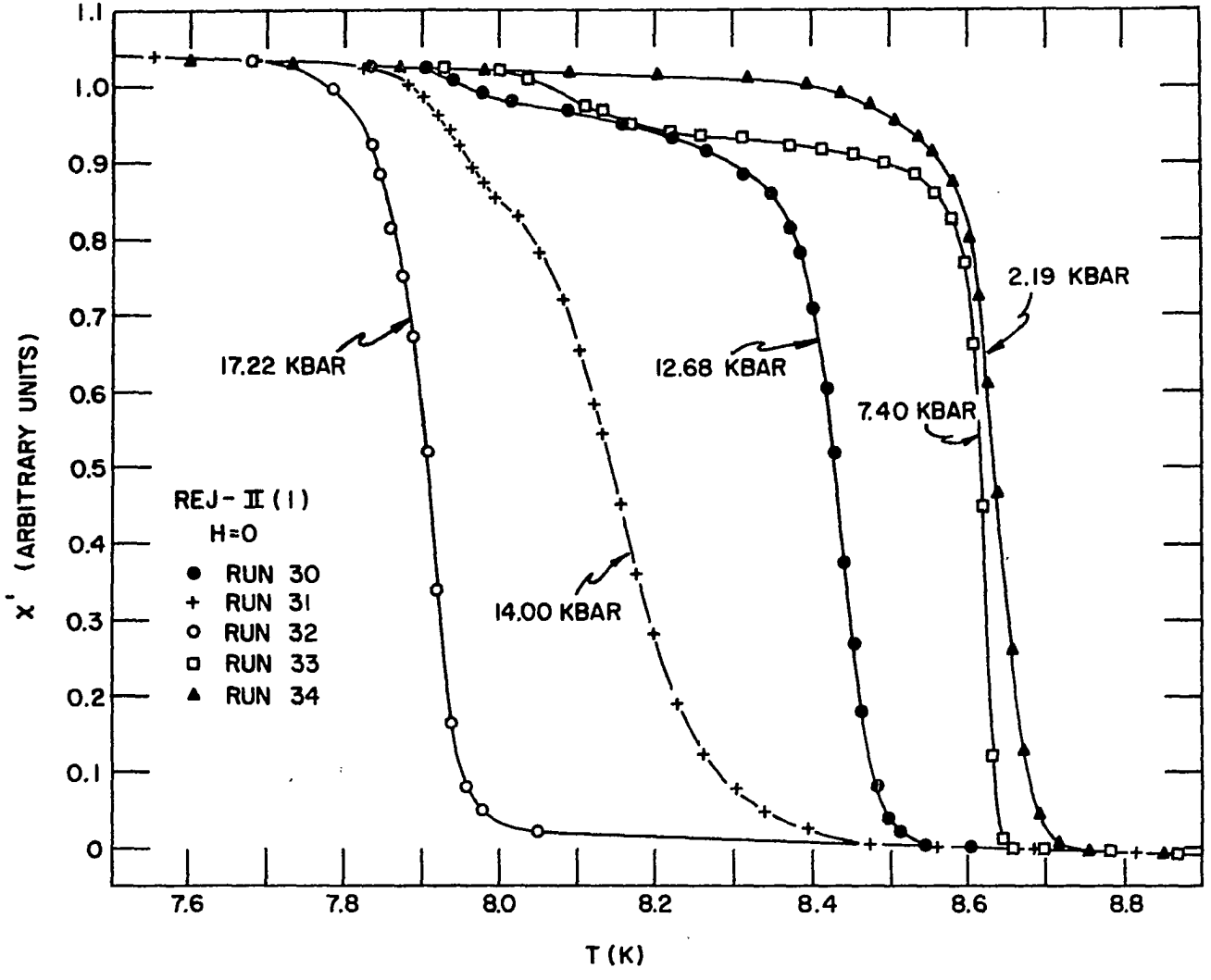

Figure 38. Zero field X' transitions of REJ-II(1) at several pressures which indicate that this sample did not readily transform from one crystal phase to another

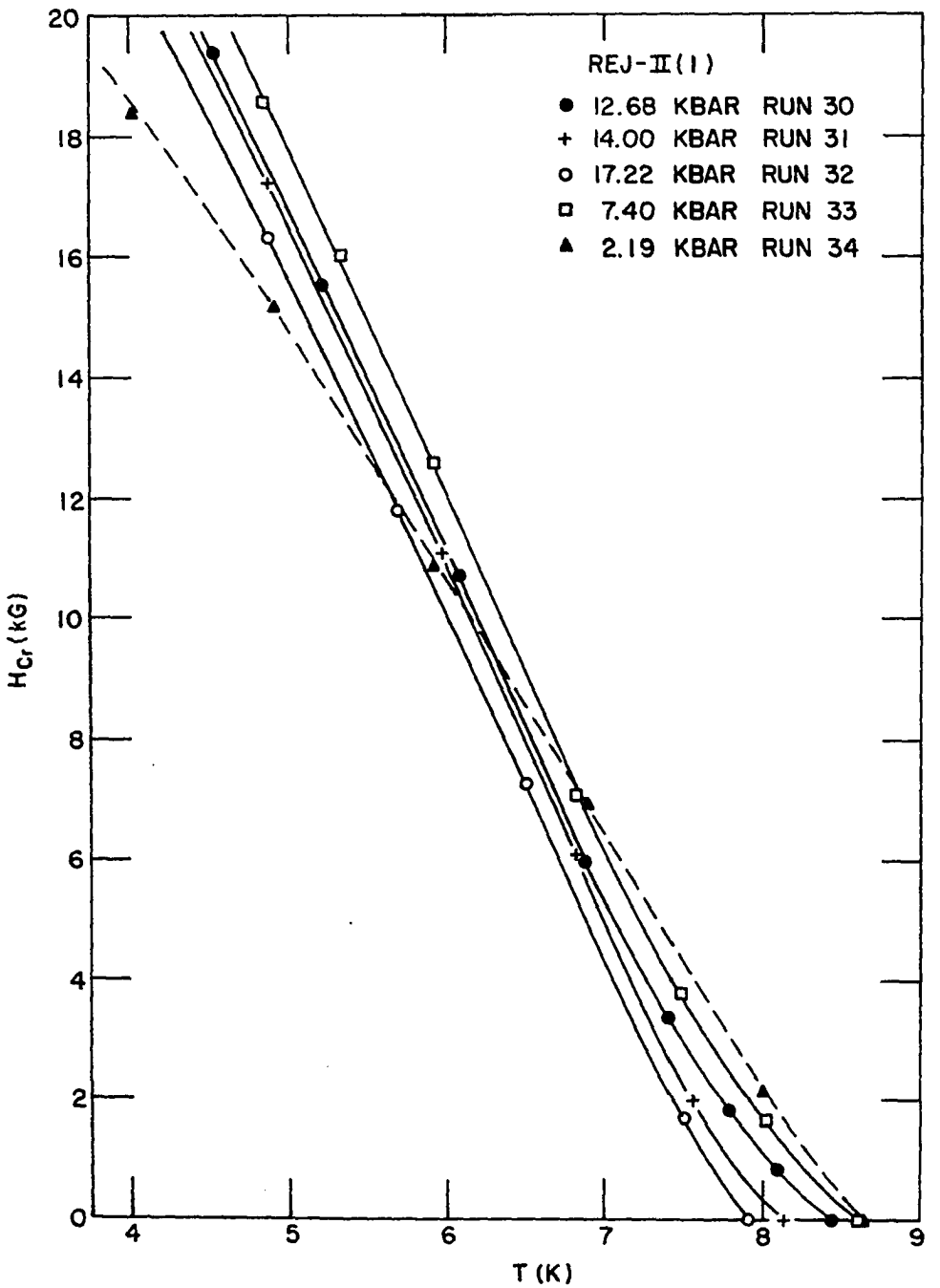

Figure 39. Critical field curves of REJ-11(1) at several pressures which indicate that this sample did not readily transform from one crystal phase to another

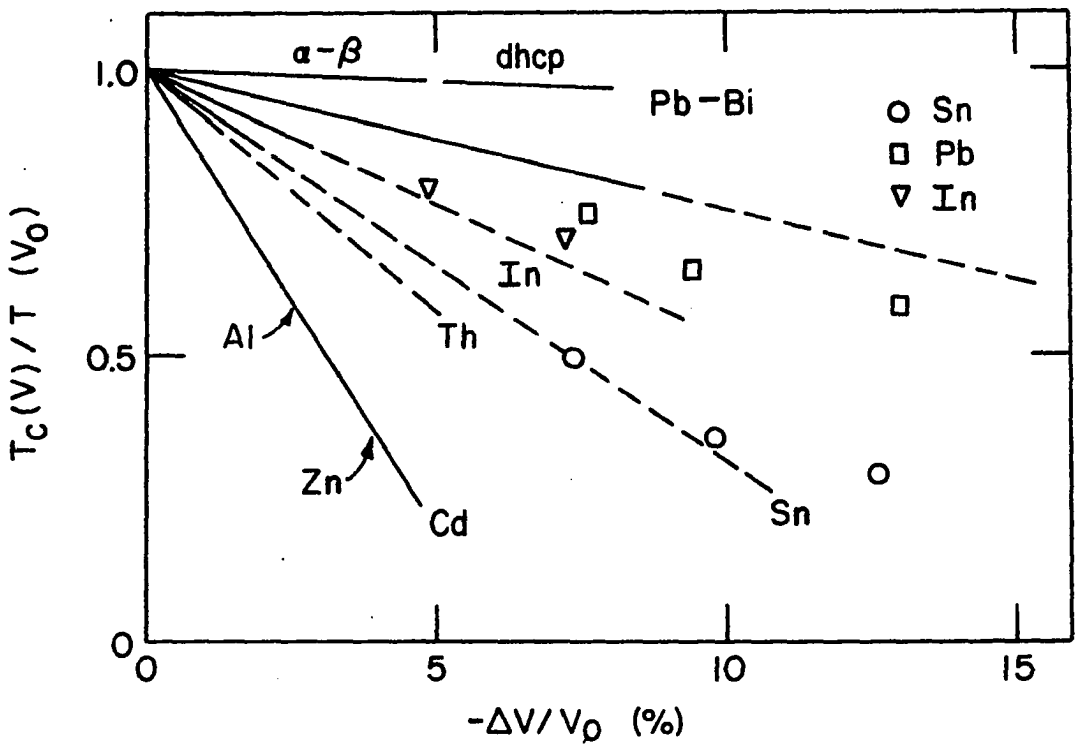

Figure 40. Depression of the reduced transition temperature as a function of percent change in volume

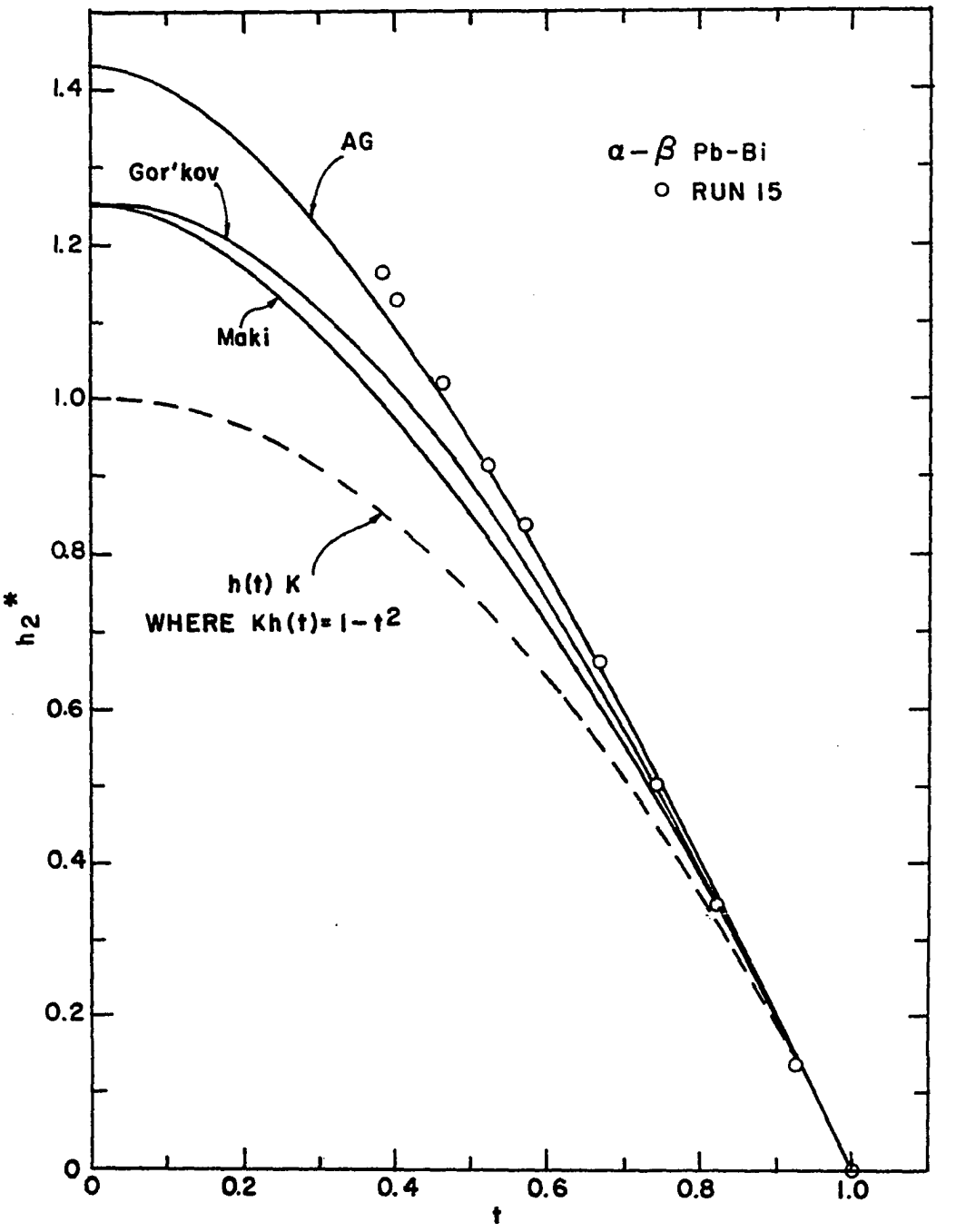

Figure 41. Comparison of observed α-β phase critical field data with theoretical critical field curves

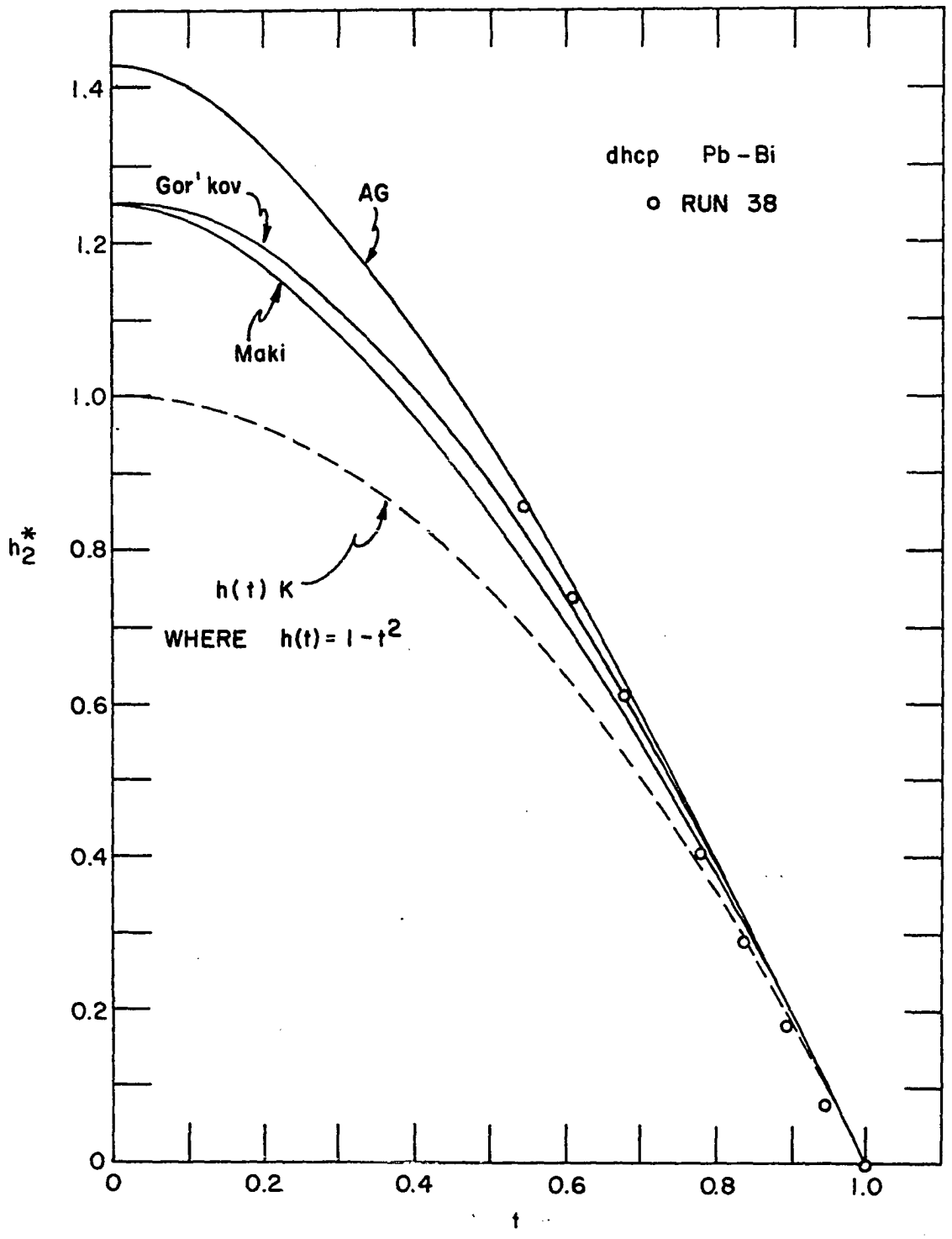

Figure 42. Comparison of observed dhcp phase critical field data with theoretical critical field curves

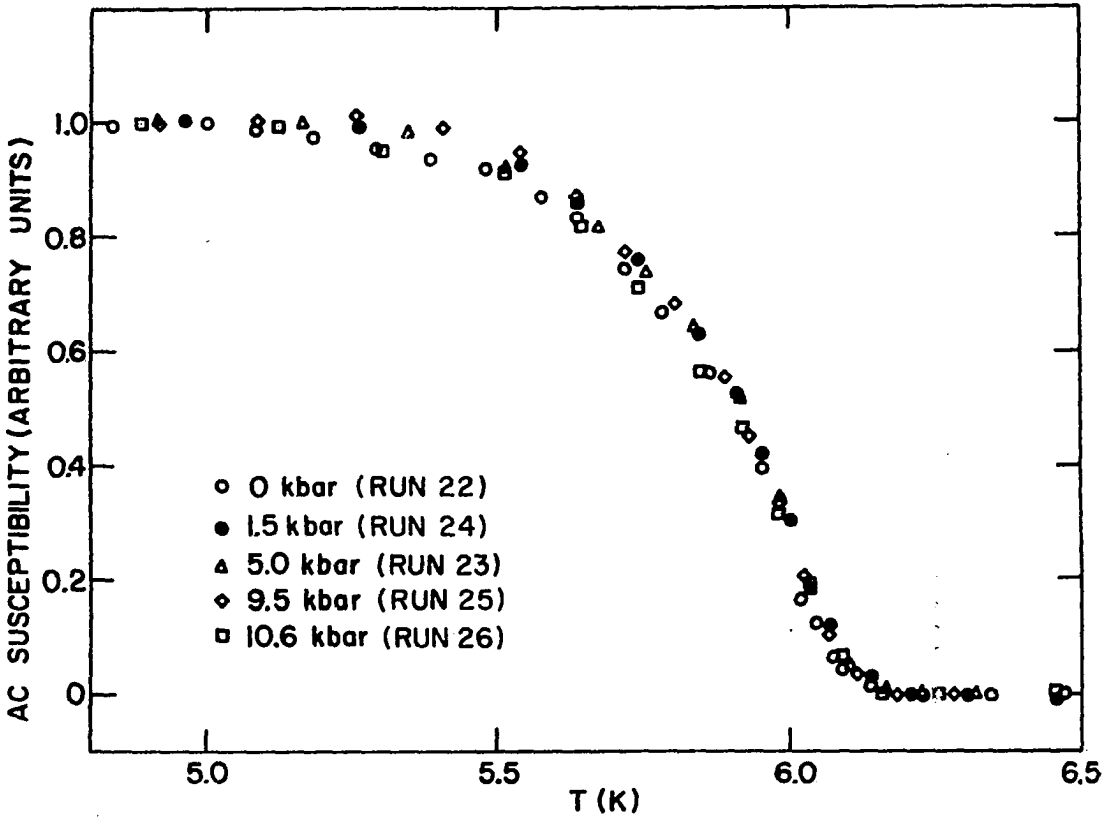

Figure 43. Zero field X' transitions for NbS_2 at various pressures

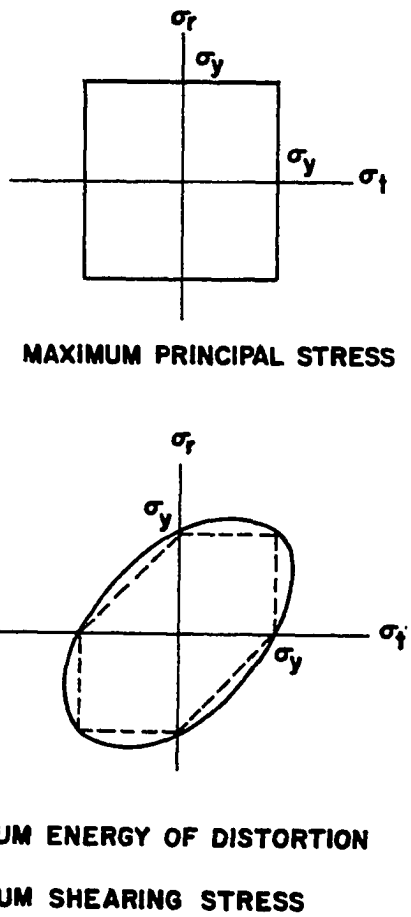

Figure 44. Elastic limit criteria. Maximum energy of distortion theory is sometimes approximated by maximum shearing stress theory

BIBLIOGRAPHY

1. D. E. Gordon and B. C. Deaton, Solid State Commun. 7, 891 (1969).

2. P. W. Bridgman, Collected Experimental Papers (Harvard University Press, Cambridge, Mass., 1964), Vol. VII, p. 4451.

3. M. Hansen, Constitution of Binary Alloys (McGraw-Hill, New York, 1958).

4. W. Klement, Jr., A. Jayaraman and G. C. Kennedy, Phys. Rev. 131, 632 (1963).

5. A. S. Balchan and H. G. Drickamer, Rev. Sci. Instr. 32, 308 (1961).

6. W. Klement, Jr., J. Chem. Phys. 38, 298 (1963).

7. K. A. Gschneidner, Rare Earth Alloys (D. Van Nostrand Company, Inc., Princeton, New Jersey, 1961) p. 13.

8. E. A. Perez-Albuerne, R. L. Clendenen, R. W. Lynch, and H. G. Drickamer, Phys. Rev. A142, 392 (1966).

9. S. E. R. Hiscocks and W. Hume-Rothery, Proc. Roy. Soc. (London) 282, 318 (1964).

10. C. J. Cooke and W. Hume-Rothery, J. Less-Common Metals 10, 42 (1966).

11. H. Kamerlingh Onnes, Afdeeling Natuurkunde, Proceedings of the section of the sciences 13, Part II, 1093 (1911), 13, Part II, 1274 (1911), 14, Part I, 113 (1911)[K. Nederlandse Akademie van Wetenschappen, Amsterdam].

12. W. Meissner and R. Ochsenfeld, Naturwiss. 21, 787 (1963).

13. A. Calverly and A. C. Rose-Innes, Proc. Roy. Soc. A255, 267 (1960).

14. T. F. Stromberg and C. A. Swenson, Phys. Rev. Letters 9, 370 (1962).

15. A. M. Campbell, J. E. Evetts, and D. Dew-Hughes, Phil. Mag. 10, 333 (1964).

16. L. N. Cooper, Phys. Rev. 104, 1189 (1956).

17. J. Bardeen, L. N. Cooper, and J. R. Schrieffer, Phys. Rev. 108, 1175 (1957).

18. L. P. Gor'kov, Zh. Eksp. Teor. Fiz. 36, 1918 (1959)[Sov. Phys. -JETP 9, 1364 (1959)].

19. T. H. Geballe, B. T. Matthias, G. W. Hull, Jr., and E. Corenzwit, Phys. Rev. Letters 6, 275 (1961).

20. J. W. Garland, Jr., Phys. Rev. Letters 11, 114 (1963).

21. B. T. Matthias, Am. Sci. 58, 80 (1970).

22. L. D. Landau and E. M. Lifshitz, in Quantum Mechanics (Pergamon Press, New York, 1958) p. 245.

23. D. C. Hamilton and M. A. Jensen, Phys. Rev. Letters 11, 205 (1963).

24. H. Suhl, B. T. Matthias, and L. R. Walker, Phys. Rev. Letters 3, 552 (1959).

25. J. Kondo, Progr. Theoret. Phys. (Kyoto) 29, 1 (1963).

26. C. G. Kuper, M. A. Jensen, and D. C. Hamilton, Phys. Rev. 134, A15 (1964).

27. J. W. Garland, Jr., Phys. Rev. Letters 11, 111 (1963).

28. D. L. Johnson and D. K. Finnemore, Phys. Rev. 158, 376 (1967).

29. H. Fröhlich, J. Phys. C 2, 1 (1968), 2, 545 (1968).

30. A. Rothwarf, Phys. Rev. 2, 3560 (1970).

31. A. A. Abrikosov, Zh. Eksp. Teor. Fiz. 32, 1442 (1957)[Sov. Phys. -JETP 5, 1174 (1957)].

32. L. P. Gor'kov, Zh. Eksp. Teor. Fiz. 37, 833 (1959) [Sov. Phys. -JETP 10, 593 (1960)].

33. L. P. Gor'kov, Zh. Eksp. Teor. Fiz. 37, 1407 (1959)[Sov. Phys. -JETP 10, 998 (1960)].

34. V. L. Ginzburg and L. D. Landau, Zh. Eksp. Teor. Fiz. 20, 1064 (1950) [English transl. in D. Ter Haar, Men of Physics: L. D. Landau (Pergamon Press, Inc., New York, 1965), p. 138].

35. K. Maki, Physics 1, 21 (1964).

36. K. Maki, Physics 1, 127 (1964).

37. C. Caroli, M. Cyrot, and P. G. de Gennes, Solid State Commun. 4, 17 (1966).

38. B. B. Goodman, Phys. Rev. Letters 6, 597 (1961).

39. D. Saint James and P. G. de Gennes, Phys. Letters 7, 306 (1963).

40. C. F. Hempstead and Y. B. Kim, Phys. Rev. Letters 12, 145 (1964).

41. J. E. Ostenson and D. K. Finnemore, Phys. Rev. Letters 22, 188 (1969).

42. D. Shoenberg, Superconductivity (Cambridge University Press, Cambridge, England, 1965). 2nd ed.

43. J. R. Schrieffer, Theory of Superconductivity (W. A. Benjamin, Inc., New York, New York, 1964).

44. P. G. de Gennes, Superconductivity of Metals and Alloys (W. A. Benjamin, Inc., New York, New York, 1964).

45. R. D. Parks, Superconductivity (Marcel Dekker, Inc., New York, 1969), Vol. I and II.

46. W. J. de Haas, E. van Aubel, and J. Voogd, Afdeeling Natuurkunde, Proceedings of the section of sciences 32, 715 (1929)[K. Nederlandse Akademie van Wetenschappen, Amsterdam].

47. W. J. de Haas, E. van Aubel, and J. Voogd, Afdeeling Natuurkunde, Proceedings of the section of sciences 32, 724 (1929)[K. Nederlandse Akademie van Wetenschappen, Amsterdam].

48. J. C. McLennan, J. F. Allen, and J. O. Wilhelm Trans. Roy. Soc. of Can III 24, 25 (1930).

49. V. W. Meissner, H. Franz, and H. Westerhoff, Ann. Physik 967 (1932).

50. J. G. Adler and S. C. Ng, Can. J. Phys. 43, 594 (1965).

51. H. W. King, C. M. Russell, and J. A. Hulbert, Phys. Letters 20, 600 (1966).

52. J. E. Evetts, A. M. Campbell, and D. Dew-Hughes, Phil. Mag. 10, 339 (1964).

53. A. M. Campbell, J. E. Evetts, and D. Dew-Hughes, Phil. Mag. 18, 313 (1968).

54. J. E. Evetts, J. M. A. Wade, J. Phys. Chem. Solids 31, 973 (1970).

55. I. Giaever, in Proceedings of the Eighth International Conference on Low-Temperature Physics, edited by R. O. Davies (Butterworth, Washington, D.C., 1963) p. 171.

56. I. Dietrich, Phys. Letters 9, 221 (1964).

57. L. D. Jennings and C. A. Swenson, Phys. Rev. 112, 31 (1958).

58. T. F. Smith and C. W. Chu, Phys. Rev. 159, 353 (1967).

59. E. Fischer and J. L. Olsen, Phys. Letters 26A, 387 (1968).

60. N. B. Brandt and N. I. Ginzburg, Usp. Fiz. Nauk 85, 485 (1965)[Sov. Phys. -Usp. 8, 202 (1965)].

61. N. B. Brandt and N. I. Ginzburg, Zh. Eksp. Teor. Fiz. 51, 59 (1966) [Sov. Phys. -JEPT 24, 40 (1967)].

62. B. T. Matthias, T. H. Geballe, and V. B. Compton, Rev. Mod. Phys. 35, 1 (1963).

63. W. E. Gardner and T. F. Smith, Phys. Rev. 138A, 484 (1965).

64. T. F. Smith and W. E. Gardner, Phys. Rev. 146, 291 (1966).

65. M. B. Maple, J. Wittig, and K. S. Kim, Phys. Rev. Letters 23, 1375 (1969).

66. W. E. Gardner and T. F. Smith, Phys. Rev. 154, 309 (1967).

67. J. Wittig, Phys. Rev. Letters 21, 1250 (1968).

68. B. T. Matthias, in Proceedings of the Seventh Rare-Earth Conference, Coronado, California, 1968 (unpublished).

69. C. F. Ratto, B. Coqblin, and E. Galleani d'Agliano, Solid State Commun. 7, 1387 (1969).

70. J. Wittig and B. T. Matthias, Phys. Rev. Letters 22, 634 (1969).

71. J. Wittig, Phys. Rev. Letters 24, 812 (1970).

72. H. Rohrer, Helv. Phys. Acta 33, 675 (1960).

73. J. L. Olsen, E. Bucher, M. Levy, J. Muller, E. Corezwit, and T. G. Aballe, Rev. Mod. Phys. 36, 168 (1964).

74. N. B. Brandt and N. I. Ginzburg, Zh. Eksp. Teor. Fiz. 44, 1876 (1963) [Sov. Phys. -JETP 17, 1262 (1963)].

75. N. B. Brandt and N. I. Ginzburg, Zh. Eksp. Teor. Fiz. 50, 1260 (1966) [Sov. Phys. -JETP 23, 838 (1966)].

76. P. E. Seiden, Phys. Rev. 179, 458 (1969).

77. W. L. McMillan, Phys. Rev. 167, 331 (1968).

78. C. A. Swenson, Solid State Phys. 11, 41 (1960).

79. N. B. Brandt and N. I. Ginzburg, Usp. Fiz. Nauk 98, 95 (1969)[Sov. Phys. -Usp. 12, 344 (1969)].

80. P. F. Chester and G. O. Jones, Phil. Mag. 44, 1281 (1953).

81. D. M. Newitt, The Design of High Pressure Plant and the Properties of Fluids at High Pressures (Oxford University Press, New York, 1940).

82. E. W. Comings, High Pressure Technology (Mc Graw-Hill, New York, 1956).

83. T. F. Smith, C. W. Chu, and M. B. Maple, Cryogenics 9, 53 (1969).

84. F. Birch, J. Geophys. Res. 57, 227 (1952).

85. D. K. Finnemore, D. L. Johnson, J. E. Ostenson, F. H. Spedding, and B. J. Beaudry, Phys. Rev. 137, A550 (1965).

86. D. L. Johnson, Ph.D. thesis, Iowa State University, 1966 (unpublished).

87. J. Nicol and T. Soller, Bull. Am. Phys. Soc. 2, 63 (1957).

88. S. Saito, T. Shiratori, G. Terui, M. Kumano, and E. Kanda, Cryophysics and Cryoengineering (Bulletin of International Institute of Refrigeration, Commission I, Tokyo, 1970).

89. J. R. Clement and E. H. Quinnell, Rev. Sci. Instr. 23, 213 (1952).

90. D. L. Decker and H. L. Lacquer, Cryogenics 9, 481 (1969).

91. W. R. Hudson, Rev. Sci. Instr. 39, 253 (1968).

92. L. J. Neuringer and Y. Shapira, Rev. Sci. Instr. 40, 1314 (1969).

93. W. C. Black, Jr., W. R. Roach, and J. C. Wheatley, Rev. Sci. Instr. 35, 587 (1964).

94. J. R. Carlson, Ph.D. thesis, University of Illinois, Urbana, 1968 (unpublished).

95. D. L. Johnson, Ames Laboratory of the United States Atomic Energy Commission Data Book DLJ-2, DLJ-3, 1965 (unpublished).

96. J. S. Blakemore, J. W. Schultz, and J. G. Myers, Rev. Sci. Instr. 33, 545 (1962).

97. J. M. Ziman, Electrons and Phonons (Oxford University Press, New York, 1960).

98. R. E. Slonaker, Jr., Ph.D. thesis, Iowa State University, 1964 (unpublished).

99. R. W. Rollins and J. Silcox, Phys. Rev. 155, 404 (1967).

100. C. A. M. van der Klein, J. D. Elen, R. Wolf, and D. de Klerk, Physica, 49, 98 (1970).

101. J. R. Clem (private communication).

102. C. F. S. Malseed, R. B. Nethercott, and W. A. Rachinger, Phys. Letters 22, 551 (1966).

103. J. E. Ostenson, M. S. thesis, Iowa State University, 1969 (unpublished).

104. A. A. Abrikosov and L. P. Gor'kov, Zh. Eksp. Teor. Fiz. 39, 1781 (1960)[Sov. Phys. -JETP 12, 1243 (1961)].

105. R. D. Parks, in Superconductivity, edited by P. R. Wallace (Gordon and Breach, Science Publishers, New York, 1969), Vol II, p. 625.

106. M. H. van Maaren and G. M. Schaeffer, Phys. Letters 20, 131 (1966).

107. J. A. Wilson and A. D. Yoffe, Adv. in Phys. 18, 193 (1969).

108. O. J. Beerntsen, G. A. Spiering, and C. H. Armitage, IEEE Trans. Aerospace 2, 816 (1964).

109. G. A. Spiering, E. Revolinsky, and D. J. Beerntsen, J. Phys. Chem. Solids 27, 535 (1966).

110. E. A. Antonova, S. A. Medvedev, and I. Yu. Shebalin, Zh. Eksp. Teor. Fiz. 57, 329 (1969)[Sov. Phys. -JETP 30, 181 (1970)].

111. E. I. Katz, Zh. Eksp. Teor. Fiz. 56, 1675 (1969)[Sov. Phys. -JETP 29, 897 (1969)].

112. E. I. Katz, Zh. Eksp. Teor. Fiz. 58, 1471 (1970)[Sov. Phys. -JETP 31, 787 (1970)].

113. F. R. Gamble, F. J. DiSalvo, R. A. Klemm, and T. H. Geballe, Science 168, 568 (1970).

114. H. Schäfer, Z. Anorg. Allgem. Chem. 286, 27 (1956).

115. H. Schäfer and W. Fuhr, J. Less-Common Metals 8, 375 (1965).

116. R. I. Beecroft and C. A. Swenson, J. Appl. Phys. 30, 1793 (1959).

117. R. H. Wentorf, Jr., Modern Very High Pressure Techniques (Butterworths, London, 1962).

ACKNOWLEDGEMENTS

The author would like to express his sincere appreciation to Dr. D. K. Finnemore for his continuing interest and advice during this research project and for his many discussions on superconductivity.

The author also wishes to express his gratitude to Dr. C. A. Swenson, Dr. C. B. Satterthwaite, Dr. J. R. Clem, and Dr. W. J. Keeler for their valuable discussions concerning various aspects of this work and in addition to Dr. C. A. Swenson for advice and criticism during the preparation of the manuscript.

The author also thanks the many other members of the low temperature research group for their assistance on a multitude of seemingly minor matters, but which together represent an important contribution.

He also extends special thanks to his wife Karen for her encouragement and understanding and for typing the final manuscript.

APPENDIX A

Superconductivity in NbS_2 under Pressure

Niobium disulfide and some other of the transition metal dichalcogenides form an interesting class of layered superconductors (106, 107). Each layer of these compounds is comprised of a hexagonal close-packed arrangement of an elementary plane of metal atoms between two chalcogenide planes. Van der Waals bonds predominate between the layers but the bonds within each layer are strong which results in a high degree of anisotropy in both the superconducting and normal state properties of these materials. Beerntsen, Spiering, and co-workers (108, 109) have reported the anisotropy of the critical currents in $NbSe_2$ for various orientations of an applied magnetic field. These critical field investigations have been extended by Antonova et al. (110) who considered the effects of deviation from stoichiometry on the anisotropy of the magnetic properties. They assumed that the superconducting behavior is associated with the niobium atoms and essentially is of a planar character since superconductivity is favored by directions in the basal plane.

Katz has developed a theory of quasi-two-dimensional superconductivity (111) which he applied to the niobium diselenide system (112). There is one result of this theory which is of particular interest in the present work since it implies through certain inequality relations that T_c should increase as the inter-layer distance decreases. The rapid decrease in T_c with deviation from stoichiometry above a critical concentration of 33.7 % niobium has been associated experimentally with excess niobium atoms leaving the plane and forming a superstructure between the layers (109, 110). Katz

considered this as effectively separating the layers and hypothesized that the decrease in T_c was due to the increase of c, the separation distance between the niobium planes. This hypothesis then established the magnitude of dT_c/dc near equilibrium for which the theory only had provided certain limits.

In related experiments (113), the layers of various transition metal dichalcogenides have been separated by intercalating a full layer of pyridine or aniline molecules, but the resulting transition temperatures usually differed by less than a factor of two or three from the initial values. These experiments do not provide an unambiguous solution of the relationship between T_c and the separation distance because of possible organic contributions to the superconducting interaction. We report here a complementary experiment in which the superconducting transition temperature of NbS_2 is studied under hydrostatic pressure.* We assume that in this experiment the principle effect will be the reduction of the interlayer separation. If the suggestion of Katz is correct, T_c should increase noticeably under pressure. For instance, extension of his hypothesis predicts an increase in T_c of greater than 1 K for a 1 % decrease in c.

For the present work, a powder of NbS_2 crystals was produced from its elemental constituents by an iodine vapor transport method (114,115). The initial mixture deliberately contained slightly more than the stoichiometric ratio of sulfur in an attempt to prevent excess niobium in the compound. The clamp technique was used with a high pressure piston-cylinder device

---

*A sharp decrease in the T_c of NbS_2 resulting from non-stoichiometry also has been reported (106) and most other properties of this compound are similar to those of the selenide.

and hydrostatic pressures were insured by placing the sample and a Sn manometer in a Teflon capsule filled with a 1:1 mixture of isoamyl alcohol and pentane. This pressure equipment and the associated apparatus have been described in Chapter II.

The results are shown in Figure 43, and the observed width of the transition (~0.6 K) could be attributed to non-stoichiometric effects, but the intrinsic T_c of about 6.1 K indicates that the desired two layer polymorph (2H-NbS_2) was obtained. The results also indicate that the transition temperature does not change by more than 0.1 K for pressures up to 10 kbar since the shape of the transition does not change. The pressure-induced changes in the lattice constants were determined approximately through compression data which were taken at room temperature on a compacted powder of NbS_2 using a piston-displacement technique similar to that described by Beecroft and Swenson (116). The pressure was cycled several times between 0 and 20 kbar until the V vs P data were reproducible although there was a large amount of hysteris which indicated internal strains in the sample. A correction for this effect was made by taking the average of the increasing and decreasing pressures for a given piston displacement, and the results indicated that $\Delta V/V$ was 2.9 % at 10 kbar. It does not seem unreasonable to assume that the inter-layer spacing c decreased by 1 % or more. Hence, our observation of a negligible change in T_c for a pressure of 10 kbar, or a decrease in c of 1%, suggests that Katz's hypothesis is not correct.

These pressure measurements presumably establish a less ambiguous value of dT_c/dc near equilibrium than that provided by the suggestion of

Katz. It appears invalid to apply the quasi-two-dimensional theory to the decrease of T_c resulting from non-stoichiometry, and therefore, the rapid destruction of superconducting behavior with increase of niobium above the critical concentration must be attributed to a mechanism other than the separation of the layers. This experiment does not provide a validity test for the theory itself, but several features of the theory have been supported by other experimental evidence.

APPENDIX B

Some Notes on the Strengths of Thick-walled Cylinders

In his book High Pressure Technology, Comings (82) has reviewed calculations for thick-walled cylinders with length relatively long compared to the diameter. The following two paragraphs present some of the results for the case where the external pressure is zero and the ends are supported.

Under elastic conditions the tangential stress at the inner radius of such a cylinder is $\sigma_t = P(K^2 + 1)/(K^2 - 1)$ and the radial stress is $\sigma_r = -P$ where P is the internal pressure and $K = r_2/r_1$, the ratio of outer to inner radii. There is not a clear cut criterion as to what stresses will exceed the elastic limit and at least five models have been proposed (also see (81)). We will consider only two of these criteria. 1) The Maximum Principal Stress Theory: the elastic limit will be reached when a principle stress (σ_t in this case) becomes equal to σ_y, the tensile yield strength. 2) The Maximum Energy of Distortion or Maximum Octahedral Shearing Stress: at the elastic limit the principle stresses are bound by the requirement

$$\sigma_r^2 + \sigma_t^2 - \sigma_t \sigma_r = \sigma_y^2 .$$

The first theory is the simplest of the criteria and the second is perhaps the most satisfactory for ductile materials. Graphic comparisons of these limits are shown in Figure 44. Remember for this case σ_r will be negative (compression) and σ_t positive (tension).

The inner radius of such a cylinder will be at the elastic limit when the internal pressure is

$$P_{el} = \frac{K^2 - 1}{K^2 + 1} \sigma_y \qquad (7)$$

according to the first criterion and

$$P_{e2} = \frac{K^2 - 1}{\sqrt{3K^4 + 1}} \sigma_y$$

according to the second. Two results for ductile materials follow from this second model. As the pressure is increased beyond P_{e2} the plastic region grows until the outer radius reaches the elastic yield strength at the overstrain pressure

$$P_o = \frac{2\sigma_y}{\sqrt{3}} \ln K \quad .$$

However, if the tensile ultimate strength, σ_u, is greater than the tensile yield strength, the cylinder will not fail until the bursting pressure

$$P_b = \frac{2}{\sqrt{3}} \left(2 - \frac{\sigma_y}{\sigma_u} \right) \sigma_y \ln K$$

is exceeded.

In this experiment all cylinders had an outside diameter of 0.60 in. but three different size bores were used. The cylinders were made of beryllium copper which had σ_y = 11.7 kbar and σ_u = 13.8 kbar. The strengths of these cylinders are shown in Table IV.

Table IV. Strengths of certain Be-Cu cylinders

r_1 (in.)	K	P_{e1} (kbar)	P_o (kbar)	P_b (kbar)
0.125	2.40	8.3	11.8	13.6
0.075	4.00	10.3	18.7	21.5
0.0625	4.80	10.7	21.2	24.4

It is an ancient practice to increase the strength of a cylinder by prestressed construction utilizing wire wrappings or multiple walls (82, 117). For part of the present experiment we have used a prestressed double-

walled cylinder. In order to obtain the maximum advantage from this procedure it was necessary to determine the proper geometry and prestressing. To simplify calculations, elastic conditions and the maximum principal stress theory were considered.

In general the tangential stress for a single-walled cylinder in the elastic case is given by

$$\sigma_t(r) = \frac{P_1 - P_2 K^2 + \frac{r_2^2}{r^2}(P_1 - P_2)}{K^2 - 1} \tag{8}$$

where P_1 is the pressure at r_1 and P_2 at r_2. Consider a double-walled cylinder for which the radii of the wall surfaces (from the inside out) are labeled r_1, r_2, r_2', and r_3. By definition, $K = r_2/r_1$, $H = r_3/r_2$, and $J = r_3/r_1$. When the cylinder is unloaded P_1 and P_3 are zero and Equation (8) yields the set of equations

$$\bar{\sigma}_{t1}(K^2 - 1) = -2pK^2 \quad , \tag{9a}$$

$$\bar{\sigma}_{t2}(K^2 - 1) = -(K^2 + 1)p \quad , \tag{9b}$$

and

$$\bar{\sigma}_{t2}'(H^2 - 1) = (H^2 + 1)p \tag{9c}$$

where P_2 is p, the prestressing pressure.

When the cylinder is loaded there is a similar set of conditions. To obtain the maximum advantage from the prestressing, we require that the stress at the inner surfaces of both walls be equal to the tensile strength. Hence

$$\sigma_y (K^2 - 1) = (K^2 + 1)P_1 - 2K^2 P_2 \quad , \tag{10a}$$

$$\sigma_{t2}(K^2 - 1) = 2P_1 - (K^2 + 1)P_2 \quad , \tag{10b}$$

and

$$\sigma_y (H^2 - 1) = (H^2 + 1)P_2 \quad . \tag{10c}$$

From (10a) and (10c), P_1 and P_2 can be solved in terms of geometry and the tensile yield strength. Then replacing H by J/K gives

$$P_1 = \frac{1}{K^2 + 1} \left[K_2 - 1 + 2K^2 \frac{J^2 - K^2}{J^2 + K^2} \right] \sigma_y \quad , \tag{11}$$

If J is kept constant so the overall cylinder dimensions are fixed, P_1 is maximized with respect to K by setting $(\partial P_1/\partial K)_J = 0$. The result is

$$H = K = \sqrt{J} \quad ,$$

so the geometrical parameter of both walls is the same. Also the maximum internal pressure for a properly prestressed double-walled cylinder is

$$P_1 = \frac{3J^2 - 2J - 1}{J^2 + 2J + 1} \sigma_y \quad ,$$

which represents a significant advantage over that for a single-walled cylinder of the same overall size (7).

Now consider the problem of how to properly prestress the cylinder. In general the radial stress in a cylinder under elastic conditions is given by

$$\epsilon_r = \frac{1}{E} (\sigma_r - \nu\sigma_t - \nu\sigma_z) \tag{12}$$

where E = elastic modulus and ν = Poisson's ratio. For this case the pistons support the force in the axial direction so σ_z is zero. Under elastic conditions the radial stress in a cylinder is

$$\sigma_r(r) = - \frac{P_2K^2 - P_1 + \left[\frac{r_2}{r}\right]^2 (P_1 - P_2)}{K^2 - 1} \quad .$$

For the unloaded cylinder $\bar{\sigma}_{r2} = -p = \bar{\sigma}'_{r2}$. When these results, (9b), and (9c) are combined with Equation (12), the changes of the radii at the interface necessary to accomplish the prestressing are

$$\frac{\Delta r_2}{r_2} = \epsilon_{r2} = \frac{1}{E}(\bar{\sigma}_{r2} - \bar{\sigma}_{t2}) = -\frac{p}{E}\left[1 - \frac{K^2 + 1}{K^2 - 1}\right],$$

and $$\frac{\Delta r_2}{r_2} = \epsilon_{r2} = -\frac{p}{E}\left[1 + \frac{K^2 + 1}{K^2 - 1}\right].$$

So the total difference in radii before assembly is

$$\frac{\Delta R_2}{r_2} = -\frac{2p}{E} .$$

The prestressing pressure can be evaluated by considering an additional restraint. Since stresses are additive the differential tangential stress at the r_2 interface must be independent of the internal pressure. For the loaded case, P_1 and P_2 obtained from (10a) and (10c) can be substituted into (10b) to give

$$\sigma_{t2} = \frac{-K^4 + 4K^2 + 1}{(K^2 + 1)^2}\ \sigma_y .$$

Since $\sigma_{t2}' = \sigma_y$,

$$\sigma_{t2}' - \sigma_{t2} = \frac{2K^2 (K^2 - 1)}{(K^2 + 1)^2}\ \sigma_y .$$

However, from (9b) and (9c) for the unloaded case,

$$\bar{\sigma}_{t2}' - \bar{\sigma}_{t2} = 2\,\frac{K^2 + 1}{K^2 - 1}\ p .$$

Equating these results gives the prestressing pressure in terms of the tensile yield strength. Then the necessary difference in radii is

$$\frac{\Delta R_2}{r_2} = -\frac{\sigma_y}{E}\ \frac{2K^2 (K^2 - 1)^2}{(K^2 + 1)^3} .$$

The double-walled cylinder used in this experiment was constructed of beryllium-copper and had $r_1 = 0.0625$ in., $r_2 = 0.125$ in., and $r_3 = 0.300$

in. The elastic modulus of age-hardened beryllium-copper (Berylco 25) is about 1310 kbar at moderate pressures, but decreases to 1190 kbar near the elastic limit. For this cylinder the elastic limit would be reached with an internal pressure of 20.4 kbar.

The necessary difference in radii at the interface is about 0.9×10^{-3} in. As mentioned in Chapter II, the interface between the two walls is tapered. Initially the two walls are assembled in a snug fit and this is considered to be the equilibrium position. The additional distance that the inner wall would have to be inserted was easily calculated from geometrical considerations. The inner wall was machined so that it extended this amount from the outer wall in the initial position. The actual prestressing was accomplished by judicious use of thermal expansion. The outer wall was heat treated at 600° F just prior to assembly and the inner wall was cooled in liquid nitrogen. (the inner wall had previously been age-hardened.) Both walls were quickly removed from their thermal environments and the inner wall driven into the outer using a small hand press. The bore was honed to final dimensions after the heat-treating and prestressing were completed.

APPENDIX C

GR-65 Thermometry Fit Coefficients

Range of Validity	Coefficients	Measuring Current
1.130-4.200 K	R0 = 18350.80 Ω	5μa
	A(0) = 1.2865066D-01	
	A(1) = -3.1063739D-01	
	A(2) = 6.9503797D-02	
	A(3) = 6.4271576D-02	
	A(4) = 5.0783040D-02	
	A(5) = 2.0449112D-02	
	A(6) = 4.3450279D-03	
	A(7) = 3.8862972D-04	
4.200-10.000 K	R0 = 955.41 Ω	5μa
	A(0) = 1.3887007D 00	
	A(1) = -5.2873387D-01	
	A(2) = 1.5369707D-01	
	A(3) = 3.6094363D-01	
	A(4) = 3.6603071D-01	
	A(5) = 2.0783642D-01	
	A(6) = 6.3146387D-02	
	A(7) = 7.8735416D-03	
10.000-20.190 K	R0 = 187.80 Ω	10μa
	A(0) = 2.2302583D 00	
	A(1) = -4.9577857D-01	
	A(2) = -1.4743807D-01	
	A(3) = -6.9903961D-01	
	A(4) = -1.4097290D 00	
	A(5) = -1.5333373D 00	
	A(6) = -8.2262089D-01	
	A(7) = -1.7093157D-01	

APPENDIX D

Data Concerning the Superconducting Properties of Pb-Bi Alloys under Pressure

The following pages list the results of the present investigations. The transition temperature, critical field, and pressure data as well as other important information about the sample are given for each run.

$H_{cr}(h_o)$ DATA+

SAMPLE INFORMATION	H_{cr}(kG)	h_o(G)	T(K)
Run 43	0.00	0.18	8.024
REJ-1a(3)		0.90	8.016
P = 15.41 kbar		3.60	7.999
dhcp		7.20	7.992
	0.20	$0.04\frac{1}{2}$	7.971
		0.18	7.966
		0.90	7.948
		3.60	7.930
		7.20	7.913
		9.00	7.910
	0.60	0.90	7.848
		7.20	7.802
	1.20	0.90	7.725
		7.20	7.667
	2.00	0.18	7.589
		0.90	7.562
		7.20	7.499
		7.20	7.502
	3.00	7.20	7.310
	5.00	0.90	7.021
		5.40	6.954
		7.20	6.943
	10.00	0.18	6.213
		0.90	6.140
		7.20	6.040
	19.60	0.18	4.604
		0.90	4.352
		7.20	4.169

+All data were obtained from temperature sweeps and the zero field data were determined from the χ'' maxima.

$H_{cr}(h_o)$ DATA+

SAMPLE INFORMATION	H_{cr}(kG)	h_o(G)	T(K)
Run 44	0.00	$0.04\frac{1}{2}$	8.415
REJ-1a(3)		0.18	8.410
P ~ 4.5 kbar		0.90	8.393
α-β		7.20	8.364
	2.00	7.20	7.807
	10.00	0.18	6.068*
		0.90	5.991*
		7.20	5.872*

*These data were obtained under non-equilibrium conditions by recording the $\mathcal{R}$ and χ' outputs of the MIB while the temperature gradually was increased.

H_{c3}* DATA

SAMPLE INFORMATION	H(kG)	$T(H_{cr})(K)^{+}$	$T(H_{c3}^*)(K)$
Run 43 REJ-1a(3) P = 15.41 kbar dhcp	0.00	8.014	8.041
	0.20	7.948	7.992
	0.40	7.896	7.935
	0.60	7.848	7.896
	0.90	7.785	7.838
	1.20	7.725	7.787
	2.00	7.562	7.633
	5.00	7.021	7.137
	10.00	6.140	6.332
	13.50	5.507	5.915
	17.00	4.857	5.476
	19.60	4.352	5.035

$^{+}h_o$ = 0.9 G.

ZERO FIELD DATA

RUN	Sn T_c(K)	P(kbar)	Sample REJ-	Pb-Bi T_c(K)	T_L(K)	T_H(K)	PHASE	t(day)+
3	3.610	2.35	Ia(2)	8.536	8.502	8.569	α-β	30
4	3.395	7.22	Ia(2)	8.476	8.438	8.513	α-β	1
5	3.221	11.37	Ia(2)	8.425	8.412	8.439	α-β	1
7	3.211	11.61	Ia(2)	7.964	7.953	7.976	dhcp	10
8	3.184	12.27	Ia(2)	7.931	7.922	7.940	dhcp	12
9	3.719	0.00	Ia(2)	8.433	sharp trans.		α-β	5
10	3.294	9.61	Ia(2)	8.427	8.400	8.455	α-β	25
11	3.721	0.00	Ia(2)	8.448	8.432	8.462	α-β	4
12	3.499	4.83	Ia(2)	8.422	8.396	8.443*	α-β	2
14	3.642	1.71	Ia(3)	8.380	8.345	8.420	α-β	195
15	3.640	1.75	Ia(3)	8.400	8.371	8.430	α-β	5
16	3.322	9.00	Ia(3)	8.504	8.477	8.530	α-β	5
17	3.117	14.00	Ia(2)	7.994	7.963	8.024	dhcp	135
28	3.052	15.64	Ia(2)	8.024	7.996	8.051	dhcp	85
29	2.998	17.02	Ia(2)	7.968	7.934	8.002	dhcp	6
30	3.170	12.68	II(1)	8.433	double trans.**		mixed	1
31	3.118	14.00	II(1)	8.136	broad trans.**		mixed	4
32	2.990	17.22	II(1)	7.907	7.864	7.950	dhcp	1
33	3.390	7.40	II(1)	8.619	double trans.**		mixed	5
34	3.620	2.19	II(1)	8.635	8.585	8.685	α-β	4
35	3.553	3.68	II(4)	8.469	8.441	8.496	α-β	25
36	3.152	13.12	II(4)	8.155	double trans.**		mixed	5
37	3.176	12.53	Ia(3)	8.048	8.017	8.077	dhcp	195
38	3.094	14.57	Ia(3)	8.020	7.990	8.051	dhcp	1
39	3.041	15.92	Ia(3)	8.005	7.979	8.031	dhcp	1
40	2.960	18.00	Ia(3)	7.974	7.937	8.010	dhcp	1
41	2.967	17.82	Ia(3)	8.042	8.020	8.065	dhcp	20
43	3.061	15.41	Ia(3)	8.009	7.992	8.025	dhcp	55
44	-----	4.5	Ia(3)	8.387	8.369	8.406	α-β	1

+Approximate time at room temperature since date of alloying or since the previous run on that sample.

*Skew transition.

**See Figure 38.

CRITICAL FIELD DATA FOR Pb-Bi ALLOYS[+]

SAMPLE INFORMATION	T(K)	H_{cr}(kG)
Run 15	8.400	0.00
REJ-1a(3)	7.774	2.28
P = 1.74 kbar	6.903	5.73
α-β	6.241	8.34
	5.606	10.96
	4.803	13.88
	4.377	15.21
	3.910	16.92
	3.392	18.73
	3.228	19.32
Run 16	8.504	0.00
REJ-1a(3)	8.079	1.52
P = 9.00 kbar	7.084	5.30
α-β	6.042	9.52
	5.025	13.70
	4.447	15.72
	3.695	18.30
Run 17	7.994	0.00
REJ-1a(2)	7.383	2.91
P = 14.00 kbar	6.840	6.05
dhcp	6.320	9.05
	5.404	14.27
	4.625	18.40
Run 29	7.968	0.00
REJ-1a(2)	7.515	1.93
P = 17.02 kbar	6.911	5.16
dhcp	6.329	8.47
	5.830	11.17
	5.169	14.82
	4.771	16.87
	4.354	18.94

[+]All data obtained with h_o = 0.9 G. All zero field data were obtained via temperature sweeps and T_c was determined from the half height of the χ' transition. All data in a magnetic field were obtained via field sweeps unless otherwise noted.

CRITICAL FIELD DATA FOR Pb-Bi ALLOYS[+]

SAMPLE INFORMATION	T(K)	H_{cr}(kG)
Run 30	8.433	0.00
REJ-11(1)	8.083	0.85
P = 12.68 kbar	7.786	1.85
mixed phase	7.397	3.36
	6.873	5.97
	6.085	10.70
	5.218	15.52
	4.549	19.36
Run 31	8.136	0.00
REJ-11(1)	7.551	2.00
P = 14.00 kbar	6.818	6.07
mixed phase	5.968	11.10
	4.868	17.23
Run 32	7.907	0.00
REJ-11(1)	7.498	1.70
P = 17.22 kbar	6.503	7.22
dhcp	5.682	11.79
	4.875	16.30
Run 33	8.619	0.00
REJ-11(1)	8.020	1.68
P = 7.40 kbar	7.473	3.76
mixed phase	6.815	7.07
	5.917	12.56
	5.333	16.01
	4.845	18.56
Run 34	8.635	0.00
REJ-11(1)	7.999	2.14
P = 2.19 kbar	6.889	6.89
α-β	5.925	10.87
	5.892*	10.87*
	4.904	15.15
	4.021	18.39

*These data were obtained using temperature sweeps.

CRITICAL FIELD DATA FOR Pb-Bi ALLOYS[+]

SAMPLE INFORMATION	T(K)	H_{cr}(kG)
Run 35	8.469	0.00
REJ-11(4)	7.030	5.03
P = 3.68 kbar	5.723	9.82
α-β	4.169	14.90
Run 38	8.020	0.00
REJ-1a(3)	7.586	1.77
P = 14.57 kbar	7.159	4.13
dhcp	6.719	6.67
	6.267	9.31
	5.437	13.99
	4.883	16.90
	4.357*	19.60*
Run 40	7.974	0.00
REJ-1a(3)	7.168	3.56
P = 18.00 kbar	6.283	8.31
dhcp	4.899	15.57
	4.069*	19.60*
Run 41	8.042	0.00
REJ-1a(3)	7.168	3.78
P = 17.82 kbar	4.895	15.71
dhcp		
Run 43	8.009	0.00
REJ-1a(3)	7.948*	0.20*
P = 15.41 kbar	7.896*	0.40*
dhcp	7.848*	0.60*
	7.785*	0.90*
	7.725*	1.20*
	7.562*	2.00*
	7.021*	5.00*
	6.140*	10.00*
	5.507*	13.50*
	4.857*	17.00*
	4.352*	19.60*
Run 44	8.387	0.00
REJ-1a(3)	5.991*	10.00*
P ~ 4.5 kbar		
α-β		